

TESI DI DOTTORATO

UNIVERSITÀ DEGLI STUDI DI NAPOLI FEDERICO II

DIPARTIMENTO DI INGEGNERIA ELETTRICA
E DELLE TECNOLOGIE DELL'INFORMAZIONE

DOTTORATO DI RICERCA IN
INFORMATION TECHNOLOGY AND ELECTRICAL
ENGINEERING

ENERGY SHAPING OF UNDERACTUATED SYSTEMS VIA
INTERCONNECTION AND DAMPING ASSIGNMENT PASSIVITY-BASED
CONTROL WITH APPLICATIONS TO PLANAR BIPED ROBOTS

Pierluigi Arpentì

Il Coordinatore del Corso di Il Tutore
Dottorato

Ch.mo Prof.
Daniele RICCIO

Ch.mo Prof.
Vincenzo LIPPIELLO

Il co-Tutore
Prof. Fabio RUGGIERO

A. A. 2020–2021

Contents

List of Acronyms	4
List of Figures	6
List of Tables	9
Abstract	10
Preface	11
1 Introduction	12
2 Literature Overview	20
2.1 Bipedal Locomotion Control Approaches	20
2.2 Energy Shaping Applied to Passive Dynamic Locomotion for Gait Generation	24
2.3 IDA-PBC Approaches to Avoid the Solution of PDEs .	25
2.4 Locomotion Control Strategies Based on HZD	28
3 Modelling	30
3.1 Underactuated Mechanical Systems in the pH Framework	30
3.1.1 The TORA System	31
3.2 Hybrid Mechanical Systems	33
3.2.1 Planar Biped Robots	34
3.2.2 Periodic Walking for Passive Bipedes	37
3.2.3 The Hybrid Zero Dynamics Concept	39

<i>CONTENTS</i>	2
3.2.4 The CBR	42
4 IDA-PBC with Explicit Solution of PDEs	46
4.1 A Mixed Parameterized-Algebraic IDA-PBC Approach	46
4.2 Constructive Methodology	48
4.2.1 Constructive Methodology with $k_1 = 0$ and $k_2 \neq 0$	53
5 Energy Shaping for Equilibrium Point Stabilization	57
5.1 Stabilization of the TORA System via IDA-PBC with Explicit solution of PDEs	57
5.1.1 Step 1	57
5.1.2 Step 2	58
5.1.3 Step 3	58
5.1.4 Step 4	59
5.1.5 Step 5	60
5.1.6 Step 6	60
5.2 Numerical Evaluation	61
6 Energy Shaping for Gait Generation	66
6.1 Total Energy Shaping VS Kinetic Energy Shaping for Gait Generation	67
6.2 Gait Generation for the CBR via IDA-PBC with Ex- plicit Solution of PDEs	68
6.2.1 Alternative choice of γ and a_{11}	70
6.3 Gait Generation for the CBR via SIDA-PBC with Dis- sipative Forces	71
6.4 Gait Generation for the CBR via EPD-PBC	73
6.5 Gait Generation for the CBR via EPOD-PBC	74
6.6 Numerical evaluation	75
6.6.1 Case Study I: Small Gait Generation via IDA- PBC With Explicit Solution Of PDEs	76
6.6.2 Case Study II: Large Gait Generation Via IDA- PBC With Explicit Solution Of PDEs	79
6.6.3 Case Study III: Small Gait Generation via SIDA- PBC with Dissipative Forces	85

<i>CONTENTS</i>	3
6.6.4 Case Study IV: Large Gait Generation via SIDA-PBC with Dissipative Forces	85
6.6.5 Case Study V: Small Gait Generation via EPD-PBC	88
6.6.6 Case Study VI: Large Gait Generation via EPD-PBC	88
6.6.7 Case Study VII: Small Gait Generation via EPOD-PBC	91
6.6.8 Case Study VIII: Large Gait Generation via EPOD-PBC	91
6.7 Performance Comparison	94
7 Energy Shaping for Gait Robustification	98
7.1 EPD-PBC Design within HZD Formulation	99
7.2 Zero Dynamics Stability Analysis	101
7.3 Full Dynamics Stability Analysis	103
7.4 Numerical Evaluation	104
7.4.1 Case Study I: Passive Gait Robustification	105
7.4.2 Case Study II: Generated Gait Robustification	108
8 Conclusion and Future Research	112
Appendix A IDA Methodologies	114
A.1 IDA-PBC for Applications to 2-DoF Mechanical Systems	115
A.2 SIDA-PBC with Dissipative Forces for Applications to 2-DoF Mechanical Systems	118
A.3 EPD-PBC for Applications to 2-DoF Mechanical Systems	120
A.4 EPOD-PBC	121
Appendix B Existence of the Integrals	122
B.1 Existence of the integral within equation (4.11)	122
B.2 Existence of the integral within equation (4.17)	123

List of Acronyms

CL	controlled Lagrangians
CS	controlled symmetries
CBR	compass-like biped robot
CoM	center of mass
DoF	degree of freedom
EPD	energy pumping-and-damping
EPOD	energy pumping-or-damping
HZD	hybrid zero dynamics
IDA	interconnection and damping assignment
KE-ME	kinetic energy matching equation
MNC	min-norm control
ODE	ordinary differential equation
PBC	passivity-based control
pH	port-Hamiltonian
PDE	partial differential equation
PE-ME	potential energy matching equation

RES-CLF	rapidly exponentially stabilizing control Lyapunov function
SIDA	simultaneous interconnection and damping assignment
TORA	translational oscillator with a rotational actuator
ZMP	zero moment point

List of Figures

1.1	Logic scheme of this doctoral thesis.	19
2.1	Complexity evolution in approximate biped robot models.	23
3.1	Scheme of a translational oscillator with a rotational actuator (TORA) system.	33
3.2	Scheme of a compass-like biped robot (CBR).	43
4.1	Flow chart of the proposed constructive solution.	54
5.1	Evolution of the potential energy of the closed-loop TORA system.	63
5.2	Time histories of the generalized coordinates of the closed-loop TORA system.	64
5.3	Time histories of the generalized momenta of the closed-loop TORA system.	65
6.1	Event histories of the step length and the step period of the CBR during Case Study I ($\gamma(q_1)$ as in (6.2) and $a_{11}(q)$ as in (6.8)).	77
6.2	Event histories of the step length and the step period of the CBR during Case Study I ($\gamma(q_1)$ as in (6.13) and $a_{11}(q)$ as in (6.14)).	78
6.3	Event histories of the step length and the step period of the CBR during Case Study II ($\gamma(q_1)$ as in (6.2) and $a_{11}(q)$ as in (6.8)).	80

6.4	Event histories of the step length and the step period of the CBR during Case Study II ($\gamma(q_1)$ as in (6.13) and $a_{11}(q)$ as in (6.14)).	81
6.5	Limit cycles comparison during Case Study II: IDA-PBC VS CL.	82
6.6	Event histories of step length and step period of the CBR during Case Study II in presence of parametric uncertainties.	83
6.7	Limit cycles comparison during Case Study II in presence of parametric uncertainties.	84
6.8	Limit cycles comparison (Case Study I and Case Study II).	84
6.9	Event histories of the step length and the step period of the CBR during Case Study III.	86
6.10	Event histories of the step length and the step period of the CBR during a Case Study IV.	87
6.11	Limit cycles comparison (Case Study III and Case Study IV).	88
6.12	Event histories of the step length and the step period of the CBR during Case Study V.	89
6.13	Event histories of the step length and the step period of the CBR during Case Study VI.	90
6.14	Limit cycles comparison (Case Study V and Case Study VI).	91
6.15	Event histories of the step length and the step period of the CBR during Case Study VII.	92
6.16	Event histories of the step length and the step period of the CBR during Case Study VIII.	93
6.17	Limit cycles comparison (Case Study VII and Case Study VIII).	94
7.1	Limit cycles comparison during Case Study I.	106
7.2	Limit cycles comparison for the first leg during Case Study I.	107
7.3	Storage function convergence during Case Study I.	108

7.4 Limit cycles comparison for the first leg during Case
Study II. 111

List of Tables

3.1	Models of the systems deployed in this thesis to test the proposed control strategies.	45
5.1	Parameters and initial conditions characterizing the TORA model used in simulations.	62
6.1	Parameters and initial conditions characterizing the CBR model used in simulations.	76
6.2	Comparison between step length values and step period values.	97
7.1	Comparison between EPD-PBC and MNC.	109

Abstract

The sought goal of this thesis is to show that total energy shaping is an effective and versatile tool to control underactuated mechanical systems. The performance of several approaches, rooted in the port-Hamiltonian formalism, are analyzed while tackling distinct control problems: *i)* equilibrium stabilization; *ii)* gait generation; *iii)* gait robustification. Firstly, a constructive solution to deal with interconnection and damping assignment passivity-based control (IDA-PBC) for underactuated two-degree-of-freedom mechanical systems is proposed. This strategy does not involve the resolution of any partial differential equation, since explicit solutions are given, while no singularities depending on generalized momenta are introduced by the controller. The methodology is applied to the stabilization of a translational oscillator with a rotational actuator system, as well as, to the gait generation for an underactuated compass-like biped robot (CBR). Then, the problem of gait generation is addressed using dissipative forces in the controller. In this sense, three distinct controllers are presented, namely simultaneous interconnection and damping assignment passivity-based control with dissipative forces, energy pumping-and-damping passivity-based control (EPD-PBC), and energy pumping-or-damping control. Finally, EPD-PBC is used to increase the robustness of the gait exhibited by the CBR over uncertainties on the initial conditions. The passivity of the system is exploited, as well as, its hybrid nature (using the hybrid zero dynamics method) to carry out the stability analysis. Besides, such an approach is applied to new gaits that are generated using IDA-PBC. Numerical case studies, comparisons, and critical discussions evaluate the performance of the proposed approaches.

Preface

This doctoral thesis is styled as a cumulative thesis. The main contents are based on publications from peer-reviewed journals and conference proceedings.

The constructive methodology for the IDA-PBC of underactuated 2-DoF mechanical systems with explicit solution of PDEs presented in Chapter 4 and then exploited in Chapter 5, as well as, in Section 6.2, has been accepted for publication in [1]. The alternative approach shown in Section 6.2.1, has been presented in [2]. The use of dissipative forces to generate gaits has been proposed in [3]. In the this thesis, the related methodologies are presented in Sections 6.3, 6.4, and 6.5, respectively. The idea to use EPD-PBC with hybrid zero dynamics to increase the robustness of the gait to uncertainties on initial conditions, as well as, the related methodology has been accepted to be published in [4]. The strategy and the numerical simulations validating this approach are presented in Chapter 7.

Chapter 1

Introduction

Complex systems require adequate control strategies which exploit, rather than suppress, their inherent nonlinear nature. As pointed out in [5], approaches that have been developed to control rigid arms deployed in structured industrial environments limit robots to move far too conservatively and to achieve only a small part of the performance that they are kinematically capable of. An alternative approach is represented by the study of underactuated robotics which leads to the development of control systems that use the natural dynamics of robots to achieve better performance in terms of speed, efficiency, or robustness [5]. A mechanical system is underactuated when the number of control inputs is less than the number of generalized coordinates which have to be controlled to accomplish the desired task. Some motivations behind such a design approach are the need to save on the cost of actuators, as well as, the need for better performance and autonomy (especially in mobile robotics). Such objectives are reachable by reducing the total number of actuators, which leads to a lightening of the whole mechanical structure. Another common motivation behind underactuation is the intrinsic difficulty (often impossibility) to actuate a given joint due to the particular kinematic structure of the robot.

Whatever motivation exists behind the underactuation, some state-of-the-art control methodologies cannot be applied. An example is the input-output linearization, which is instead broadly used for fully actu-

ated robots. Exceptions occur when restrictive conditions on the inertia matrix hold, hence limiting the range of applicability of the methodology, which leads to a partial feedback linearization approach [6]. Anyway, even in those cases for which partial feedback linearization is applicable, this control policy does not fully exploit the nonlinear nature of the system, implying a worsening in the performance exhibited by the controlled system.

Great research effort has been put into developing control strategies tailored for underactuated mechanical systems. Passivity-based control (PBC) plays a key role in this quest. A mechanical system is passive respect to input-output signals if the variation of its energy during a certain time interval is less than or equal to the energy exchanged by the system with the external environment. Hence, control methodologies based on passivity are those which duly take into account the nonlinear nature of systems, regarded as energy exchanging devices. Given the desired equilibrium point, PBC passivizes the system with a storage function that has a minimum exactly at that point. This methodology proved to be useful for stabilizing simple mechanical systems, shaping their potential energy only. Nevertheless, some applications, including underactuated mechanical systems, require to shape also kinetic energy [7, Section 10.3.1]. Energy shaping is a subclass of PBC which exploits the intrinsic physical and passive properties of the systems by assigning a desired energy to the closed-loop, resulting in a fundamental tool to control nonlinear systems [8]. As seen, some applications require to shape only the potential energy whereas others need to shape also the kinetic one. Motivated by the need for a total energy shaping which extends the range of applicability of PBC to a broader class of systems (e.g., underactuated mechanical systems), interconnection and damping assignment passivity-based control (IDA-PBC) has been proposed in [9]. IDA-PBC is rooted in the port-Hamiltonian (pH) framework, a modeling formalism which explicitly models nonlinear systems highlighting their energy-conserving/dissipating properties. The pH framework allows to describe the system in terms of Hamiltonian, interconnection and dissipation structures, and input ports, resulting to be an elegant tool

to describe passive systems. What makes the pH framework so useful to cope with underactuation is the set of control techniques that have been developed to exploit such formalism. The main class of control strategies is represented by the IDA methodologies that are those based on IDA-PBC. This latter control approach results from the matching between the dynamics of the plant (potentially underactuated) and those of the desired system. Such matching consists in the solution of a set of partial differential equations (PDEs) which are the main stumbling block to a widespread diffusion of such kind of control methodologies. IDA-PBC is well suited to cope with underactuated systems due to the presence of a skew-symmetric matrix in the matching equations, resulting from the inclusion of gyroscopic (workless) forces in the desired dynamics, that can be profitably designed to reduce the number of PDEs to be solved. Despite this, research paths are still pursuing a systematic procedure to avoid the solution of such PDEs [10, 11]. This could have beneficial effects not only in the quest for a control law able to stabilize underactuated mechanical systems at sought equilibrium points but also for different control tasks. One of such tasks is the gait generation, which is addressed when dealing with the locomotion control of legged robots.

Gait generation is the creation, through a feedback control action, of a walking pattern (usually periodic) for a legged robot. Biped robots constitute a subclass of legged robots that are those with only two legs and upright posture. In particular, this thesis addresses the gait generation for the compass-like biped robot, which belongs to the class of the point-feet passive bipeds. Point-feet synthesizes some of the properties encompassed by human feet where the former ones rotate around a single axis (the tip of the leg) while the latter rotate around two axes (the heel and the toe of each foot), although a freely rotating point of contact is more difficult to control than the heel-strike or toe-roll phases of human walking [12]. Point-feet bipeds are often designed with unactuated ankles. If gait generation can be achieved when zero control torque is applied at stance ankle, then it is likely that flat-footed walking can be accomplished with arbitrary small torques [12]. Moreover, based on previous work in planar robots [13], there is good reason to believe that

a gait consisting of a full walking cycle (heel strike, flat foot, and toe roll) can be realized stably. For these reasons, walking with an unactuated point-feet presents an interesting case study for any locomotion control design methodology. In this situation, underactuation arises when no control torque is applied at the ankle's joints, but it is not the only possibility. Studies on the natural human gait show that the primary energy source for the forward motion comes from ankles and that an ankle-only actuation is more energetically efficient than a hip-only one [14, 15]. In human walking, the ankle is the main source of the energy required for the forward motion of the body [14], contributing more than the knee or hip [15]. Such studies, which show that zero control torque at the hip joint faithfully resembles human locomotion from an energetic point of view, have thus motivated control strategies for underactuated bipeds with a passive hip joint [16]. Hence there are two alternative approaches: those for which underactuation represent the best test-bed to propose robust control strategies to achieve stable walking, *i.e.*, methodologies which consider unactuated ankle's joints, and, at the opposite end of the spectrum, those for which underactuation is an opportunity to propose more human-like and efficient gaits, *i.e.*, approaches that consider an unactuated hip joint. In both cases, underactuation is motivated by the necessity to exploit distinct properties endowed by the biped's model during control design, to propose robust and efficient walking. Since biped's gait is underactuated, gait generation has necessarily to cope with underactuation. Moreover, the key features of biped locomotion are synthesized by passive dynamic walking, which is exhibited by passive walkers, *i.e.*, biped robots able to walk down a shallow slope with no actuation, under the influence of the gravitational field only [17]. Conservation of mechanical energy is the physical principle which explains passive dynamic locomotion. For this reason, studying passive locomotion from an energetic point of view is a profitable way to enter the core mechanism which underscores efficient and human-like locomotion. Because of the pivotal role that conservation of energy plays in generating efficient walking, it feels natural to shape the energy of the biped in such a way to modify the gait. Energy shaping was proved to be an effective strategy to

control passive walkers, albeit it has been poorly used. Passive gaits suffer from weak stability properties since the associated limit cycles (*i.e.*, the solutions representing the gaits in the phase plane) usually exhibit a restricted basin of attraction. Therefore, the advantage of shaping the energy during continuous dynamics is twofold. First, the passive gait's basin of attraction can be enlarged, second, the gait can be modified by changing the way the robot and the ground exchange energy [16, 18, 19, 20].

This thesis shows the effectiveness of IDA methodologies, which have been originally developed to stabilize systems at desired equilibrium points, to tackle the gait generation of planar, passive biped robots. The investigation about the effects of IDA methodologies, which are strategies perfectly fitted to shape the energy of underactuated systems, on the gait generation for passive walkers follows immediately from the importance assumed by underactuation and energy conservation in passive locomotion.

As the first contribution, this thesis shows a novel control methodology, firstly presented in [1], inspired by IDA-PBC, aimed at avoiding the explicit solution of the PDEs arising during the matching process, while not introducing any singularity in the controller. Since controller design is simplified, this new procedure is applied to tackle both the equilibrium stabilization of a translational oscillator with a rotational actuator (TORA) system and the gait generation for a compass-like biped robot (CBR), proving the versatility of IDA methodologies to also cope with control problems differing by standard equilibrium stabilization, thus extending the range of applications of IDA methodologies.

The second contribution is the application of the simultaneous interconnection and damping assignment passivity-based control (SIDA-PBC) with dissipative forces to accomplish gait generation, as originally shown in [3]. Unlike IDA-PBC, which firstly accomplishes energy shaping and, successively, dissipates energy, SIDA-PBC accomplishes energy shaping and damping injection simultaneously. As claimed in [21], SIDA-PBC with dissipative forces represents a generalization of IDA-PBC, meaning that it applies to a wider class of systems. SIDA-

PBC uses dissipative forces, in contrast to IDA-PBC which uses gyroscopic ones. This difference might justify the fact that the former is more suited to generate small gaits while IDA-PBC exhibits good performance in generating both large and small ones, as will be shown in the sequel of the thesis.

Another control strategy investigated in this thesis, which exploits dissipative forces too, is the energy-pumping and damping passivity-based control (EPD-PBC). Such methodology represents a valid alternative to SIDA-PBC, as outlined in [3], due to the similar performance displayed and to the simpler control design because it does not require solving any PDEs. Hence the third contribution is the application of EPD-PBC to tackle gait generation.

Moreover, as firstly proposed in [4], in this thesis EPD-PBC is adopted in conjunction with the Hybrid Zero Dynamics (HZD) approach. In this way, by explicitly taking into account the hybrid nature of walking, the exponential stabilization to a reference energy value for a planar biped robot is achieved. This is instrumental to enlarge the basin of attraction of an existing gait, as firstly shown in [22]. The target energy in the EPD-PBC can be related to the passive gait or another one if an inner energy shaping control loop is applied. Non-passive gaits are created through energy shaping, which is motivated by the necessity to change the way the robot and the ground exchange energy [23]. Compared with the approach exploited in [22], which is based on Poincaré maps, the methodology used in this thesis, based on invariant set theory, leads to less conservative results [24] in determining the stability of the controlled system.

The outline of this thesis is organized as follows.

In Chapter 2, a summary overview of the most common approaches deployed to control simple biped robot models is given. Subsequently, a literature review about energy shaping approaches applied to passive locomotion, focused on gait generation, is carried out. Then, a specific energy shaping methodology, namely IDA-PBC, is revised, with particular emphasis on the strategies which have been proposed to avoid the solution of PDEs. Finally, some state-of-the-art approaches to stabilize gaits taking into account the hybrid nature of walking, each one rooted

in the HZD approach, are summarized. Chapter 3 is devoted to the pH modeling of underactuated mechanical systems firstly. The TORA system is described, which is the test-bed employed in this thesis to show the effectiveness of the proposed stabilization approach. Then, hybrid mechanical systems are presented with particular emphasis to planar biped robots able to walk exhibiting a periodic gait without actuation. Finally, the HZD concept is introduced and the CBR model, which is the test-bed deployed to show the effectiveness of gait generation methodologies, as well as, of the approach aimed at enlarging the basin of attraction of the passive gait, is presented. Chapter 4 presents a variant of standard IDA-PBC aimed at shaping the total energy of a given 2-DoF underactuated mechanical system without solving any PDE explicitly. In Chapter 5 the IDA-PBC methodology, previously presented in Chapter 4, is applied to tackle the stabilization task of the TORA system. Chapter 6 proposes several approaches to face the gait generation problem of the CBR, namely IDA-PBC with explicit solutions of PDEs, SIDA-PBC with dissipative forces, EPD-PBC, and EPOD-PBC. Performance comparison among methodologies exploited is done, pointing out the advantages of total energy shaping with respect to kinetic energy shaping. Chapter 7 presents an alternative use of EPD-PBC, aimed at enlarging the basin of attraction of an existing gait by duly taking into account the hybrid nature of the CBR and using HZD. In Chapter 8, conclusions and ongoing projects are outlined.

Figure 1.1 may help the reader to go through this thesis, outlining the logic connections between the chapters and the appendices.

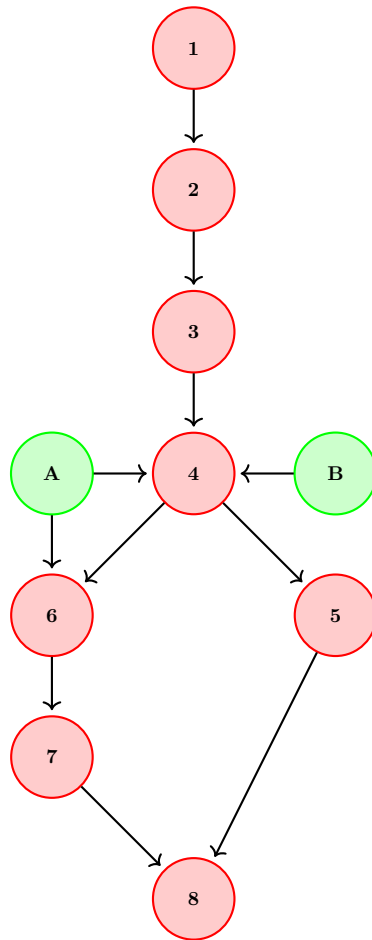


Figure 1.1: Logic scheme of this doctoral thesis. Numbers and letters refer respectively to chapters (red) and appendices (green).

Chapter 2

Literature Overview

2.1 Bipedal Locomotion Control Approaches

This section is inspired on the survey proposed in [12], which is warmly recommended to deepen the arguments that are about to be addressed in the following.

When studying locomotion control strategies of biped robots, the most popular concept used in literature is the *zero moment point* (ZMP), *i.e.*, the contact point between the ground and the foot at which the reaction forces produce no horizontal moment. ZMP-based control approaches plan the motion of the robot's center of mass (CoM) to keep the ZMP within the convex hull of the stance foot. As consequence, the foot remains flat on the ground while not rotating, thus leading the robot to walk without falling [25].

It is common to reduce the complexity of control design by referring to a lower-dimensional model. If the robot is approximated as a point mass, legs are assumed to be massless and telescoping and, additionally, if the height of the CoM is assumed to not change throughout the whole gait, then the biped can be approximated by a *linear inverted pendulum model* (LIPM) [26], which is the most simple low-dimensional model for a biped robot. Besides, such kind of model finds some motivations in the study of human posture and balance [27]. To achieve walking with such a simplified model, the ZMP can be expressed in

a simplified way, as the dynamics of the CoM via a linear ordinary differential equation (ODE) [28, 29]. ZMP has been extensively investigated to tackle the gait generation task leading to several solutions, some of the most relevant are [30, 31, 32]. Moreover, it was first demonstrated in practice on the WL10-RD biped in [33]. Since gait design via ZMP methods does not take care of the hybrid nature of walking, some limitations arise. For instance, the swing foot trajectory must be planned in such a way as to hit the ground with low velocity, which can be hard to achieve. Moreover, it is shown in [34] that fulfilling ZMP conditions does not guarantee the asymptotic stability of a periodic walking motion. More complex models have been successively considered to overcome such limitations. An additional point mass has been added at the location of the swing foot in [35] to explore a gravity-compensated LIPM, to achieve better modeling accuracy.

The *inverted pendulum with flywheel* (IPF) is used to achieve posture control and analysis of push recovery in [36], and to mitigate the effects of modeling error on gait generation in [37]. The concept of the capture point, *i.e.*, a point on the ground on which a biped can stop, keeping an upright posture without toppling [38], has been proposed using IPF. Then such a concept has been used to design a stabilizing control law for a biped in [39] and for achieving robust walking combined with learning (due to the large errors present in the set of all capture points) in [40].

A simplified model which was developed based on observations on hopping and running of several terrestrial animals is the *spring-loaded inverted pendulum* (SLIP) model [41], which well approximates their body CoM motion during steady-state running gaits [42]. Moreover, the SLIP model behavior is endowed by effectively running robots such as the Planar Hopper [43], ARL Monopod II [44], and CMU Bowleg Hopper [45]. In [41, 44] the original control methodologies of such kind of robots are presented, aimed at regulating forward propulsion of the robot at the desired speed by placing the toe at the desired position with respect to the CoM during flight phases, regulating the vertical hopping height of the body by adjusting the length of the leg at the bottom of the stance phase through a fixed amount of thrust, and

keeping the body at the desired posture exploiting hip torque during contact phases.

LIPM, IPF, and SLIP approximate complex bipeds with simplified models. An alternative modeling approach is to design robots with dynamics that approximately realize a simplified model, where a specific mechanical design helps to achieve dynamic stability, also without feedback control in some peculiar conditions. Analysis and synthesis methods developed on such simple models can be deployed in more complex bipeds. The simpler mechanical design facilitates a more deepened mathematical modeling, thus allowing to take care of impact dynamics during control design and, consequently, to take into account the full hybrid model which is generally neglected from the design process of control policies used to stabilize LIPM, as well as, IPF and SLIP models. After some preliminary studies [46], which pointed out a tight connection between the swing phase of human walking and the motion of a double inverted pendulum, enlightening the passive nature of human walking, planar, passive bipedal walkers, *i.e.*, biped robots without any actuation which could walk stably down shallow slopes were built. The rise of such pendulum-like bipeds, whose presentation coincided with the birth of the concept named *passive dynamic walking*, began with the *compass-like biped robot* (CBR), *i.e.*, a simple inverted-pendulum model, firstly proposed in its original version without knees [17] and then adding them [47]. The interest in studying passive dynamic walking is twofold. At first, passive walking exhibits similarities with human gait features, serving as a testbed to investigate human locomotion [48]. Secondly, this kind of motion is energetically efficient compared to the other state-of-the-art biped locomotion control strategies based on walking primitives preplanning and on the zero moment point stability criterion [49]. Passive dynamic walking served as the leading principle in the design of several robots, all of them sharing the “human-looking” walking and the efficiency, rising as unrivaled effective devices in periodic walking and running. For this class of walkers, the main drawback is the lack of flexibility in achieving tasks other than walking at a fixed speed, making them ineffective in realizing more articulated tasks, such as the ones requiring to climb

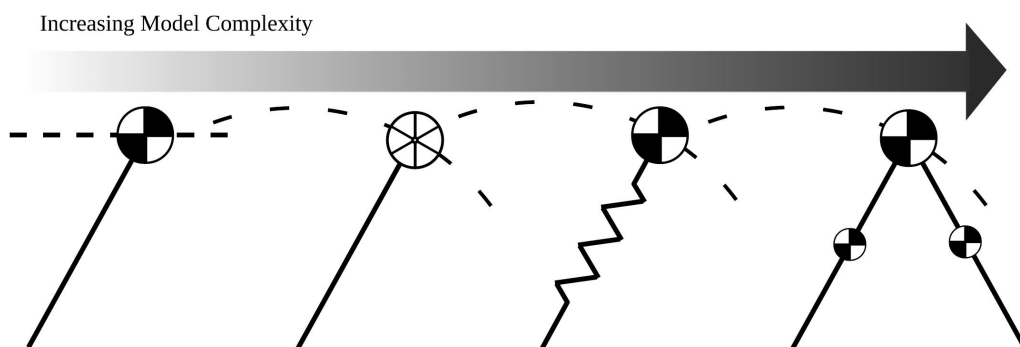


Figure 2.1: Complexity evolution in approximate biped robot models as proposed in [12]. From left to right: the Linear Inverted Pendulum Model (LIPM) which exhibits the whole mass of the robot lumped at a point moving at a fixed height, with massless legs; the Inverted Pendulum with Flywheel (IPF) which accounts for the internal angular momentum of the robot by adding a flywheel and which relaxes the assumption on fixed height; the Spring-Loaded Inverted Pendulum (SLIP) which incorporates a spring to model legs as massless pogo sticks; and the Compass-Like Biped Robot (CBR) which represents the biped as a double inverted pendulum with lumped masses on the stance and swing legs, as well as, on the hip.

stairs or to pause and turn. One example of biped robot realized with this design philosophy at the core is the one proposed in [50], where gait is generated by injecting small amounts of energy into passive-type bipeds, and where a mix between mechanical design and learning algorithms helps to find the efficient control policy. A passive dynamic for multiple degrees of freedom underactuated biped is generated in [51] by combining a passive controller and a proportional-derivative one.

A more deepened presentation about a sub-class of PBC strategies developed for bipeds exhibiting passive dynamic walking, CBR in particular, is proposed in the next section. The complexity-evolution of low-dimensional biped models is synthetically sketched in Figure 2.1. Another broad overview about how generic legged robots are modeled and how they are controlled is given in [52].

2.2 Energy Shaping Applied to Passive Dynamic Locomotion for Gait Generation

Passive dynamic walking is the stable gait performed by an unactuated biped robot descending a moderate slope under the effect of the gravitational field only. The biped robot's dynamic parameters must be suitably chosen to realize such a stable gait. Firstly investigated in [17], this phenomenon emerges when an inelastic impact with the ground dissipates the increment of kinetic energy at the end of every single step, resetting the potential energy to its initial value. If both the robot and the environment meet particular geometrical and inertial conditions, the mechanical (total) energy of the biped is constant during each step, and thus the whole process evolves indefinitely. A limit-cycle represents such behavior in the phase plane of the robot state variables.

Since such a passive gait is naturally exhibited by the unactuated biped robot when the initial conditions are precisely on the associated limit cycle, adding a control action is useful for two reasons. One is the possibility to enlarge the basin of attraction of the passive (uncontrolled) gait. The other is the possibility to generate additional gaits to the original one exhibited without actuation. Therefore, studying passive dynamic walking can be the starting point to develop energy-saving control strategies.

This thesis focuses on a specific passive walker, the CBR which, despite its simple kinematic structure, exhibits a very complicated dynamic behavior due to the hybrid nature of the system [53]. An effective, but still poorly used, strategy to control the CBR is the energy shaping [54] which represents a dominant class of methodologies, belonging to the more general realm of passivity-based control approaches, able to exploit the intrinsic passive nature of such a type of systems. Most of the works proposed in the literature derive the control laws starting from a Lagrangian modeling framework. For example, a potential energy shaping finalized to make the biped's gait

slope invariant is applied in [18] using a particular technique called *controlled symmetries* (CS). A potential energy shaping is instead employed in [20] to regulate the biped's forward walking speed. The former cited works [18, 20] consider a fully actuated biped robot model. However, studies on the natural human gait show that the primary energy source for the forward motion comes from ankles and that an ankle-only actuation is more energetically efficient than a hip-only one and a fully actuated system. These biomechanical considerations are explained in [16], motivating a kinetic energy shaping control for an underactuated CBR which creates new walking gaits based on the *controlled Lagrangian* (CL) methodology [55, 56].

Starting from the port-Hamiltonian (pH) modeling framework, a similar result is achieved in [49] where the proposed control strategy is based on the interconnection and damping assignment passivity-based control (IDA-PBC) [9, 57], that is capable to generate robust gaits characterized by small step lengths and slow forward speed by shaping only kinetic energy. In particular, the methodology followed in [49], based on [58], requires that the open-loop inertia matrix does not depend on actuated generalized coordinates, forcing to perform a preliminary change of coordinates to get a suitable dynamic model. Other energy-efficient control approaches which exploit the pH framework are proposed in [59] for several walking robots.

Besides, a total energy shaping approach enlarges the basin of attraction of the limit cycle (making the gait more robust over uncertainties on the initial conditions), increases the rate of convergence, and is more effective in generating new gaits compared to those methodologies which shape only potential or kinetic energy.

2.3 IDA-PBC Approaches to Avoid the Solution of PDEs

As stated in Section 2.2, IDA-PBC can be profitably used to force new gaits during passive dynamic walking. The main drawback behind such control methodology is the solution of a set of PDEs, which is

instrumental to design the control law. This section presents some of the approaches proposed in the literature to avoid the solution of such PDEs.

IDA-PBC [9] is a nonlinear control methodology that is rooted in the pH framework of nonlinear systems. Differently from other nonlinear control strategies, IDA-PBC does not cancel nonlinear dynamics out but, conversely, it takes advantage of the nonlinear nature of the plant. IDA-PBC stabilizes a given plant at the desired equilibrium point by matching the original dynamics with desired ones. The desired total energy in the closed-loop must exhibit a minimum in such an equilibrium. The matching involves the solution of a set of PDEs, called matching equations, which represent the main bottleneck of the control design. These PDEs, which include plant dynamics and the desired closed-loop total energy, are parameterized by three matrices that are related to the interconnection between the subsystems, the damping, and the kernel of the input matrix, respectively. The role played by these matrices has several interpretations, as explained in [60]. Throughout the years, several strategies have addressed constructive procedures avoiding the solution of the PDEs [61], and they are distinguished by how the matching process is tackled. Referring to the taxonomy introduced in [60], the described methodology can be grouped into three main classes: *i)* non-parameterized IDA-PBC; *ii)* algebraic IDA-PBC; *iii)* parameterized IDA-PBC. The non-parameterized IDA-PBC represents the standard formulation proposed in [9]. In this case, the desired interconnection and the damping matrices are fixed, as well as the input matrix. The procedure leads to a set of PDEs defining the family of the proper desired total energy functions. A solution, having a minimum in the desired equilibrium, is selected among such a family. A constructive methodology based on a dynamic extension is provided in [62], exploiting the notion of the algebraic solution of the matching equations. The authors proposed to asymptotically stabilize an equilibrium point without involving the solution of any PDE by constructing an auxiliary energy function in an extended state-space. As firstly proposed in [54], the algebraic IDA-PBC fixes the desired energy function for the closed-loop. This choice transforms the matching equations

into algebraic ones with the interconnection matrix, the damping matrix, and the input mapping port as unknowns. This approach, which is inherently constructive and straightforward, is based on the exact knowledge of the desired energy function that, in turn, requires proper physical considerations that are not always easy to derive. The parameterized IDA-PBC fixes the structure (*i.e.*, the family) of the desired energy function. This is convenient in those physical systems which always exhibit the same structure of the total energy. An example is given by the mechanical systems whose desired energy function is the sum of a potential energy term, depending only on the generalized positions, and the kinetic energy, which is quadratic in the generalized momenta. According to [63], relatively to the class of underactuated two-degree-of-freedom (2-DoF) mechanical systems with underactuation degree one, such a parameterization yields to the decomposition of the original matching equations in two separate PDEs. The former is referred to as *kinetic energy matching equation* (KE-ME), and it depends on the generalized momenta; the latter is referred to as *potential energy matching equation* (PE-ME). Besides, such a parameterization introduces some degrees of freedom which are helpful for the solution of the PDEs. Several constructive solutions were presented for this methodology. For instance, the results presented in [58] show that if the original system's inertia matrix, as well as the forces induced by the potential energy, does not depend on the unactuated coordinates, and given a particular parameterization of the desired inertia matrix, then the KE-ME can be solved as an algebraic equation. Besides, the PE-ME admits a general solution, which is a given integral. Conversely, a solution that can be applied only to those systems having an inertia matrix depending exclusively on the unactuated coordinates, and endowing a constant sub-block matrix, is proposed in [11]. However, in this last case, the pH structure of a mechanical system in the closed-loop is not preserved. The recent methodology from [64] proposes a constructive solution for underactuated 2-DoF mechanical systems by relaxing some of the constraints imposed by the previous works. In particular, the plant's inertia matrix can depend on both the actuated and the unactuated variables. Such a procedure avoids the explicit

solution of the matching equations by parameterizing the desired inertia matrix. However, it introduces a singularity in the interconnection matrix depending on generalized momenta.

2.4 Locomotion Control Strategies Based on HZD

Energy shaping methodologies presented in Section 2.2, such as CS, CL, and IDA-PBC, have been originally developed to stabilize mechanical systems in absence of impacts. For such kind of a task, it is usually sufficient to achieve asymptotic convergence to the desired energy level to realize the sought goal. IDA-PBC guarantees that target dynamics are asymptotically stabilized at an equilibrium point corresponding to the minimum of the target Hamiltonian, for instance. As outlined in [12, 22], methods that stabilize a biped robot to a specific gait are those which construct a zero dynamics manifold. As clearly explained in [12, 65], reset maps that characterize hybrid systems push away solutions that do not lie in the zero dynamics manifold. Hence, the convergence of the continuous dynamics to the manifold must be sufficiently rapid to counteract such a repulsive behavior of the reset map. Energy shaping approaches presented in Section 2.2 neither construct a zero dynamics manifold nor guarantee exponential convergence of continuous dynamics to it. Hence they can stabilize the biped robot to neither a specific gait nor a target energy level (due to the presence of impacts), while they effectively generate new gaits.

The approaches that duly take into account the hybrid nature of the system should address closed-loop exponential stability [12]. Some of them ensure exponential convergence by exploiting the notion of hybrid zero dynamics (HZD) [66, 67, 68]. While these preliminary works were based on an input-output linearization, an approach based on a Lyapunov analysis was proposed in [65], where rapidly exponentially stabilizing control Lyapunov functions (RES-CLF) were used to make the output dynamics converge exponentially fast to the HZD manifold with a rate of convergence which can be modified by gain adjustments.

Later, the same framework was extended in [22] to achieve energy-shaping to increase the robustness of the passive gait of the CBR with respect to perturbations in initial conditions. Based on the HZD, but not relying on RES-CLF, the work in [69] proposed a passivity-based approach to keep the natural dynamics of the system and enhance the performance in terms of robustness and control effort minimization.

Chapter 3

Modelling

The underactuated mechanical systems addressed in this thesis have $n = 2$ degrees of freedom, $m = 1$ control inputs, no natural dissipation, constant input matrix, and continuous bounded elements of the inertia matrix. Such assumptions are reasonable and cover a very broad class of 2-DoF mechanical systems [70].

For the sake of generality, the sections of this chapter have been presented for n -DoF mechanical systems, apart from Section 3.1.1 and Section 3.2.4 which introduce the models of the test-bed used to evaluate the performance of the proposed control approaches.

3.1 Underactuated Mechanical Systems in the pH Framework

Consider an underactuated mechanical system with n degrees of freedom and $m = n - 1$ control inputs, let $q \in \mathbb{R}^n$ and $p \in \mathbb{R}^n$ be the vector of generalized coordinates and momenta, respectively.

The pH model of such system is

$$\begin{bmatrix} \dot{q} \\ \dot{p} \end{bmatrix} = \begin{bmatrix} 0_n & I_n \\ -I_n & 0_n \end{bmatrix} \begin{bmatrix} \frac{\partial H(q,p)}{\partial q} \\ \frac{\partial H(q,p)}{\partial p} \end{bmatrix} + \begin{bmatrix} 0_{n \times m} \\ G_p(q) \end{bmatrix} u(q,p), \quad (3.1)$$

with $I_n \in \mathbb{R}^{n \times n}$ and $0_n \in \mathbb{R}^{n \times n}$ the identity matrix and the zero matrix

of proper dimensions, respectively, $0_{n \times m} \in \mathbb{R}^{n \times m}$ the zero matrix of proper dimension, $G_p(q) \in \mathbb{R}^{n \times m}$ is the full rank matrix mapping the input, and $u(q, p) \in \mathbb{R}^m$ the control input.

The scalar function $H(q, p) \in \mathbb{R}$ is the Hamiltonian

$$H(q, p) = \frac{1}{2}p^T M^{-1}(q)p + V(q), \quad (3.2)$$

representing the total energy (kinetic plus potential) with $M(q) = M(q)^T > 0 \in \mathbb{R}^{n \times n}$ the symmetric and positive definite inertia matrix, $V(q) \in \mathbb{R}$ the potential energy.

Defined

$$J = \begin{bmatrix} O_n & I_n \\ -I_n & O_n \end{bmatrix} \quad (3.3)$$

such that $J = -J^T \in \mathbb{R}^{2n \times 2n}$, the skew-symmetric interconnection matrix mapping the principle of conservation of energy, the pH system (3.1) can be synthetically represented as

$$\dot{x} = J \nabla_x H(x) + G(x)u(x) \quad (3.4)$$

where $x = [q^T \ p^T]^T$ is the state vector, $\nabla_x H(x) = [\nabla_q H(x) \ \nabla_p H(x)]^T = [\partial H(x)/\partial q \ \partial H(x)/\partial p]^T$ is the Hamiltonian gradient vector, and $G(x) = [0_{m \times n} \ G_p^T(q)]^T$ is the input port.

The rationale behind the use of formulation (3.4) is its easiness to be rewritten in the zero dynamics formulation, which is instrumental to developing HZD-based methodologies to control a planar biped robot, as will be shown in Section 3.2.3.

3.1.1 The TORA System

The TORA is an underactuated 2-DoF mechanical system firstly studied in [71] and commonly employed in the literature as a benchmark for several nonlinear control systems designs addressing underactuation.

In the literature, the model of the TORA system through the pH formalism and the use of the standard IDA-PBC approach is proposed

in [72], where a constant closed-loop mass matrix reduces the complexity of the matching equations related to the kinetic energy. A dynamic extension is proposed in [73] to asymptotically stabilize the system with only position measurements. The procedure to address this goal is to shape the potential energy only, equating the open and the closed-loop inertia matrices, canceling the assigned interconnection matrix to get rid of the kinetic energy PDEs, and then the resulting controller is independent of the velocity measurements because they are not present in the potential energy. Besides, in the literature, the TORA system is used as an example to test different feedback-stabilizing controllers [74]. Several controllers based on cascade (linear cascade control, integrator backstepping) and passivity (feedback passivation, passivation without cancellation) paradigms can be used to asymptotically stabilize the system. The former class leads to algorithms requiring full state feedback linearization and nonlinearities cancellation, while the latter class, for input-output passive systems with relative degree one and weakly minimum-phase, leads to controllers with a reduced set of measurements and no cancellations. A Lagrangian-based change of coordinates along with a partial feedback linearization to reshape the system as a nonlinear cascade system in a strict feedback form is addressed in [75]. The global asymptotic stability is then achieved via a backstepping procedure. An experimental output regulation for the TORA system is performed in [76], while a piecewise multi-linear model is considered in [77]. Finally, fuzzy-based controls are proposed in [78, 79].

The TORA consists of a translational oscillating cart with mass $m_2 > 0$ that is controlled via a rotational eccentric mass, here schematized by a pendulum with mass $m_1 > 0$, radius $r > 0$, inertia $I = m_1 r^2$, and a rigid link to the cart of length $l > 0$. The (actuated) variable $q_1(t)$ denotes the angle of the mass m_1 with respect to the vertical, while the displacement of the cart with mass m_2 is denoted by the (unactuated) variable $q_2(t)$. The relative generalized momenta are identified by p_1 and p_2 , respectively. The cart is forced to oscillate in the horizontal plane by a spring with elastic coefficient $k > 0$. The actuated eccentric mass damps the horizontal oscillations of the platform. The TORA is

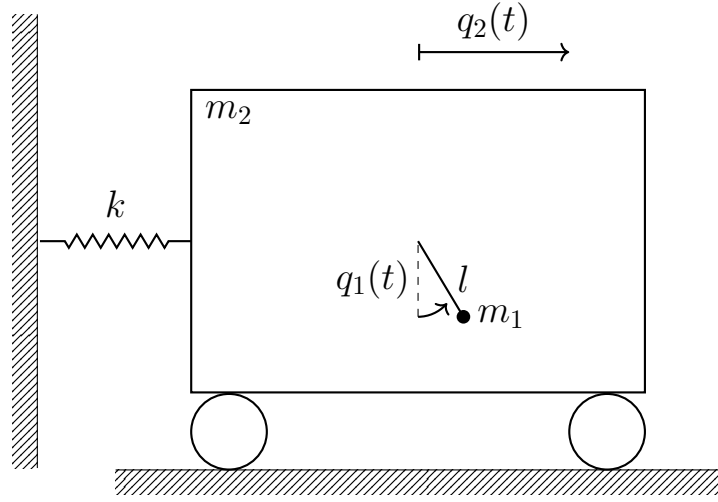


Figure 3.1: Scheme of a translational oscillator with a rotational actuator (TORA) system.

illustrated in Figure 3.1.

The pH model of the TORA system is given by (3.1) with the elements of $M(q)$ given below

$$b_{11} = m_1 l^2 + I, b_{12}(q) = m_1 l \cos(q_1), b_{22} = m_1 + m_2. \quad (3.5)$$

The Hamiltonian function $H(q)$ for the TORA is (3.2), with

$$V(q) = \frac{1}{2} k q_2^2 + m_1 l g (1 - \cos(q_1)). \quad (3.6)$$

3.2 Hybrid Mechanical Systems

The continuous pH system (3.4) can be more generally rewritten as

$$\dot{x} = f(x) + g(x)u(x), \quad (3.7)$$

with

$$f(x) = J(x)\nabla H(x), \quad g(x) = G(x). \quad (3.8)$$

If the system undergoes impacts, its dynamics can be exhaustively described by

$$\Sigma = \begin{cases} \dot{x} = f(x) + g(x)u(x) & x \in X \setminus S \\ x^+ = \Delta(x^-) & x^- \in S \end{cases} \quad (3.9)$$

which represents a hybrid mechanical system, where $x \in X$ is the state, x^- and x^+ indicate the states just before and just after the impact event, respectively, $X \subseteq \mathbb{R}^{2n}$ is the admissibility domain of continuous dynamics with cardinality $2n$, $f(x) \in X$ is the C^1 vector field describing continuous dynamics, $g(x) \in X$ is the C^1 vector field mapping the control input $u(x)$ in the continuous dynamics, S is the switching surface, and $\Delta(x^-) \in X$ is the C^1 reset map.

$J(x)$ in (3.8) has been expressed in a general form intentionally, without assuming any particular structure for it. With such a choice, it can represent the interconnection matrix of both uncontrolled (3.3) and controlled (A.4) mechanical systems, as long as the latter ones preserve the principle of conservation of energy characterizing uncontrolled systems. This can be achieved using an energy shaping control action, carried out by IDA-PBC, for instance. Such a general structure enables the application of EPD-PBC to enlarge the basin of attraction of a passive gait, as well as, of a gait created via energy shaping, combining EPD-PBC with IDA-PBC as will be shown in Section 7.4.2, for instance. Albeit (A.4) is the interconnection matrix of a 2-DoF controlled mechanical system, the above considerations have general validity. Hence they hold for controlled mechanical systems of any dimension.

3.2.1 Planar Biped Robots

Biped robots are hybrid, mechanical systems which can be profitably described using (3.9). Their dynamics can be usefully partitioned in swing phases and impact events.

Swing Phase

As outlined in [12, Section 3.2], the nature of the foot-ground interface determines the number of independently actuated joints and, in turn, whether the dynamic model of the biped robot is fully actuated or underactuated. If the biped has all the joints independently actuated, including the ankle, and moves using flat feet, hence its model is fully actuated whereas feet which are not flat on the ground, *i.e.*, feet which rotate, necessarily lead to underactuation [12, Section 3.3]. Biped robots with rotating point feet, the CBR for instance, belong to the class of underactuated mechanical systems [12, Section 3.4]. During the swing phase, the stance leg is continuously in contact with the ground, behaving like a pivot. Zero control torque is applied at the stance ankle. The other one, the swing leg, moves freely in the air. Therefore, the interaction between the stance foot and the ground is uncontrolled, yielding to one degree of underactuation in the related model. No double-support phase is admitted, *i.e.*, only one leg at a time is in contact with the ground and, when left and right legs exchange their roles at the impact, the double support phase is only instantaneous.

Continuous dynamics are usually modeled through Lagrangian formalism. Nevertheless, in this thesis, swing dynamics are modeled through the pH formalism, as in (3.4). This choice is motivated by the relationship connecting conservation of mechanical energy and dynamics, especially in passive dynamic locomotion, which has given room to plenty of energy shaping control methodologies well suited for underactuated mechanical systems.

The following hypotheses about the robot model, during swing phase, are assumed throughout this thesis:

- RH.1** the robot constitutes a single open kinematic chain made by n rigid links, connected by $n - 1$ rigid and frictionless revolute joints;
- RH.2** the robot is planar, *i.e.*, its motion is constrained to the sagittal plane only;

- RH.3** the robot is biped with symmetric legs which are connected at a common point which is the hip, and are terminated in points (no flat foot assumed);
- RH.4** the torque applied at stance foot is zero, thus the robot is underactuated with one degree of underactuation.

Impact Event

Let $y_{sw}(q) \in \mathbb{R}$ be a scalar function mapping the vertical distance between the tip of the swing leg and the walking surface. Swing phase continues as long as $y_{sw}(q) > 0$, meaning that dynamics (3.7) is followed until swing leg does not land. When $y_{sw}(q) = 0$ and $\dot{y}_{sw}(q) < 0$, an impact between the swing leg and the ground occurs. If the impact is assumed to be rigid, *i.e.*, a perfectly inelastic contact occurs, without nor slipping or rebound between the hitting foot and the ground, then the effect of the impact event on the state of the system can be reasonably approximated as a discontinuous variation in generalized velocities, which undergo a jump. On the other hand, there is no effect on generalized coordinates which do not change (apart from a relabelling procedure due to the left-right symmetry of the gait).

Therefore, if the following hypothesis on an impact event hold:

- IH.1** an impact between the swing leg and the ground is instantaneous, *i.e.*, double support phase is instantaneous;
- IH.2** an impact does not give rise to neither slipping nor rebounds of the swing leg;
- IH.3** an impact is regarded as an impulsive force;
- IH.4** an instantaneous change in generalized velocities arises at the impact while the configuration variables remains unchanged.

Then, the dynamics of the biped robot, during an impact event, are described by

$$(q^+, \dot{q}^+) = \Delta(q^-, \dot{q}^-) \quad (3.10)$$

which relates coordinates and conjugated velocities just before the impact, (q^-, \dot{q}^-) , with those just after it, (q^+, \dot{q}^+) , on the basis of the law of conservation of angular momentum. Last equation leads to

$$(x^+, \dot{x}^+) = \Delta(x^-, \dot{x}^-). \quad (3.11)$$

since a discontinuous change in generalized velocities implies a proportional variation in generalized momenta, due to the constancy of the inertia matrix at the impact.

Subsequently, it is possible to define the switching surface as

$$S = \{x \in X | y_{sw}(x) = 0, \dot{y}(x)_{sw} < 0\}. \quad (3.12)$$

3.2.2 Periodic Walking for Passive Biped

In many practical applications, the biped is required to walk with a periodic gait, during running for instance. Moreover, a steady-state stable, periodic walking is exhibited by passive bipeds without any control action, under the effects of gravity only. Such kind of walking is known as *passive-dynamic walking* [17]. Such passive periodic motion, that, for sake of brevity, will be referred to as *passive gait* in this thesis, arises when some geometric, as well as, inertial conditions are met. Besides, initial conditions must fall inside the basin of attraction of the *passive limit* cycle, which is the representation of natural gait in the robot's state space [53]. When dealing with periodic walking, a step is defined as two consecutive foot-ground impacts [53, 16, 49]. Then, two parameters characterize the gaits of a passive biped: the space covered on the slope by each step, that is referred to as *step length* S , and its duration, *i.e.*, the time between two consecutive foot-ground impacts, which is referred to as *step period* T . For this specific class of walkers, the control problem reduces to two alternatives:

- 1) make the robot walking with a periodic gait that differs from the natural one;
- 2) enlarge the basin of attraction of the limit cycle, *i.e.*, make the robot walking with a periodic gait that has the same features (in

terms of step length and step period, for instance) as the passive one but which is more robust concerning uncertainties over initial conditions.

The first problem is addressed by two different tasks, namely *gait generation* and *gait stabilization* (usually referred to as *orbital stabilization*). If there is no preliminary assumption on the new gaits, the control problem can be recast as gait generation. Gait generation leads to stable periodic gaits, unexhibited by the uncontrolled biped, by changing the energy of the passive walker, *i.e.*, by changing the way the robot and the ground interact. Methods currently existing for gait generation do not have an intrinsic concept of stabilization to a specific gait through gain adjustment [49, 18, 20, 16], hence their design does not rely on the whole hybrid model presented in (3.9) but only on the continuous part. Conversely, if the new gait has some sought features, such as desired S , T , and H , for instance, the gait design has to explicitly deal with impacts occurring at swing-foot landing. In such situations, the control problem is recast as gait stabilization. Gait stabilization assumes the desired orbit that is associated with a specific gait, with target characteristics, usually different from those of the natural gait.

The second problem is addressed by *gait robustification*, which requires stabilizing the passive orbit while making it more robust compared to uncertainties on initial conditions. This is equivalent to enlarge the basin of attraction of the related limit-cycle which, for passive bipeds, is narrow. In both cases, the sought periodic orbit, to which stabilize the system at, has to be defined.

Given a finite time $T \in \mathbb{R} > 0$ such that $x(t) = x(t + T)$ is a periodic solution of the swing dynamics in (3.7), a periodic orbit is a set $O \subset X$ such that

$$O = \{x \in X | x(t) = x(t + T)\}. \quad (3.13)$$

When dealing with hybrid systems with impulsive effects, there is an additional difficulty represented by the presence of the impact map. In other words, the gait has to be periodic even if the swing leg hits the

ground. Gait stabilization and gait robustification are the processes of designing a control strategy that renders a given periodic orbit O (a new one or the passive one) stable during both swing phase and impacts.

In this thesis, gait generation and gait robustification will be faced, while the gait stabilization is left as future work.

3.2.3 The Hybrid Zero Dynamics Concept

Although gait generation does not explicitly take into account the hybrid nature of walking during control synthesis, stabilization either to a specific periodic orbit or to a target energy level does. To simplify the solution of the task, a common approach is to tackle it in a lower-dimensional space which is invariant under both the vector field $f(x)$ and the reset map $\Delta(x)$. Such low-dimensional manifold is usually taken as a submanifold, called Z , of the domain of admissibility X . Defined $T_x Z$ as the tangent space of the submanifold Z at the point x , Z is

- 1) *forward invariant* if $f(x) \in T_x Z \forall x \in Z$;
- 2) *impact invariant* if $\Delta(x) \in Z \forall x \in S \cap Z$;
- 3) *hybrid invariant* if it is both forward invariant and impact invariant.

Hybrid invariance ensures that a sought periodic motion preserves its stability properties even in presence of impulsive forces exerted when the swing leg hits the walking surface. In other words, the stabilization of a periodic orbit of a hybrid mechanical system reduces to find a control strategy which creates a hybrid invariant manifold $Z \subset X$ containing the desired orbit O among its solutions, and then to stabilize such orbit. To find a suitable submanifold Z and the related dynamics which are invariant under continuous dynamics only, it is possible to exploit the notion of *maximal internal dynamics which are compatible with the output being identically zero*, also known as *zero dynamics*,

firstly introduced in [80]. The creation of a zero dynamics submanifold usually depends on the imposition of a set of *virtual constraints* on the output variables [12].

Continuous system (3.7) can be rewritten in a formulation that is compatible with zero dynamics. There are several ways to accomplish such a task, each one depending on the particular choice of the output variables [22, 65]. In this thesis, a transformation similar to the one proposed in [22] is exploited. The sought zero-dynamics formulation of (3.7) is

$$\begin{cases} \dot{x} = f(x) + g(x)u(x, e) & (x, e) \in X \setminus S, \\ \dot{e} = r(x) + w(x)u(x, e) & (x, e) \in X \setminus S. \end{cases} \quad (3.14)$$

In this context, e is referred to as the output variable. In [22] e depends on the energy of (3.7) as it does in this thesis, as will be clearly shown in Section 7. On the other hand, x variables are the zero dynamics ones. The output can be generally defined as a function of the zero dynamics variables such that

$$e|_O = 0, \quad (3.15)$$

that is, assumed that output variables are defined as virtual constraints, such constraints are asymptotically (exponentially, if the system is hybrid) realized on the orbit O . The zero dynamics submanifold, according to [80], is the restricted subset $Z \subset X$ defined as

$$Z = \{x \in X | e = 0\}. \quad (3.16)$$

Additionally, if $\dot{e} = 0$, then the zero dynamics submanifold Z is forward invariant, *i.e.*, it is invariant under the swing dynamics,

$$Z = \{x \in X | e = 0, \dot{e} = 0\}. \quad (3.17)$$

The zero dynamics manifold Z defined as in (3.17) is only forward invariant. To achieve invariance under both continuous and discrete dynamics, the concept of *hybrid zero dynamics* has been developed in [66], which represents the extension of the concept of maximal internal

dynamics compatible with the output being identically zero to the class of hybrid systems with impulse effects. According to (3.14), the zero dynamics formulation of (3.9) is

$$\Sigma_{zd} = \begin{cases} \dot{x} = f(x) + g(x)u(x, e) & (x, e) \in X \setminus S, \\ \dot{e} = r(x) + w(x)u(x, e) & (x, e) \in X \setminus S, \\ x^+ = \Delta(x^-) & (x^-, e^-) \in S, \\ e^+ = \Delta(e^-) & (x^-, e^-) \in S, \end{cases} \quad (3.18)$$

besides, $f(x)$, $r(x)$, $g(x)$, and $w(x)$ are assumed to be locally Lipschitz continuous functions.

Then, the control problem reduces to solve two lower dimensional ones:

- 1) establish the stability of an orbit contained in the hybrid zero dynamics submanifold;
- 2) ensure the exponential convergence of the output variables to the hybrid zero dynamics submanifold.

There are several approaches to face this problem, ranging from those based on input-output linearization [66, 67] to those based on control Lyapunov functions [22, 65] and passivity-based control [69]. All these methodologies share the same overall architecture, based on the two-steps approach discussed before, as well as, the requirement that output dynamics converge exponentially fast to the hybrid zero dynamics submanifold. As explained in [12, 65], the impact map has an expansive behavior that rejects output dynamics from converging to the hybrid zero dynamics submanifold. To overcome the resulting divergence, such submanifold, in particular the orbit contained in it, must be sufficiently fast-attracting, hence exponential convergence is required. Besides, if the addressed biped is planar, it is sufficient to guarantee exponential convergence of output dynamics to Z and make it hybrid invariant, that is invariant under both swing dynamics and foot-strikes [67, 68]. If exponential convergence of output dynamics is

guaranteed, hence hybrid invariance follows from nominal virtual constraints vanishing along the orbit [12]. Indeed, for 2D biped models with one degree of underactuation, no compliance, and a rigid impact map, it is showed in [67] that any forward invariant manifold Z , containing a periodic orbit O , is also impact invariant and hence hybrid invariant. In particular, as demonstrated in [67, Theorems 5.2, 6.2], this result holds if the hypotheses on the robot model, as well as, those on both the gait nature and the impact model are assumed. On the other hand, this result does not hold for 3D biped models, for which is necessary to extend (3.18) using a *hybrid deadbeat extension*, as outlined in [12, 68].

3.2.4 The CBR

The compass-like biped robot (CBR) is a 2-DoF, planar, and bipedal walking robot belonging to the class of passive walkers, which satisfies the hypothesis on the robot model, as well as, those on the impact event, **RH.1-RH.4** and **IH.1-IH.4**, respectively. In particular, the CBR consists of two legs joined by the hip of mass $m_H > 0$. Each leg has mass $m > 0$ and length $l = a + b$, where $a > 0$ is the length of the legs between m and the feet while $b > 0$ is the length of the legs between m_H and m , supposing both m_H and m to be point masses. A representation of such a biped robot is depicted in Figure 3.2, where q_1 is the angle between the vertical relative to the ground and the stance leg while q_2 is the angle between the vertical relative to the ground and the swing leg. The conjugated momenta are denoted by p_1 and p_2 , respectively.

The behavior of the CBR consists of two distinct phases. The swing phase of the CBR is described by (A.1) with the elements of the inertia matrix $M(q)$ as

$$\begin{aligned} b_{11} &= (m_H + m)l^2 + ma^2, \\ b_{12}(q) &= -mlb \cos(q_1 - q_2), \\ b_{22} &= mb^2, \end{aligned} \tag{3.19}$$

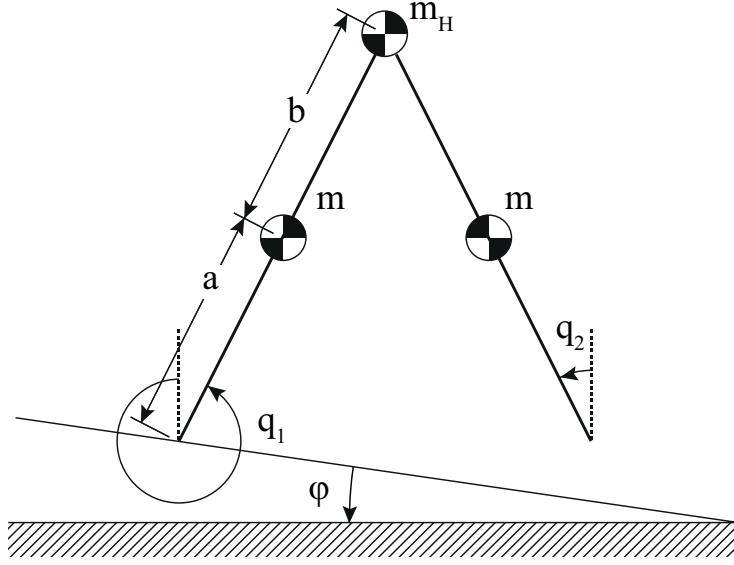


Figure 3.2: Scheme of a compass-like biped robot (CBR).

with $H(q)$ as in (3.2), where

$$V(q) = (m(a + l) + m_H l)g \cos(q_1) - mbg \cos(q_2) \quad (3.20)$$

with $g \simeq 9.81 \text{ m/s}^2$ the gravity acceleration. The impact phase is described by (3.11). An impact occurs when the conditions

$$\begin{aligned} y_{sw}(q) &= l[\cos(q_1 + \varphi) - \cos(q_2 + \varphi)] = 0, \\ \dot{y}_{sw}(q) &= l[\sin(q_2 + \varphi)\dot{q}_2 - \sin(q_1 + \varphi)\dot{q}_1] < 0, \end{aligned} \quad (3.21)$$

hold. The change in generalized velocities, assuming true **IH.1-IH.4**, is described by

$$\dot{q}(t^+) = P(q(t^-))\dot{q}(t^-), \quad (3.22)$$

where $\dot{q} = [\dot{q}_1 \ \dot{q}_2]^T \in \mathbb{R}^2$ is the velocity vector, while the time instants just before and just after the impact are given by t^- and t^+ , respectively. From now on $q^\pm = q(t^\pm)$ as well $\dot{q}^\pm = \dot{q}(t^\pm)$ to ease the notation. The conservation of angular momentum law is used to derive the expression of the matrix $P(q^-) \in \mathbb{R}^{2 \times 2}$, which is

$$P(q^-) = \begin{bmatrix} p_{11}^+ & p_{12}^+ \\ p_{21}^+ & p_{22}^+ \end{bmatrix}^{-1} \begin{bmatrix} p_{11}^- & p_{12}^- \\ p_{21}^- & p_{22}^- \end{bmatrix}, \quad (3.23)$$

with

$$\begin{aligned}
p_{11}^+ &= ml(l - b \cos(q_1^- - q_2^-)) + ma^2 + m_H l^2, \\
p_{12}^+ &= mb(b - l \cos(q_1^- - q_2^-)), \\
p_{21}^+ &= -mb l (\cos(q_1^- - q_2^-)), \\
p_{22}^+ &= mb^2, \\
p_{11}^- &= -mab + (m_H l^2 + 2mal) \cos(q_1^- - q_2^-), \\
p_{12}^- &= p_{21}^- = -mab, \\
p_{22}^- &= 0.
\end{aligned} \tag{3.24}$$

Since the CBR exhibits a gait with left-right symmetry, at each impact the angles are swapped and relabelled (*i.e.*, when an impact occurs, the former swing leg becomes the stance one and vice-versa). Hence, these angles are not associated with a physical leg, but they are referred to as the action played by the leg during the gait. This procedure is taken into account via the matrix

$$R = \begin{bmatrix} 0 & 1 \\ 1 & 0 \end{bmatrix} \tag{3.25}$$

which results in

$$q^+ = Rq^- \tag{3.26}$$

at each impact. The interested reader can refer to the work in [53] for further details. It must be underscored that such kind of robot is not physically realizable due to the scuffing between the nonsupport foot and the the ground. In real prototypes foot scuffing is avoided by particular mechanical designs, as the one proposed in [81], whereas in this paper it is avoided by ignoring (3.21) whenever the nonsupport leg is behind the support one [16].

A summary of the TORA and CBR models, with their equations fully and explicitly written, is incorporated in Table 3.1 to simplify the reading of next sections.

Table 3.1: Models of the systems deployed in this thesis to test the proposed control strategies.

system	model
TORA	$\begin{bmatrix} \dot{q} \\ \dot{p} \end{bmatrix} = \begin{bmatrix} 0_2 & I_2 \\ -I_2 & 0_2 \end{bmatrix} \begin{bmatrix} \frac{\partial H(q,p)}{\partial q} \\ \frac{\partial H(q,p)}{\partial p} \end{bmatrix} + \begin{bmatrix} 0_{n \times m} \\ G_p(q) \end{bmatrix} u(q,p)$ $H(q,p) = \frac{1}{2} p^T \begin{bmatrix} b_{11} & b_{12}(q) \\ b_{12}(q) & b_{22} \end{bmatrix} p + V(q)$ $b_{11} = m_1 l^2 + I, b_{12}(q) = m_1 l \cos(q_1), b_{22} = m_1 + m_2$ $V(q) = \frac{1}{2} k q_2^2 + m_1 l g (1 - \cos(q_1))$
CBR	$\begin{cases} \begin{bmatrix} \dot{q} \\ \dot{p} \end{bmatrix} = \begin{bmatrix} 0_2 & I_2 \\ -I_2 & 0_2 \end{bmatrix} \begin{bmatrix} \frac{\partial H(q,p)}{\partial q} \\ \frac{\partial H(q,p)}{\partial p} \end{bmatrix} + \begin{bmatrix} 0_{n \times m} \\ G_p(q) \end{bmatrix} u(q,p) & (q,p) \in X \setminus S \\ q^+ = R q^- & q^- \in S \\ \dot{q}^+ = P(q^-) \dot{q}^- & (q^-, \dot{q}^-) \in S \end{cases}$ $H(q,p) = \frac{1}{2} p^T \begin{bmatrix} b_{11} & b_{12}(q) \\ b_{12}(q) & b_{22} \end{bmatrix} p + V(q)$ $b_{11} = (m_H + m) l^2 + m a^2, b_{12}(q) = -m l b \cos(q_1 - q_2), b_{22} = m b^2$ $V(q) = (m(a+l) + m_H l) g \cos(q_1) - m b g \cos(q_2)$ $R = \begin{bmatrix} 0 & 1 \\ 1 & 0 \end{bmatrix}$ $P(q(t^-)) = \begin{bmatrix} p_{11}^+ & p_{12}^+ \\ p_{21}^+ & p_{22}^+ \end{bmatrix}^{-1} \begin{bmatrix} p_{11}^- & p_{12}^- \\ p_{21}^- & p_{22}^- \end{bmatrix}$ $p_{11}^+ = m l (l - b \cos(q_1^- - q_2^-)) + m a^2 + m_H l^2$ $p_{12}^+ = m b (b - l \cos(q_1^- - q_2^-))$ $p_{21}^+ = -m b l (\cos(q_1^- - q_2^-))$ $p_{22}^+ = m b^2$ $p_{11}^- = -m a b + (m_H l^2 + 2 m a l) \cos(q_1^- - q_2^-)$ $p_{12}^- = p_{21}^- = -m a b$ $p_{22}^- = 0$

Chapter 4

IDA-PBC with Explicit Solution of PDEs

Remark. Refer to Appendix A.1 for details about the IDA-PBC methodology for 2-DoF mechanical systems, as well as, for the standard procedure to solve matching equations.

4.1 A Mixed Parameterized-Algebraic IDA-PBC Approach

The key idea of the methodology presented in [1] is to combine the advantages of the parameterized IDA-PBC and the algebraic IDA-PBC. After giving a suitable parameterization for $M_d(q)$ complying with **C.1**¹, it is possible to retrieve a family for the desired potential energy $V_d(q)$ in which impose the condition **C.2**. For the considered 2-DoF mechanical systems, to comply with **C.3**, the interconnection matrix can be uniquely defined as

$$J_2 = \begin{bmatrix} 0 & j_2(q, p) \\ -j_2(q, p) & 0 \end{bmatrix}, \quad (4.1)$$

¹Conditions **C.1**, **C.2**, and **C.3** are listed in Appendix A.1

where $j_2(q, p) : \mathbb{R}^2 \times \mathbb{R}^2 \rightarrow \mathbb{R}$ is a scalar function. Having at disposition both $M_d(q)$ and $V_d(q)$, as for the algebraic IDA-PBC, the KE-ME becomes an algebraic equation in $j_2(q, p)$

$$\begin{aligned} G_p^\perp \nabla_q (p^T M^{-1}(q)p) - G_p^\perp M_d(q) M^{-1}(q) \nabla_q (p^T M_d^{-1}(q)p) \\ - 2j_2(q, p) G_p^T M_d^{-1} p = 0, \end{aligned} \quad (4.2)$$

whose solution is given by

$$j_2(q, p) = \frac{G_p^\perp (\nabla_q (p^T M^{-1}(q)p) - M_d(q) M(q)^{-1} \nabla_q (p^T M_d^{-1}(q)p))}{2G_p^T M_d^{-1}(q)p}. \quad (4.3)$$

Define $G_p = [1 \ 0]^T$ and, as a consequence, $G_p^\perp = [0 \ 1]$. This particular choice, which does not affect in any way the generality of the methodology, holds true throughout whole Chapters 4, 5, and 6. Solution (4.3) exhibits a singularity in the generalized momenta p

$$\begin{aligned} G_p^T M_d^{-1}(q)p = 0 &\Rightarrow \\ [1 \ 0] \begin{bmatrix} m_{d22}(q) & -m_{d12}(q) \\ -m_{d12}(q) & m_{d11}(q) \end{bmatrix} \begin{bmatrix} p_1 \\ p_2 \end{bmatrix} = 0 &\quad (4.4) \\ \iff (m_{d22}(q)p_1 - m_{d12}(q)p_2) = 0. & \end{aligned}$$

Hence, the singularity appears when either $m_{d22}(q)p_1 = m_{d12}(q)p_2$ or the system is at the equilibrium, $p^* = 0_2$. The former condition is not predictable a priori. The latter is a consequence of the detectability-like condition required to guarantee the asymptotic stability of the closed-loop equilibrium when (A.11) is introduced in the control action. Such a condition requires that the passive output $y_d = G_p^T M_d^{-1}(q)p$, which is exactly the denominator of (4.3), nullifies at the equilibrium. This singularity due to the generalized momenta p is a problem for mechanical systems and it is present in many works [64, 82]. In these papers, the problem was worked around either numerically or with an ad-hoc solution for the peculiar addressed case study. In [64], an analysis on the order of the various terms appearing in (4.3) is carried out. Despite the

numerator of (4.3) tends toward zero faster than the denominator, due to the quadratic dependence on p exhibited by the first, the same analysis cannot address the singularity condition $m_{d22}(q)p_1 = m_{d12}(q)p_2$ because it arises far from the equilibrium $p = 0$. Hence, a different approach to remove it is required. In the next section, it will be shown how the methodology proposed in [1] can remove such a singularity in p structurally. Notice that further fractional functions may be introduced within (4.3) from the choice of $M_d(q)$: singularities in the generalized coordinates q must be managed during the design of the target inertia matrix.

4.2 Constructive Methodology

In this section, with a little abuse of notation, it will also be highlighted the dependency on some parameters to be tuned. Besides, in the following, given a generic function $f(q)$, the notation $f([q_a \ q_b])$ means that the variable q_1 is substituted by q_a and the variable q_2 is substituted by q_b , respectively.

As explained before, the key idea is to combine the advantages of both the parameterized IDA-PBC and the algebraic IDA-PBC, solving each singularity issue. Hence, the resulting approach provides an explicit solution of the PE-ME and requires to solve the KE-ME as an algebraic equation, just like the algebraic IDA-PBC does, without assigning the exact values of $M_d(q)$ and $V_d(q)$, in the spirit of the parameterized IDA-PBC, and without introducing any singularity in $j_2(q, p)$. As expressed in [64], the starting point is the parameterization of the desired inertia matrix in (A.3) as

$$\begin{aligned} M_d(q, c_1) &= \begin{bmatrix} m_{d11}(q, c_1) & m_{d12}(q, c_1) \\ m_{d12}(q, c_1) & m_{d22}(q, c_1) \end{bmatrix} \\ &= \Delta(q) \begin{bmatrix} a_{11}(q, c_1) & a_{12}(q, c_1) \\ a_{12}(q, c_1) & a_{22}(q, c_1) \end{bmatrix} \end{aligned} \quad (4.5)$$

where

$$\Delta(q) = b_{11}(q)b_{22}(q) - b_{12}(q)^2, \quad (4.6)$$

is the determinant of $M(q)$, $c_1 \in \mathbb{R}^{n_{c_1}}$ is a set of gains useful to design the controller, with $n_{c_1} > 0$, and $a_{ij}(q, c_1) \in \mathbb{R}$ are scalar functions to be defined and related to $M_d(q, c_1)$. Under this parameterization, the PE-ME (A.9) becomes

$$G_p^\perp (\nabla_q V(q) - \Gamma(q, c_1) \nabla_q V_d(q, c_2)) = 0, \quad (4.7)$$

with $c_2 \in \mathbb{R}^{n_{c_2}}$ a set of gains useful to design the controller, with $n_{c_2} > 0$, and

$$\Gamma(q, c_1) = M_d(q, c_1) M(q)^{-1} = \begin{bmatrix} \Gamma_{11}(q, c_1) & \Gamma_{12}(q, c_1) \\ \Gamma_{21}(q, c_1) & \Gamma_{22}(q, c_1) \end{bmatrix} \quad (4.8)$$

where

$$\begin{aligned} \Gamma_{11}(q, c_1) &= a_{11}(q, c_1)b_{22}(q) - a_{12}(q, c_1)b_{12}(q), \\ \Gamma_{12}(q, c_1) &= a_{12}(q, c_1)b_{11}(q) - a_{11}(q, c_1)b_{12}(q), \\ \Gamma_{21}(q, c_1) &= a_{12}(q, c_1)b_{22}(q) - a_{22}(q, c_1)b_{12}(q), \\ \Gamma_{22}(q, c_1) &= a_{22}(q, c_1)b_{11}(q) - a_{12}(q, c_1)b_{12}(q). \end{aligned}$$

The key of the approach is to introduce a scalar function $\gamma(q, c_1) \in \mathbb{R}$ that parameterizes the second row of $\Gamma(q, c_1)$ as

$$a_{22}(q, c_1)b_{12}(q) - a_{12}(q, c_1)b_{22}(q) = k_1\gamma(q, c_1), \quad (4.9a)$$

$$a_{12}(q, c_1)b_{12}(q) - a_{22}(q, c_1)b_{11}(q) = k_2\gamma(q, c_1), \quad (4.9b)$$

with $k_1, k_2 \in \mathbb{R}$ and $k_1 \neq 0$. The specific case with $k_1 = 0$ and $k_2 \neq 0$ is presented in the next subsection. Such a choice simplifies (4.7) as

$$\nabla_{q_2} V(q) + \gamma(q, c_1)(k_1 \nabla_{q_1} V_d(q, c_2) + k_2 \nabla_{q_2} V_d(q, c_2)) = 0, \quad (4.10)$$

which is a linear PDE, hence a modified version of Frobenius Theorem can be invoked to claim existence of solutions (for the sake of brevity, this analysis will be omitted from this thesis). As shown in [64], an

explicit solution of (4.10) is

$$V_d(q, c_2) = - \int_1^{q_1} \frac{\nabla_{q_2} V \left(\left[\sigma \frac{k_1 q_2 - k_2 q_1 + k_2 \sigma}{k_1} \right] \right)}{k_1 \gamma \left(\left[\sigma \frac{k_1 q_2 - k_2 q_1 + k_2 \sigma}{k_1} \right] \right)} d\sigma \quad (4.11)$$

$$+ f_1 \left(\frac{k_1 q_2 - k_2 q_1}{k_1}, c_2 \right),$$

with $f_1(\cdot, \cdot) \in \mathbb{R}$ any scalar function of its arguments.

Indeed, the PDE (4.10) admits an explicit solution provided that a right $\gamma(q, c_1)$ is found to: (i) guarantee a closed-form solution for the integral in (4.11); (ii) shape $V_d(q, c_2)$ such as to comply with **C.2**; and (iii) avoid the singularity in the interconnection matrix. The fulfillment of the first requirement is explained in Appendix B.1. Concerning the second requirement, the degrees of freedom given by $f_1(\cdot, \cdot)$ and $\gamma(q, c_1)$ may help in satisfying **C.2** as well as to avoid singularities in the generalized coordinates q . Otherwise, other choices for $\gamma(q, c_1)$ must be done. The fulfillment of the last requirement is addressed in the following. For the moment, consider that the $V_d(q, c_2)$ is found. Then, the desired inertia matrix can be computed through (4.5) and (4.9). In particular, it is possible to retrieve the scalar functions $a_{12}(q, c_1)$ and $a_{22}(q, c_1)$ as

$$a_{12}(q, c_1) = - \frac{k_1 \gamma(q, c_1) b_{11}(q) + k_2 \gamma(q, c_1) b_{12}(q)}{\Delta(q)}, \quad (4.12a)$$

$$a_{22}(q, c_1) = - \frac{k_1 \gamma(q, c_1) b_{12}(q) + k_2 \gamma(q, c_1) b_{22}(q)}{\Delta(q)}, \quad (4.12b)$$

while $a_{11}(q, c_1)$ is left free such as to satisfy **C.1**. If it is not possible to find a desired inertia matrix which matches the criteria expressed by **C.1**, it is then necessary to design again the set of gains c_1 , as well as, the scalar function $f_1(\cdot, \cdot)$, and eventually $\gamma(q, c_1)$, until both **C.1** and **C.2** are simultaneously met. Once that $M_d(q, c_1)$ and $V_d(q, c_2)$ are found, the KE-ME (4.2) is an algebraic equation with

$j_2(q, p)$ as unknown and whose solution is (4.3). However, as said, the solution (4.3) suffers of a singularity problem. To avoid this, a suitable $\gamma(q, c_1)$ must be found to fix this problem. Therefore, not any $\gamma(q, c_1)$ can be thus considered to deal with **C.1** and **C.2** through $M_d(q)$ and $V_d(q, c_1)$ in (4.12) and (4.11), respectively. The key for the solution is to recognize $j_2(q, p)$ as a fractional function

$$\begin{aligned} j_2(q, p) &= \frac{n(q, p)}{d(q, p)} \\ &= \frac{G_p^\perp (\nabla_q (p^T M^{-1}(q)p) - M_d(q)M(q)^{-1}\nabla_q (p^T M_d^{-1}(q)p))}{2G_p^T M_d^{-1}(q)p}. \end{aligned} \quad (4.13)$$

Let $\zeta(q, p) \in \mathbb{R}$ and $\eta(q, p) \in \mathbb{R}$ the quotient and the remainder of $j_2(q, p)$, respectively. The expression (4.13) becomes

$$\frac{n(q, p)}{d(q, p)} = \zeta(q, p) + \frac{\eta(q, p)}{d(q, p)}. \quad (4.14)$$

Nullifying the remainder $\eta(q, p)$ brings the solution $\eta(q, p) = 0$ implying $j_2(q, p) = \zeta(q, p)$, which is structurally not affected by any singularity in p . Taking into account (4.12) and (4.13), the equation $\eta(q, p) = 0$ to nullify the remainder can be written as

$$\begin{aligned} &\gamma(q, c_1)(k_1\gamma(q, c_1)(-k_1\nabla_{q_2}b_{11}(q) \\ &\quad - k_2\nabla_{q_2}b_{12}(q) + k_1\nabla_{q_1}b_{12}(q) + k_2\nabla_{q_1}b_{22}(q)) \\ &\quad + (k_1b_{12}(q) + k_2b_{22}(q))(k_2\nabla_{q_2}\gamma(q, c_1) + k_1\nabla_{q_1}\gamma(q, c_1))) = 0, \end{aligned} \quad (4.15)$$

which is a PDE in the scalar function $\gamma(q, c_1)$. The PDE (4.15) has two explicit solutions. The first one is trivial, $\gamma(q, c_1) = 0$, and it is not allowed because it would imply both (4.12a) and (4.12b) to be zero, preventing the fulfilling of **C.1**. The second solution is

$$\gamma(q, c_1) = f_2(q, c_1)f_3\left(\frac{k_1q_2 - k_2q_1}{k_1}, c_1\right), \quad (4.16)$$

where $f_3(\cdot, \cdot) \in \mathbb{R}$ is any scalar, continuous, and nonzero function of its arguments, while $f_2(q, c_1)$ is

$$f_2(q, c_1) = \exp \left(\int_1^{q_1} \frac{k_1(\nabla_{q_2} b_{11}(\cdot) - \nabla_{q_1} b_{12}(\cdot))}{k_1 b_{12}(\cdot) + k_2 b_{22}(\cdot)} + \frac{k_2(\nabla_{q_2} b_{12}(\cdot) - \nabla_{q_1} b_{22}(\cdot))}{k_1 b_{12}(\cdot) + k_2 b_{22}(\cdot)} d\sigma \right), \quad (4.17)$$

where $b_{ij}(\cdot) = b_{ij}([\sigma \ f_4(q, \sigma)])$ to compact notation, with $i, j = \{1, 2\}$, $\exp(k) = e^k$, and $f_4(q, \sigma) = (k_1 q_2 - k_2 q_1 + k_2 \sigma)/k_1$. The expression (4.17) holds if the integral exists: the discussion and the proof is within Appendix B.2. The solution (4.16) gives the structure on how construct $\gamma(q, c_1)$ to avoid the singularity in $j_2(q, p)$. Hence, the function $\gamma(q, c_1)$ is given by two parts: (i) $f_2(q, c_1)$ that is fixed by (4.17) depending on k_1 , k_2 , and $M(q)$; (ii) $f_3(\cdot, \cdot)$ that is free to be chosen to comply with **C.1** and **C.2** through $V_d(q, c_2)$ and $M_d(q, c_1)$ in (4.11) and (4.12), respectively. The gains are also useful to avoid singularities in the generalized coordinates q within the introduced functions. Any other choice of $\gamma(q, c_1)$ may bring to a valid controller, but resulting in $j_2(q, p)$ with a singularity in the generalized momenta that has to be managed in other ways [64]. Finally, once got $j_2(q, p)$ as in (4.13), being sure that no singularity in p will appear, the control law can be computed as in (A.13). The flow-chart represented in Figure 4.1 resumes the derived constructive solution, whose existence is guaranteed by the existence of the integrals within equations (4.11) and (4.17) (see Appendix B.1, B.2).

The novelties introduced within this methodology do not jeopardize the property of asymptotic stability of the sought equilibrium guaranteed by the introduction of the u_{di} control term. To check the detectability of the passive output (A.12), it is sufficient to show that $q \rightarrow q^*$ when $y_d = 0$. Recalling the expression of y_d in (A.12), since $M_d(q)$ is always positive definite because of **C.1**, then $y_d = 0 \iff p = 0_2$. When $p = 0_2$, the closed-loop (A.3) becomes

$$\begin{bmatrix} 0_2 \\ -M_d(q, c_1)M(q)^{-1}\nabla_q V_d(q, c_2) \end{bmatrix} = 0_4. \quad (4.18)$$

Given the expression of the target closed-loop Hamiltonian function $H_d(q, p) = \frac{1}{2}p^T M_d(q, c_1)p + V_d(q, c_2)$, the equations in the last two rows of (4.18) are satisfied if one of the following relationships holds:

- 1) $\det(-M_d(q, c_1)M(q)^{-1}) = 0$;
- 2) $\nabla_q V_d(q, c_2) = 0_2$.

The former condition is not met because it requires that $\det(M_d(q, c_1)) = 0$ which is false because **C.1** holds. The latter is satisfied at the equilibrium q^* because of the validity of **C.2**. Hence, the detectability condition of the passive output is locally guaranteed: the desired equilibrium is locally asymptotically stable with a basin of attraction that can be estimated using the LaSalle's invariance principle, as shown in [9, 83].

Remark *The proposed methodology can be applied to an underactuated mechanical system in the form (A.1). Indeed, the parameterization of the desired inertia matrix does not pose limits on the applicability range of such a methodology. Besides, unlike the method proposed in [64], it does not introduce any singularity depending on generalized momenta in the control law.*

4.2.1 Constructive Methodology with $k_1 = 0$ and $k_2 \neq 0$

A particular solution can be achieved through the choice $k_1 = 0$ and $k_2 \neq 0$. In detail, the expressions (4.9) become

$$a_{22}(q, c_1)b_{12}(q) - a_{12}(q, c_1)b_{22}(q) = 0, \quad (4.19a)$$

$$a_{12}(q, c_1)b_{12}(q) - a_{22}(q, c_1)b_{11}(q) = k_2\gamma(q, c_1). \quad (4.19b)$$

Such a choice further simplifies (4.10) as

$$\nabla_{q_2} V(q) + \gamma(q, c_1)k_2\nabla_{q_2} V_d(q, c_2) = 0, \quad (4.20)$$

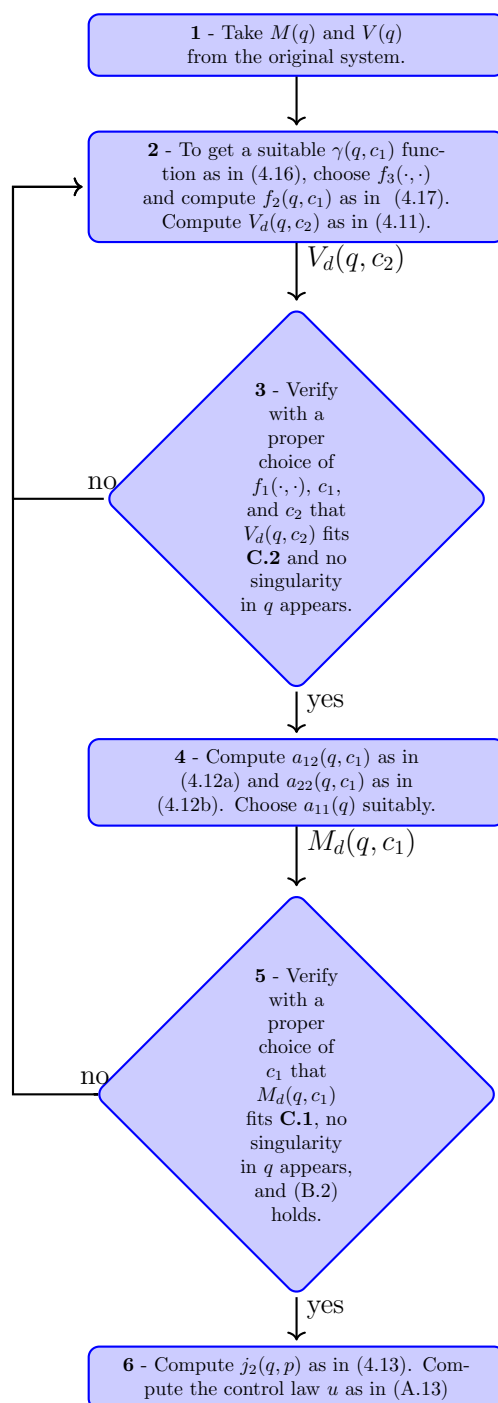


Figure 4.1: Flow chart of the proposed constructive solution.

whose explicit solution is

$$V_d(q, c_2) = - \int_1^{q_2} \frac{\nabla_{q_2} V([\sigma \ q_1])}{k_2 \gamma([\sigma \ q_1])} d\sigma + f_1(q_1, c_2), \quad (4.21)$$

with $f_1(q_1, c_2) \in \mathbb{R}$ is now function of q_1 only and some gains. Once that the $V_d(q, c_2)$ is found and **C.2** is established, the desired inertia matrix can be computed as done for $k_1 \neq 0$. The scalar functions $a_{12}(q, c_1)$ and $a_{22}(q, c_1)$ are now equal to

$$a_{12}(q, c_1) = - \frac{k_2 \gamma(q, c_1) b_{12}(q)}{\Delta(q)}, \quad (4.22a)$$

$$a_{22}(q, c_1) = - \frac{k_2 \gamma(q, c_1) b_{22}(q)}{\Delta(q)}, \quad (4.22b)$$

while $a_{11}(q, c_1)$ is left free to satisfy **C.1**. The remaining part of the procedure is the same. Therefore, once that $M_d(q, c_1)$ and $V_d(q, c_2)$ are found, the function $j_2(q, p)$ should be computed. However, the function $\gamma(q, c_1)$ should be chosen properly to avoid singularity in the generalized momenta in the denominator of $j_2(q, p)$. Following the same idea, the equation to nullify the remainder (4.15) simplifies into

$$k_2^2 \gamma(q, c_1) b_{22}(q) \nabla_{q_2} \gamma(q, c_1) = 0, \quad (4.23)$$

which is a PDE in the scalar function $\gamma(q, c_1)$. The previous PDE has again two explicit solutions. The first is trivial, $\gamma(q, c_1) = 0$, and it is not allowed because it would imply (4.22a) and (4.22b) to be zero, preventing the fulfilling of **C.1**. The latter solution is $\gamma(q, c_1) = f_3(q_1, c_1)$, where now $f_3(q_1, c_1) \in \mathbb{R}$ is any scalar, continuous, and nonzero function of q_1 only and some gains. Therefore, in the particular case $k_1 = 0$ and $k_2 \neq 0$, the degrees of freedom given by $f_1(\cdot, \cdot)$ and $\gamma(\cdot, \cdot)$ depend on q_1 only and some gains. These should be employed to fulfil **C.1** and **C.2**, as well as to avoid singularities in q . Notice that, given the arguments in the Appendix B, the existence of the integral within (4.21) is trivial. The flow-chart represented in Figure 4.1 holds also in the case of $k_1 = 0$ and $k_2 \neq 0$ with the described changes. The possibility

of choosing $k_1 = 0$ and $k_2 \neq 0$ or not depends on the particular case study. It indeed simplifies the solution but bestows fewer degrees of freedom to the control design. In the following, both approaches will be employed for two different case studies.

Chapter 5

Energy Shaping for Equilibrium Point Stabilization

To ease the understanding of the procedure presented in Chapter 4, the design of the stabilizing controller for the TORA system has been divided into steps that have been numbered as in the flow chart in Figure 4.1.

5.1 Stabilization of the TORA System via IDA-PBC with Explicit solution of PDEs

5.1.1 Step 1

Without loss of generality, the procedure presented in this paper is applied to stabilize the TORA (with $M(q)$ and $V(q)$ summarized in Table 3.1) at the desired equilibrium point $(q^*, p^*) = (\pi, 0, 0, 0)$.

5.1.2 Step 2

The following procedure assumes $k_1 \neq 0$. To get a proper function $\gamma(q)$, a constant $f_3 ((k_1q_2 - k_2q_1)/k_1) = k_3$ is picked up, with $k_3 \neq 0$ a suitable gain. Taking into account (3.5), the expression (4.17) becomes

$$f_2(q) = \frac{1}{(k_2(m_1 + m_2) + k_1m_1l \cos q_1)},$$

with $k_2 > k_1m_1l/(m_1 + m_2)$ to avoid any singularity in $f_2(q)$. Then, the suitable scalar function $\gamma(q, c_1)$ in (4.16) becomes

$$\gamma(q) = \frac{k_3}{(k_2b_{22} + k_1lm_1 \cos q_1)}.$$

The $f_1 ((k_1q_2 - k_2q_1)/k_1)$ function in (4.11) is chosen as follows

$$f_1 \left(\frac{k_1q_2 - k_2q_1}{k_1} \right) = k_4 \left(\frac{k_1q_2 - k_2q_1}{k_1} \right)^2, \quad (5.1)$$

with $k_4 \in \mathbb{R}$ a suitable gain. With the above choice and expressions, the desired potential energy in (4.11) is

$$\begin{aligned} V_d(q) = & \frac{b_{22}kk_2^2q_1^2 - 2b_{22}kk_1k_2q_1q_2 - 2kk_1k_2lm_1 \cos q_1}{2k_1^2k_3} \\ & - \frac{2kk_1^2lm_1q_2 \sin q_1 + 2k_1^2k_3k_4 \left(\frac{k_1q_2 - k_2q_1}{k_1} \right)^2}{2k_1^2k_3}. \end{aligned} \quad (5.2)$$

5.1.3 Step 3

The evaluation of the gradient $\nabla_q V_d(q)$ in $q^* = (\pi, 0)$ yields

$$\nabla_q V_d(q) \Big|_{q^*} = \begin{bmatrix} \frac{k_2^2(b_{22}k + 2k_3k_4)\pi}{k_1^2k_3} \\ -\frac{k_2(b_{22}k + 2k_3k_4)\pi}{k_1k_3} \end{bmatrix}, \quad (5.3)$$

which becomes

$$\nabla_q V_d(q) \Big|_{q^*} = 0_2, \quad (5.4)$$

if the condition $k_4 = -b_{22}k/(2k_3)$ holds. The Hessian of $V_d(q)$, evaluated in $q^* = (\pi, 0)$, is

$$\nabla_q^2 V_d(q) \Big|_{q^*} = \begin{bmatrix} \frac{2b_{22}kk_2^2 + 4k_2^2k_3k_4 - 2kk_1k_2m_1l}{2k_1^2k_3} \\ -\frac{2b_{22}kk_1k_2 - 4k_1k_2k_3k_4 + 2kk_1^2m_1l}{2k_1^2k_3} \\ -\frac{2b_{22}kk_1k_2 - 4k_1k_2k_3k_4 + 2kk_1^2m_1l}{2k_1^2k_3} \\ 2k_4 \end{bmatrix}. \quad (5.5)$$

This last is positive definite if the conditions

$$k_1 > 0, k_2 > \frac{k_1m_1l}{b_{22}}, k_3 < 0, k_4 = -\frac{b_{22}k}{2k_3} \quad (5.6)$$

are met. Since these conditions are not in contrast with the ones found previously for the same gains, the procedure can continue. The condition **C.2** is thus checked.

5.1.4 Step 4

The scalar functions $a_{12}(q)$ and $a_{22}(q)$ are evaluated using (4.12), while $a_{11}(q)$ is free and it is here computed as proposed in [64]

$$a_{11}(q) = k_5 \frac{a_{12}^2(q)}{a_{22}(q)}, \quad (5.7)$$

which does not show any dependence on the generalized momenta at the denominator and, therefore, on the passive output, as expected. However, to avoid any singularity in the q variables, the conditions $k_2 > k_1 m_1 l / b_{22}$ and $k_2 \neq k_1 (l^2 + r^2) / l$ must hold. Both the conditions can be dropped because already contained within (5.6) and (5.10), respectively. Therefore, the set of gains avoiding any singularities and satisfying **C.1**, **C.2**, and **C.3** are

$$\begin{aligned} k_1 > 0, \quad k_2 > \frac{k_1 m_1 l}{m_1 + m_2} \wedge k_2 \neq \frac{k_1 (l^2 + r^2)}{l}, \quad k_3 < 0, \\ k_4 = -\frac{b_{22} k}{2k_3}, \quad k_5 > 1. \end{aligned} \tag{5.13}$$

Notice that the constant terms b_{11} and b_{22} were often not explicitly expressed due to space constraints and for the sake of clarity. In addition, the condition $k_2 > k_1 m_1 l / (m_1 + m_2)$ agrees with (B.2), ensuring the existence of the integral in (4.17) and in (4.11).

Finally, the sum between the energy shaping (A.10) and the damping injection (A.11) is the total control action.

5.2 Numerical Evaluation

The current section aims to demonstrate the effectiveness of the designed controller for the TORA. To recap, the sought control goal is to stabilize the system, described by (3.6) and (3.5) at the desired equilibrium point $(q^*, p^*) = (\pi, 0, 0, 0)$. The nominal dynamic parameters chosen for the TORA model are $m_1 = 1$ kg, $m_2 = 10$ kg, $l = 1$ m, $r = 0.1$ m, $k = 5$ and $g = 9.81$ m/s². The performance of the proposed control law is evaluated in presence of parametric uncertainties, noisy measurements, and a time delay introduced by the discretization of the controller. The test is carried out on a standard personal computer in the MATLAB/Simulink environment using the *ODE45* routine. The robustness in the presence of parametric uncertainties is tested by considering, in the control law, an increment of the 20 % in the value of the parameters m_1 , m_2 , l , r and k contained inside the

Table 5.1: Parameters and initial conditions characterizing the TORA model used in simulations.

inertial and kinematic parameters	initial conditions
$m_1 = 1 \text{ kg}, m_2 = 10 \text{ kg}$	$q_1(0) = \pi/2 \text{ rad}, q_2(0) = 0.1 \text{ m}$
$l = 1 \text{ m}, r = 0.1 \text{ m}$	$p_1(0) = 0 \text{ (kg rad)/s}, p_2(0) = 0 \text{ (kg m)/s}$
$k = 5, g = 9.8 \text{ m/s}^2$	

model. Moreover, in order to evaluate the performance in presence of noisy measurements, a white noise is added to the signals $q_1(t)$, $q_2(t)$, $p_1(t)$, and $p_2(t)$, with a variance of 0.05, 0.01, 0.05, and 0.01, respectively. The discretization of the controller is also taken into account by sampling the control law each 0.01 s. The controller has been designed with gains $k_1 = 1$, $k_2 = 0.14$, $k_3 = -1$, $k_4 = 39.6$, $k_5 = 2$, $k_d = 20$. They comply with the conditions in (5.13). The simulation starts with initial conditions $q_1(0) = \pi/2 \text{ rad}$, $q_2(0) = 0.1 \text{ m}$, $p_1(0) = 0 \text{ (kg rad)/s}$, $p_2(0) = 0 \text{ (kg m)/s}$ and lasts for 100 s. A summary of the inertial and kinematic parameters characterizing the TORA model deployed in the following simulations, as well as, of the initial conditions selected, is given in Table 5.1.

Figure 5.1 depicts the time evolution of the closed-loop systems potential energy which, as expected, reaches its local minimum located in q^* . As shown in Figure 5.2 and Figure 5.3, the state trajectories of the system asymptotically converge to the desired values in roughly 40 s, with performance comparable with the methodologies belonging to the state of art in the control of the TORA, exhibiting small amplitude oscillations due to the presence of noisy measures.

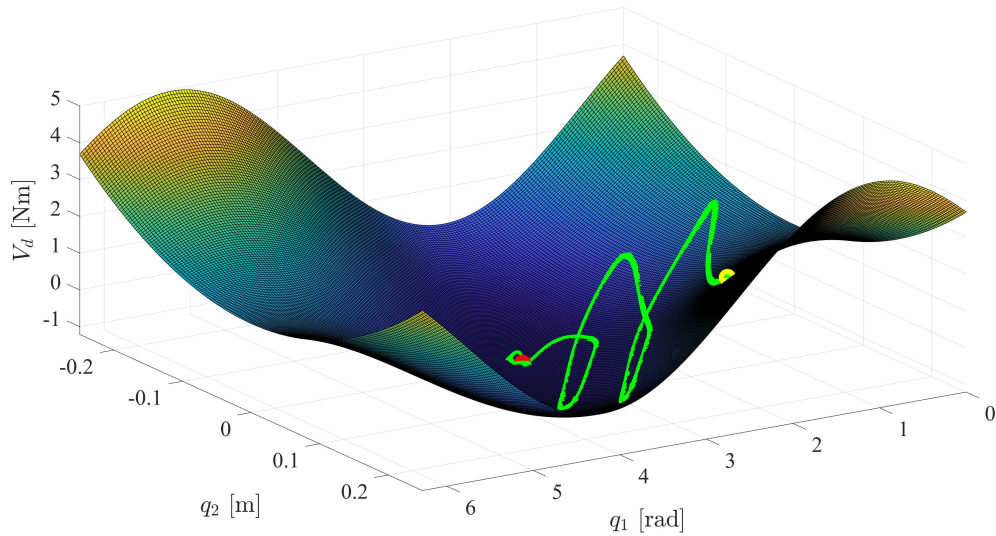
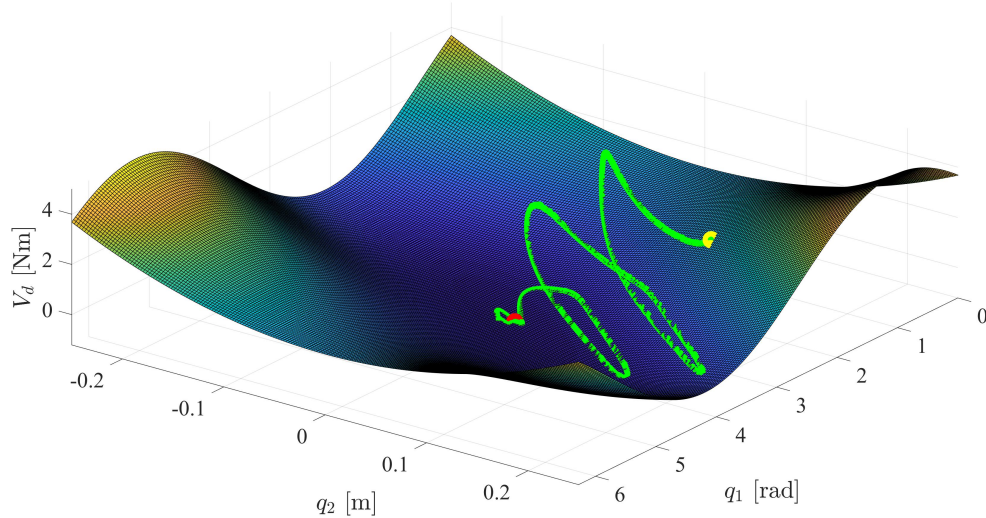
(a) Front view of $V_d(q)$ surface.(b) Top view of $V_d(q)$ surface.

Figure 5.1: Evolution of the closed-loop system potential energy during a test carried out with perturbed conditions. Potential energy (the green curve) evolves from its initial value (the yellow dot) until it reaches its minimum (the red dot).

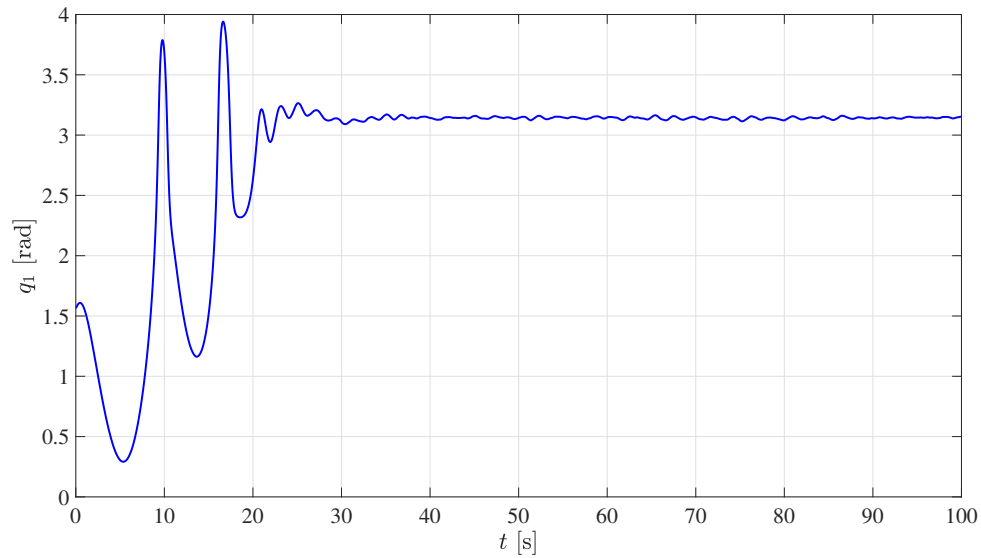
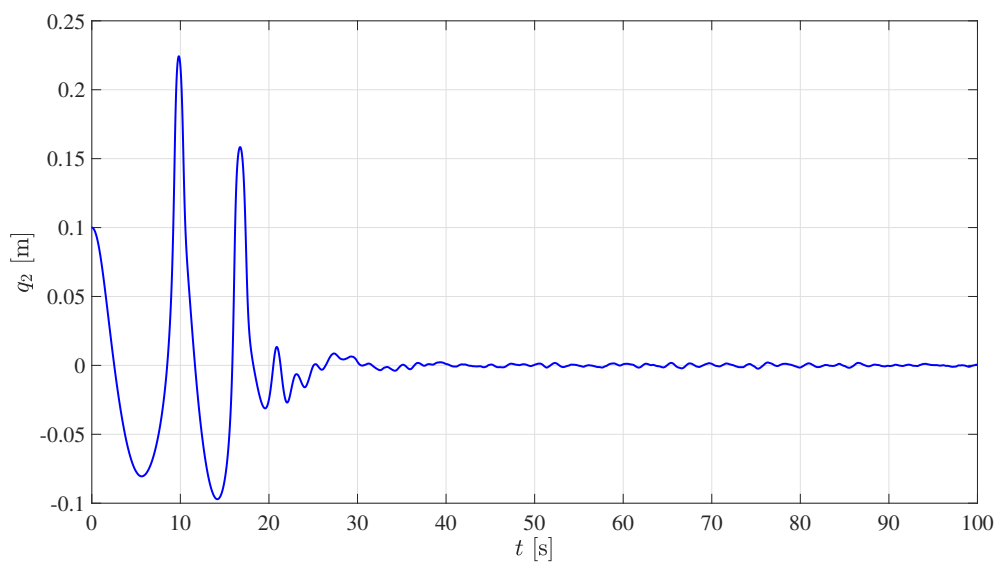
(a) Time history of q_1 (b) Time history of q_2

Figure 5.2: Time histories of the generalized coordinates during a test carried out in presence of parametric uncertainties, noisy measurements, and controller discretization.

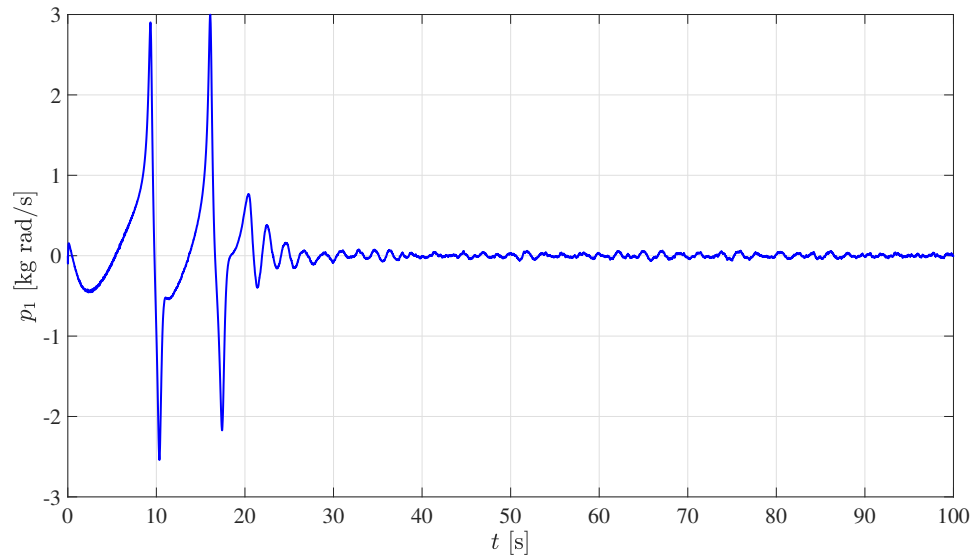
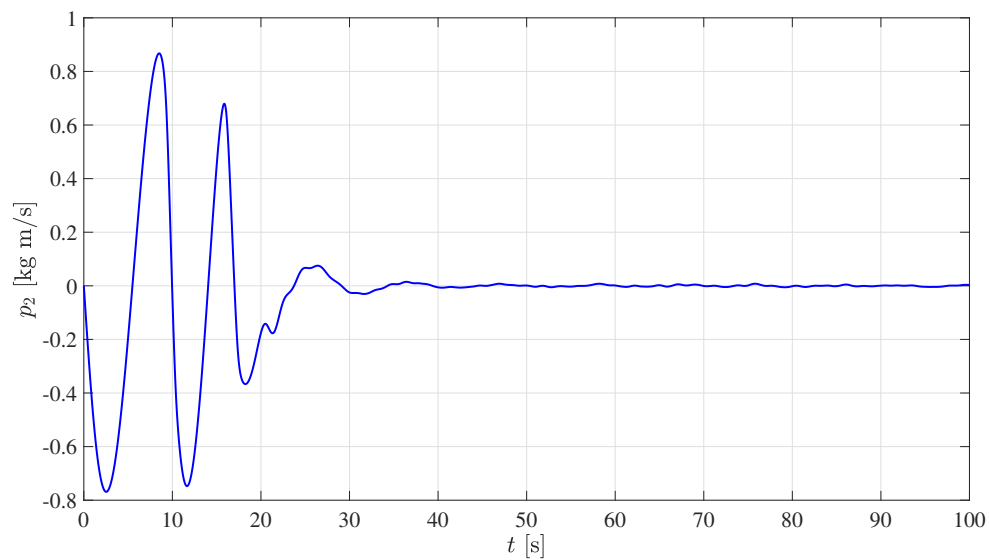
(a) Time history of p_1 (b) Time history of p_2

Figure 5.3: Time histories of the generalized momenta during a test carried out in presence of parametric uncertainties, noisy measurements, and controller discretization.

Chapter 6

Energy Shaping for Gait Generation

The objective of this chapter is to demonstrate the effectiveness of IDA methodologies to generate gaits that cannot be exhibited by the uncontrolled CBR. The introduction of a controller, which exerts his action during the swing phase, gives birth to gaits that the uncontrolled CBR cannot exhibit unless to change the mass/geometrical properties of the robot and/or the slope of the surface on which the robot walks. These artificial gaits are associated with several limit cycles in the state space of the CBR. These limit cycles, representing the asymptotic behavior of the closed-loop, are due to the impacts between the swing leg and the ground. Specifically, the focus is on efficient periodic locomotion, more than on robust walking, hence more effort has been put to achieve a gait that is as close as possible to the human one, from an energetic point of view. This choice is motivated by results in robotics and biomechanics showing that actuation from the ankle alone requires less energy to sustain continuous walking than hip-only actuation does [84]. Hence, as already done in [16, 49], based on such biomechanics arguments, the control schemes proposed in this chapter are designed to take into account actuation at the ankles instead of the hip. Nevertheless, presented approaches are general, hence they hold even if the actuation is at the hip. As proof of this, the methodology

proposed in Section 6.2 is also deployed in Section 7.4.2 to implement an inner-loop energy shaping control in the context of the gait robustification for a biped with unactuated ankles.

6.1 Total Energy Shaping VS Kinetic Energy Shaping for Gait Generation

As already stated in Chapter 1, underactuated mechanical systems require total energy shaping to be stabilized at a certain equilibrium point, whereas an approach based on potential energy shaping only, fails due to an unnatural inversion of the system which is imposed along the reference trajectories [7, Section 10.3.1]. On the other hand, when dealing with the periodic walking exhibited by an underactuated passive walker, kinetic energy shaping alone has proved to be effective in changing the forward speed of the biped. The choice to shape only kinetic energy is motivated by studies on human and animal locomotion [85, 86], which demonstrate that step length is adjusted simultaneously to speed change, during walking, to minimize energy consumption. Based on such results, modifications of the closed-loop kinetic energy are proposed in [16], firstly, and in [49], lately, with two different approaches, the former based on CL and the latter on IDA-PBC. Such modified kinetic energies result in simultaneous speed and step length change, in a biomimetic fashion.

One of the objectives of the current chapter is to show that total energy shaping impacts more dramatically, compared to kinetic-energy shaping only, on the gait generation of a CBR and, in turn, that the extra computational cost related to the solution of the PE-ME is worth the price. In other words, this chapter aims to show that the introduction of a total energy shaping control action, like the ones exploited in this work, effectively generate gaits that cannot be exhibited by the uncontrolled biped and that go beyond the ones achievable via kinetic energy shaping only (in terms of S and T parameters), and whose stability is verified numerically a posteriori.

6.2 Gait Generation for the CBR via IDA-PBC with Explicit Solution of PDEs

The following procedure follows the constructive methodology presented in Section 4.2.1. To get a proper function $\gamma(q_1)$, a constant

$$f_3(q_1) = -\frac{1}{k_2^2} \quad (6.1)$$

function is picked up. With such a choice, results that

$$\gamma(q_1) = -\frac{1}{k_2^2}. \quad (6.2)$$

Then, choosing the function $f_1(q_1)$ in (4.21) as

$$f_1(q_1) = k_3(ma + (m + m_h)l)g \cos(q_1), \quad (6.3)$$

with $k_3 \in \mathbb{R}$ a suitable gain, the desired potential energy in (4.21) becomes

$$V_d(q) = k_3g(ma + (m + m_H)l) \cos(q_1) - k_2bmg \cos(q_2). \quad (6.4)$$

Notice that the two gains k_2 and k_3 weigh the components of the original system's potential energy relative to the swing and the stance leg, respectively. Since the CBR without the impact resembles a double inverted pendulum, the most natural choice seems to assign $q^* = [\pi \ 0]^T$ as equilibrium, like the one in the mathematical model of the plant. The sought goal is not to stabilize the system at the desired equilibrium but rather to generate new gaits. The gradient of $V_d(q, c_2)$ is

$$\nabla_q V_d(q, c_2) = \begin{bmatrix} -k_3(ma + (m + m_H)l)g \sin(q_1) \\ k_2bmg \sin(q_2), \end{bmatrix} \quad (6.5)$$

which, evaluated in q^* , becomes

$$\nabla_q V_d(q, c_2) \Big|_{q^*} = 0_2. \quad (6.6)$$

The Hessian of $V_d(q, c_2)$, evaluated in q^* , is

$$\nabla_q^2 V_d(q, c_2) \Big|_{q^*} = \begin{bmatrix} k_3(ma + (m + m_H)l)g & 0 \\ 0 & k_2 b m g \end{bmatrix}. \quad (6.7)$$

This Hessian matrix is positive definite if the conditions $k_2 > 0$, $k_3 > 0$ hold. Therefore, if k_2 and k_3 are simultaneously positive, **C.2** is satisfied. The scalar functions $a_{12}(q)$ and $a_{22}(q)$ are evaluated using, respectively, (4.22a) and (4.22b) while the free term $a_{11}(q)$ is chosen as

$$a_{11}(q) = k_4 \frac{b_{11}}{k_2 \Delta(q)}, \quad (6.8)$$

with $k_4 \in \mathbb{R}$ a suitable gain. Thereby, the desired inertia matrix becomes

$$M_d(q, c_1) = \frac{1}{k_2} \begin{bmatrix} k_4 b_{11} & b_{12}(q) \\ b_{12}(q) & b_{22} \end{bmatrix}, \quad (6.9)$$

whose determinant is

$$\Delta_d(q) = \frac{k_4 b_{11}(q) b_{22}(q) - b_{12}^2(q)}{k_2^2}. \quad (6.10)$$

To comply with **C.1**, it should be proven that the desired inertia matrix is positive definite. Thanks again to the Sylvester's criterion, this is true if both $a_{11}(q) > 0$ and $\Delta_d(q) > 0$. The former is true if both $k_2 > 0$ and $k_4 > 0$. On the other hand, the latter condition is true if $k_4 > (mlb)^2 / (b_{11} b_{22})$. Hence, the choice

$$k_2 > 0, k_3 > 0, k_4 > \frac{(mlb)^2}{b_{11} b_{22}} \quad (6.11)$$

satisfies both **C.1** and **C.2**.

The scalar interconnection term $j_2(q, p)$, computed as in (4.13), has the following expression

$$j_2(q, p) = \frac{\psi_1(q, p) + \psi_2(q, p)}{\psi_3(q)}, \quad (6.12)$$

with

$$\begin{aligned}
\psi_1(q, p) &= b b_{11}(-1 + k_4)lm(-8b_{11}^2 b_{22}^2 k_4 p_2 \\
&\quad + 3b^4 l^4 m^4 p_2 + 4b b_{22}lm(-2b_{11}b_{22}(1 + k_4) \\
&\quad + 3b^2 l^2 m^2)p_1 \cos(q_1 - q_2)), \\
\psi_2(q, p) &= b b_{11}(-1 + k_4)lm(4b^4 l^4 m^4 p_2 \cos(2(q_1 \\
&\quad - q_2)) + 4b^3 b_{22} l^3 m^3 p_1 \cos(3(q_1 - q_2)) \\
&\quad + b^4 l^4 m^4 p_2 \cos(4(q_1 - q_2)) \sin(q_1 - q_2)). \\
\psi_3(q) &= 8k_2(b_{11}b_{22} - b^2 l^2 m^2 \cos(q_1 - q_2))^2 (b_{11}b_{22}k_4 \\
&\quad - b^2 l^2 m^2 \cos(q_1 - q_2)^2).
\end{aligned}$$

Both the denominator of (6.12) and the passive output are independent from the generalized momenta. The gains chosen as in (6.11) avoid any singularity depending on q , assuring that the denominator of (6.12) never becomes zero. Notice that the terms b_{11} , b_{22} , and $b_{12}(q)$ were often not explicitly expressed due to space constraints. The total control action is given by (A.13).

6.2.1 Alternative choice of γ and a_{11}

An alternative control contribution can be retrieved following the procedure presented in [2]. With

$$\gamma(q_1) = -\frac{1}{k_2^3}, \quad (6.13)$$

and $f_1(q_1)$ as in (6.3), while no substantial difference there is in the expression of the desired potential energy which is exactly the same as in (6.4), the main change is in the scalar functions $a_{12}(q)$ and $a_{22}(q)$, evaluated using, respectively, (4.22a) and (4.22b), and, most of all, in the free term $a_{11}(q)$ which is chosen as

$$a_{11}(q) = k_4 \frac{k_5 \Delta + k_7 f_5(q) b_{12}(q)^2}{\Delta(k_6 \Delta + k_7 f_5(q) b_{22})}, \quad (6.14)$$

with $f_5(q) \in \mathbb{R}$ a function to be selected, and $k_4, k_5, k_6, k_7 \in \mathbb{R}$ some gains.

6.3 Gait Generation for the CBR via SIDA-PBC with Dissipative Forces

Remark. Notice that condition (A.20) can be relaxed in this section since the main objective is not the regulation of the equilibrium point, but the gait generation. Moreover, notice that the dissipative forces in the controller are represented by the mapping $C(q, p)$, as indicated in [21].

A particular family of solutions is computed from the matching PDEs related to SIDA-PBC. First, the PE-ME is solved by imposing that the closed-loop and the open-loop dependency to the potential energy with respect to q_2 are equal, *i.e.*,

$$\nabla_{q_2} V(q) = \nabla_{q_2} V_d(q). \quad (6.15)$$

Then, the KE-ME is solved by fixing the structure of the Q_i matrices.

Let

$$M_d(q) = \begin{bmatrix} m_{d11}(q) & m_{d12}(q) \\ m_{d12}(q) & m_{d22}(q) \end{bmatrix} \quad (6.16)$$

be the desired inertia matrix and

$$\Gamma(q) = M_d(q)M^{-1}(q) = \begin{bmatrix} \Gamma_{11}(q) & \Gamma_{12}(q) \\ \Gamma_{21}(q) & \Gamma_{22}(q) \end{bmatrix}, \quad (6.17)$$

the product between the desired inertia matrix and the inverse of the open-loop one, similarly as expressed in (4.8). Then, the PE-ME (A.9) becomes

$$G_p^\perp (\nabla_q V(q) - \Gamma(q)\nabla_q V_d(q)) = 0. \quad (6.18)$$

Since the actuation is on the stance ankle, meaning that $G_p = [1 \ 0]^T$ and $G_p^\perp = [0 \ 1]^T$, results that the PE-ME (6.18) can be expressed as

$$\nabla_{q_2} V(q) - \Gamma_{21}\nabla_{q_1} V_d(q) - \Gamma_{22}\nabla_{q_2} V_d(q) = 0. \quad (6.19)$$

The PDE (6.19) is solved choosing $\Gamma_{21}(q) = 0$ and $\Gamma_{22}(q) = 1$. Hence, $m_{d_{22}} = b_{22}$ and $m_{d_{12}} = b_{12}(q)$. This implies that $\nabla_{q_1} V_d(q)$ is left free to be chosen. The desired closed-loop potential energy is finally defined as

$$V_d(q) = g(ma + (m + m_H)l) \cos(q_1 + k_3\varphi) - bmg \cos(q_2). \quad (6.20)$$

In order to solve the KE-ME, folding G_p^\perp into (A.15) yields

$$\nabla_{q_2} (p^T M^{-1}(q)p) - \nabla_{q_2} (p^T M_d^{-1}(q)p) + 2C(q, p) = 0. \quad (6.21)$$

By fixing the structure of the Q_2 matrix as

$$Q_2 = \begin{bmatrix} Q_{11} & Q_{12} \\ Q_{12} & Q_{22} \end{bmatrix}, \quad (6.22)$$

the component $\Lambda_{22}(q)$ can be written in terms of \dot{q}_1 , for simplicity reasons, and $m_{d_{11}}(q)$, which is the only free component of the desired inertia matrix $M_d(q)$ so far, as

$$\Lambda_{22}(q) = \frac{-mlb b_{22} \sin(q_1 - q_2) (b_{11} - m_{d_{11}}(q))}{2b_{12}^2(q) - 2b_{22}m_{d_{11}}(q)} \dot{q}_1. \quad (6.23)$$

Setting $\Lambda_{12}(q) = \Lambda_{21}(q)$ and $\Lambda_{11}(q) = \Lambda_{22}(q)$, a family of solutions for the KE-ME is obtained through an appropriate selection of $m_{d_{11}}(q)$. A possible choice for $m_{d_{11}}(q)$ is

$$m_{d_{11}}(q) = \frac{b_{11}^2 b_{22} - [b_{11} + k_2 \sin(q_1 - q_2)] b_{12}^2(q)}{b_{11} b_{22} - b_{12}^2(q) - b_{22} k_2 \sin(q_1 - q_2)}, \quad (6.24)$$

with k_2 a gain to be selected in order to meet **C.1**. Hence, $\Lambda_{ii}(q)$, with $i = 1, 2$, yields to

$$\Lambda_{ii}(q) = \frac{-mlb b_{22} k_i \sin^2(q_1 - q_2)}{2(b_{11} b_{22} - b_{12}^2(q))} \dot{q}_1. \quad (6.25)$$

Notice that, although $\Lambda_{ii}(q)$ depends on the velocity \dot{q}_1 , this is always negative during a gait, since the the support leg rotates always clock wise (see Figure 3.2).

By fixing the structure of the matrices Q_2 and $\Lambda(q)$, then the mapping $C(q, p)$ is completely defined. Therefore, the matrix Q_1 is determined intrinsically. Notice that, due to the switching conditions (3.21), the equilibrium point of the closed-loop system will be never reached if a stable limit cycle is generated. This implies that the stability condition can be relaxed to generate gaits.

6.4 Gait Generation for the CBR via EPD-PBC

Remark. *The main objective of the controller is the gait generation, and not the asymptotic stabilization of an equilibrium point, hence the classical dissipation condition (A.24) can be relaxed.*

Similarly to the considerations made in [16] relying on bio-mechanic arguments, pumping energy at the beginning of each step while dissipating it at the end

$$\begin{aligned} \dot{H}(q, p) &> 0 \quad \text{for } \zeta < q_1 < \pi \\ \dot{H}(q, p) &= 0 \quad \text{for } q_1 = \zeta \\ \dot{H}(q, p) &< 0 \quad \text{for } -\zeta < q_1 < 0 \end{aligned} \tag{6.26}$$

seems to be an effective way to achieve larger step lengths and shorter step periods for the generated gait. The other way round

$$\begin{aligned} \dot{H}(q, p) &< 0 \quad \text{for } \zeta < q_1 < \pi \\ \dot{H}(q, p) &= 0 \quad \text{for } q_1 = \zeta \\ \dot{H}(q, p) &> 0 \quad \text{for } -\zeta < q_1 < 0 \end{aligned} \tag{6.27}$$

leads instead to shorter step lengths and greater step periods for the generated gait. The introduction of the offset $\zeta > 0$ in the transition between the pumping regime and the damping one (and vice-versa) is motivated by the intuition that feeding energy to the system in a wider region of the phase plane should lead to a faster gait as, equivalently, subtracting it should take to a slower one if compared to a transition in

$q_1 = 0$. This is realized by designing the scalar function $e(q) : \mathbb{R}^2 \rightarrow \mathbb{R}$ such as

$$e(q) = \begin{cases} e_1(q) > 0 & \text{if } q \in Z \\ e_2(q) \leq 0 & \text{if } q \in \mathbb{R}^2 - Z \end{cases} \quad (6.28)$$

where $Z \subset \mathbb{R}^2$. Therefore, given (A.28), the controller (A.27) which realizes the sought behavior in (6.26) and (6.27) is

$$u_{pd}(q, p) = k_{pd} \sin(q_1) G_p^T M^{-1}(q) p, \quad (6.29)$$

where the function $e(q) = \sin(q_1)$, which meets (6.28), defines the sign of $\dot{H}(q, p)$ once that the gain $k_{pd} \in \mathbb{R}$ is fixed.

6.5 Gait Generation for the CBR via EPOD-PBC

The choice $e(q) = |\sin(q_1)q_1|$ transforms the control action (6.29) into the following energy pumping or damping controller

$$u_{pod}(q, p) = k_{pd} |\sin(q_1)q_1| G_p^T M^{-1}(q) p. \quad (6.30)$$

The control law (6.30) is equivalent to a damping injection control law for $k_{pd} < 0$, while it pumps energy for $k_{pd} > 0$ in the sense that

$$\begin{aligned} \dot{H}(q, p) &< 0 && \text{for } k_{pd} < 0 \text{ and } \forall q_1 \\ \dot{H}(q, p) &= 0 && \text{for } q_1 = 0 \text{ and } \forall k_{pd} \\ \dot{H}(q, p) &> 0 && \text{for } k_{pd} > 0 \text{ and } \forall q_1 \end{aligned} \quad (6.31)$$

where the time derivative of the total energy, obtained by substituting $e(q) = |\sin(q_1)q_1|$ into (A.28), is given by

$$\dot{H}(q, p) = k_{pd} |\sin(q_1)q_1| \dot{q}_1^2. \quad (6.32)$$

6.6 Numerical evaluation

The current section aims to demonstrate the effectiveness of the designed controllers for the CBR in generating new gaits. The nominal dynamic parameters chosen for the CBR are $m_H = 10$ kg, $m = 5$ kg, $a = 0.5$ m, $b = 0.5$ m, $g = 9.8$ m/s², and $\varphi = 3$ deg. Eight case studies will be analyzed in the following and they are compared with the passive gait. They start with the initial conditions

$$x(0) = [0.2187 \quad -0.3234 \quad -1.0918 \quad -0.3772]^T,$$

where the first two components are the generalized coordinates, while the last two are the generalized velocities. Initial conditions have been defined in terms of coordinates and velocities (as in [16, 49]) rather than coordinates and momenta. Notice that the momenta are linearly related to the velocities through the inertia matrix. All the gains are experimentally tuned. The objective is the generation of two different gaits which cannot be exhibited by the uncontrolled CBR. Recalling the S and T parameters describing a generic gait, the uncontrolled gait, which will be referred to as *passive gait*, is characterized by $S = 0.5347$ m and $T = 0.7347$ s. The first desired gait is characterized by a smaller step length S and a bigger period T : it will be referred to as *small gait*. The second desired gait features an increased step length S and a reduced period T : it will be referred to as *large gait*. Tests are performed on a standard personal computer, using the Matlab *ODE45* routine together with the event detection option active, to evaluate the hits between the swing foot and the ground. The controller is implemented at a discrete-time step of 0.01 s. A summary of the inertial and kinematic parameters characterizing the biped's model deployed in the following simulations, as well as, of the initial conditions belonging to the limit cycles, is given in Table 6.1.

Table 6.1: Parameters and initial conditions characterizing the CBR model used in simulations.

inertial and kinematic parameters	initial conditions
$m_H = 10 \text{ kg}, m = 5 \text{ kg}$	$q_1(0) = 0.2187 \text{ rad}, q_2(0) = -0.3234 \text{ rad}$
$a = 0.5 \text{ m}, b = 0.5 \text{ m}$	$\dot{q}_1(0) = -1.0918 \text{ rad/s}, \dot{q}_2(0) = -0.3772 \text{ rad/s}$
$g = 9.8 \text{ m/s}^2, \varphi = 3 \text{ deg}$	

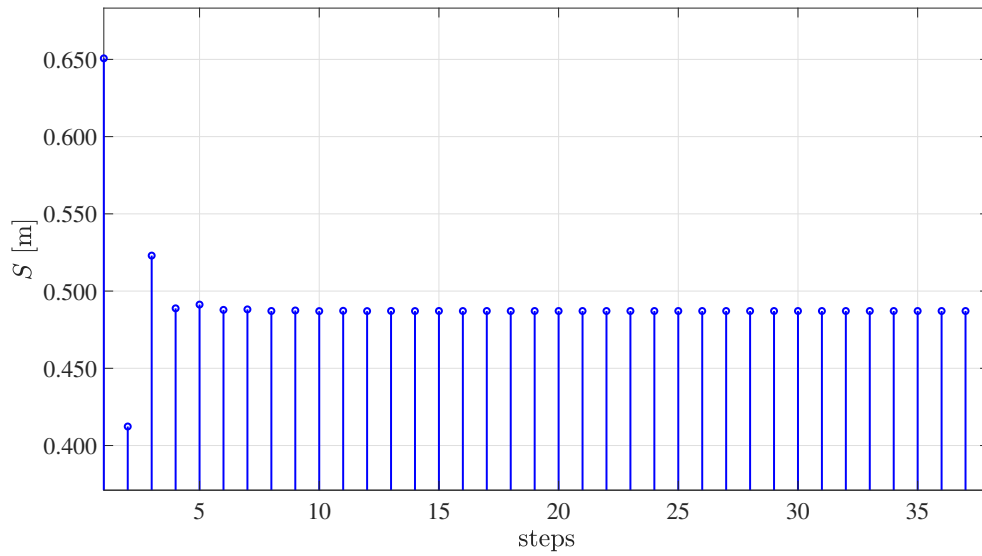
6.6.1 Case Study I: Small Gait Generation via IDA-PBC With Explicit Solution Of PDEs

In order to generate the small gait, the controller (A.13) is designed as shown in Section 6.2, with $\gamma(q_1)$ as in (6.2) and $a_{11}(q)$ as in (6.8), through the following set of gains $k_2 = 1.25$, $k_3 = 0.45$, $k_4 = 1.05$ and $k_d = 0.1$, experimentally tuned complying with (6.11). The simulation is carried out for 30 s. As shown in Figure 6.1, the step length S and the step period T asymptotically converge to values 0.4871 m and 0.7854 s, which are respectively smaller and bigger than the parameters $S = 0.5347$ m and $T = 0.7347$ s characterizing the passive gait. The last one is generated by turning off the controller and using the same initial conditions.

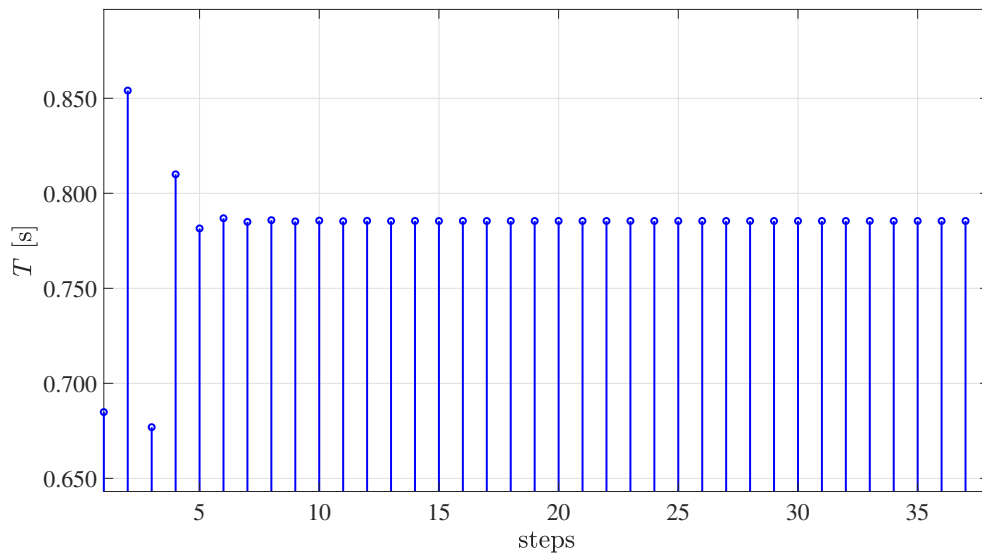
In a different way, the same controller is designed with $\gamma(q_1)$ as in (6.13) and $a_{11}(q)$ as in (6.14), through the following set of gains $k_2 = 1.1$, $k_3 = 1$, $k_4 = 1/k_2$, $k_5 = 0.04$, $k_6 = 0$, $k_7 = 1$, and $k_d = 0.1$. The function $f_5(q)$ in (6.14) is chosen equal to 1 yielding

$$a_{11}(q) = k_4 \frac{k_5 \Delta + b_{12}(q)^2}{\Delta b_{22}}. \quad (6.33)$$

To check the fulfillment of **C.1**, see [2]. The resulting controller is similar to the one proposed in [49], apart from the potential energy shaping stage and the damping injection. The designed controller leads to a symmetric gait with $S = 0.0417$ m and $T = 1.149$ s, which is slower than the slowest symmetric one proposed in [49] having $S = 0.2012$ m and $T = 0.9996$ s. The gait parameters S and T converge to these very small values as in Figure 6.2.



(a) Event history of S .



(b) Event history of T .

Figure 6.1: Event histories of the step length and the step period during Case Study I ($\gamma(q_1)$ as in (6.2) and $a_{11}(q)$ as in (6.8)).

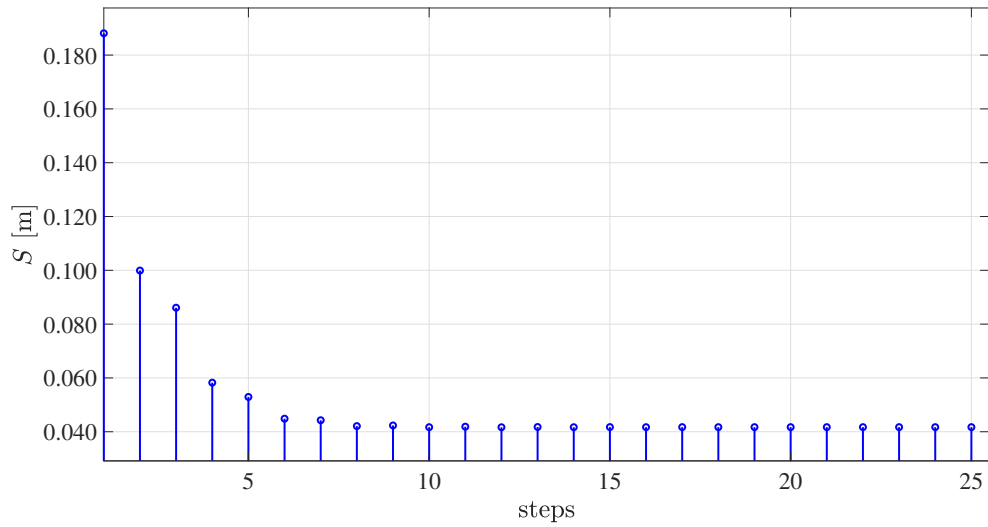
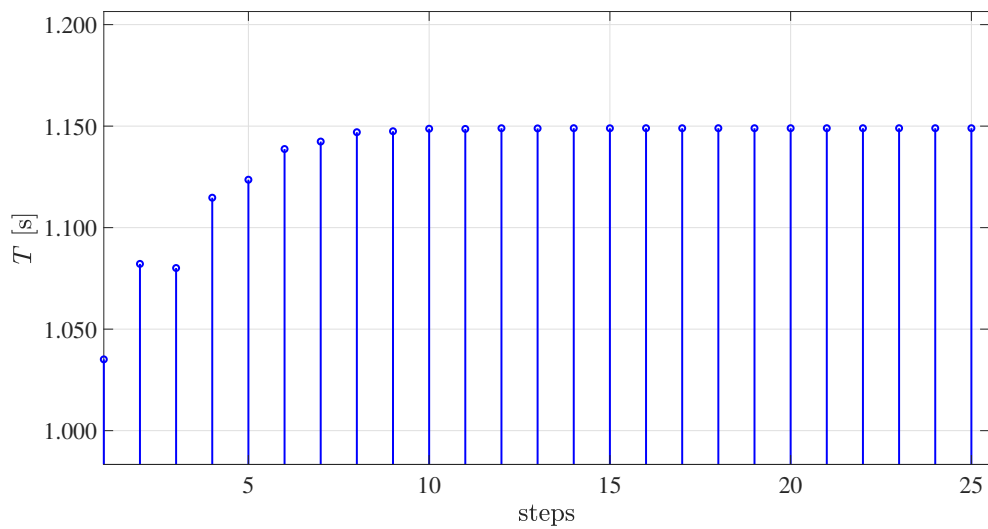
(a) Event history of S .(b) Event history of T .

Figure 6.2: Event histories of the step length and the step period during Case Study I ($\gamma(q_1)$ as in (6.13) and $a_{11}(q)$ as in (6.14)).

6.6.2 Case Study II: Large Gait Generation Via IDA-PBC With Explicit Solution Of PDEs

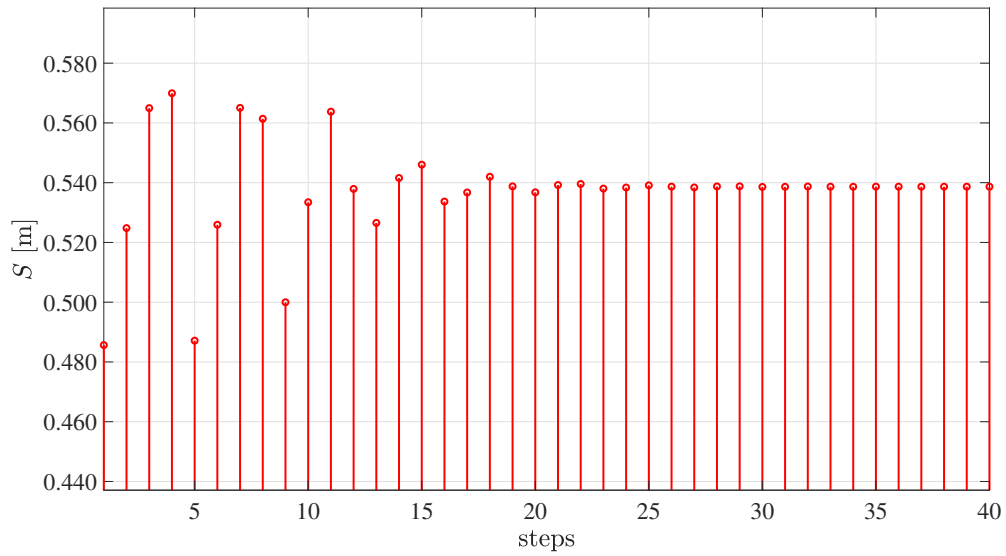
A large gait is achieved by designing the controller (A.13) as shown in Section 6.2 with $\gamma(q_1)$ as in (6.2) and $a_{11}(q)$ as in (6.8) and gains $k_2 = 0.8$, $k_3 = 1.1$, $k_4 = 0.9$ and $k_d = 0.0$, which fulfill again (6.11). The simulation, as for Case Study I, lasts for 30 s. Figure 6.3 depicts the step length S and the step period T which asymptotically converge to values 0.5387 m and 0.7322 s, which are respectively bigger and smaller than the parameters S and T characterizing the passive gait.

Complementary to previous test, the same controller is designed with $\gamma(q_1)$ as in (6.13) and $a_{11}(q)$ as in (6.14). For this task, $f_5(q) = \sin(q_1 - q_2)$ which transforms (6.14) into

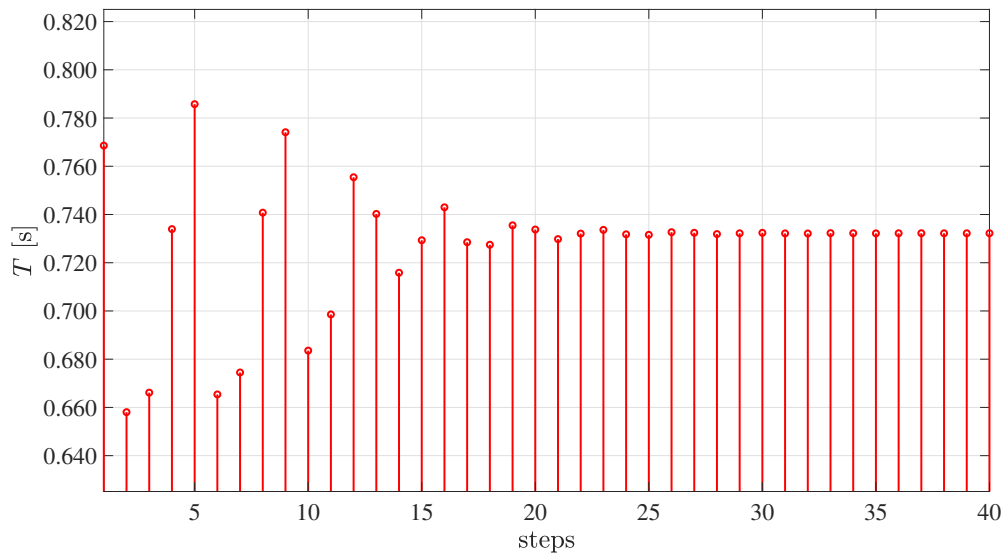
$$a_{11}(q) = k_4 \frac{k_5 b_{11} b_{22} - b_{12}(q)^2 (k_5 - k_7 \sin(q_1 - q_2))}{\Delta(k_6(b_{11} b_{22} - b_{12}(q)^2) + k_7 \sin(q_1 - q_2) b_{22})}, \quad (6.34)$$

where the selected gains ensuring **C.1** ([2]) are $k_2 = 1.7$, $k_3 = 1$, $k_4 = 0.588$, $k_5 = b_{11} = 16.25$, $k_6 = 1$, $k_7 = 6.2$, and $k_d = 0$. The simulation shows the generation of a symmetric gait characterized by $S = 0.8738$ m and $T = 0.6806$ s, as depicted in Figure 6.4. This gait is faster than the one in [16], characterized by $S = 0.7784$ m and $T = 0.7118$ s.

Figure 6.5 shows the comparison between the large limit cycle generated using the controller (A.13) with $\gamma(q_1)$ as in (6.13) and $a_{11}(q)$ as in (6.14) and the limit cycle obtained through CL method, where it is visible that the area of the cycle limit obtained through CL is almost totally contained by the area of limit cycle generated by the proposed IDA-PBC approach.

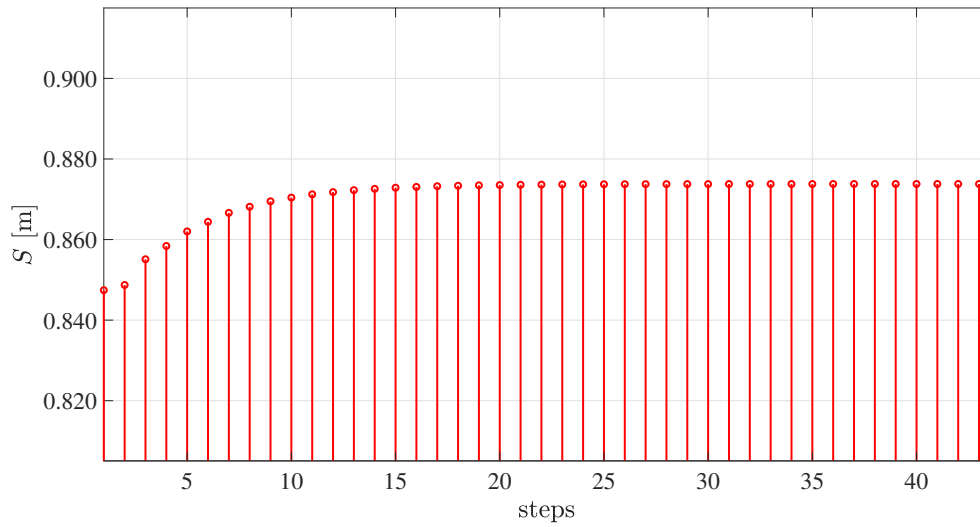


(a) Event history of S .

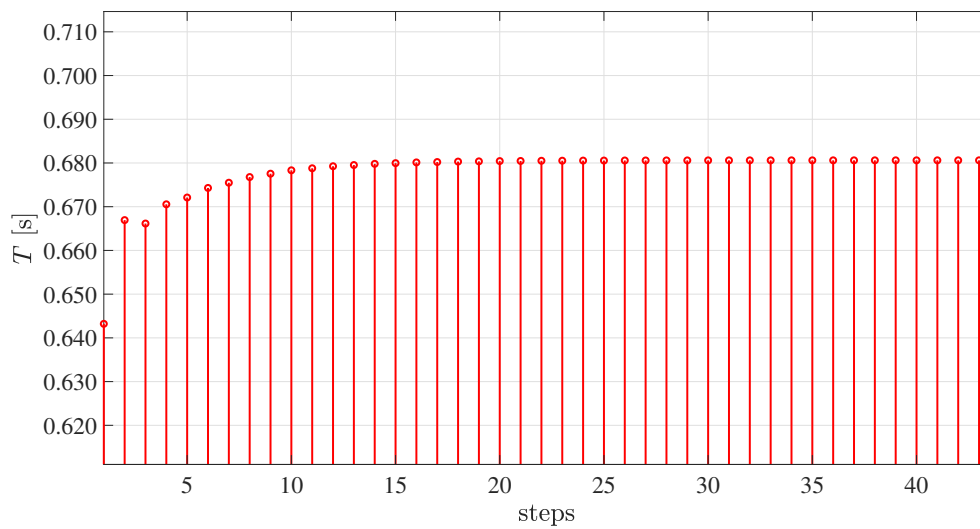


(b) Event history of T .

Figure 6.3: Event histories of the step length and the step period during Case Study II ($\gamma(q_1)$ as in (6.2) and $a_{11}(q)$ as in (6.8)).



(a) Event history of S .



(b) Event history of T .

Figure 6.4: Event histories of the step length and the step period during Case Study II ($\gamma(q_1)$ as in (6.13) and $a_{11}(q)$ as in (6.14)).

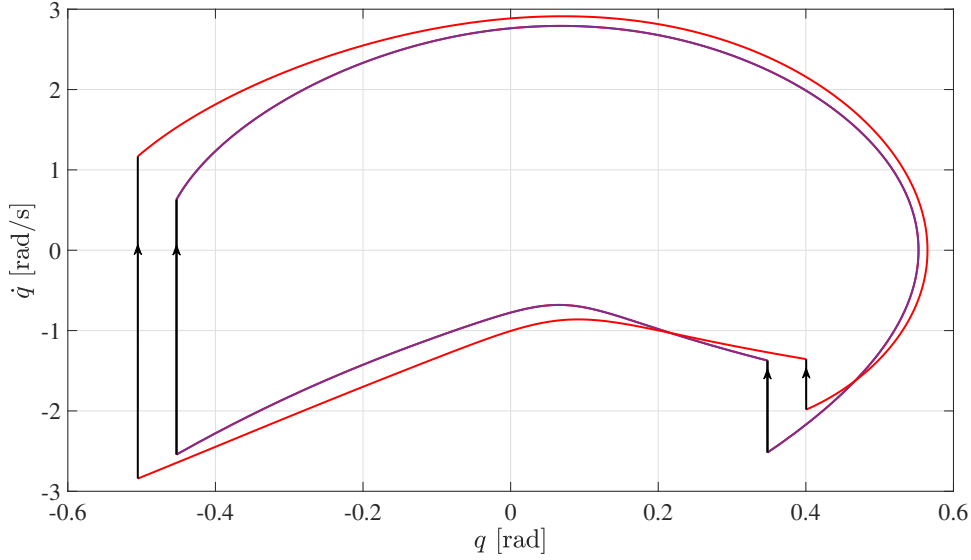


Figure 6.5: Limit cycles comparison during Case Study II. In red, the limit cycle generated with the proposed IDA-PBC. In purple, the limit cycle generated using CL. In black, the discontinuities occurring at impacts. The arrows indicate the time evolution.

The proposed controller is robust to parametric uncertainties. It is designed on the nominal values of the dynamic parameters, while the ODE45 function simulating the system dynamics sees an increment of 10% for the masses and the lengths of the CBR. A different, but symmetric, gait is generated with the same gains which lead to $T = 0.6806$ s and $S = 0.8738$ m in nominal conditions. The event histories of gait parameters, shown in Figure 6.6, testify the robustness of the approach. Figure 6.7 shows that the gait is symmetric and that it is very close to the gait obtained in case of perfect knowledge of the dynamic parameters. Figure 6.8 represents the comparison between the limit cycles associated respectively to the small gait (blue), the passive gait (green), and the large gait (red), the former and the latter generated with the controller (A.13) with $\gamma(q_1)$ as in (6.2) and $a_{11}(q)$ as in (6.8). As a consequence of the designs proposed in Case Study I and Case Study II, the small-gait limit cycle is enclosed by the passive limit cycle, which is, in turn, contained by the large-gait limit cycle.

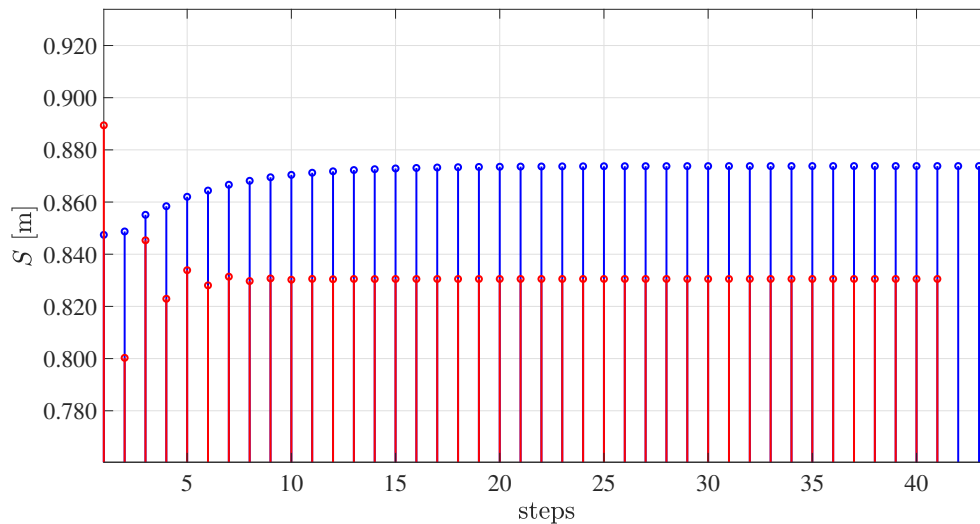
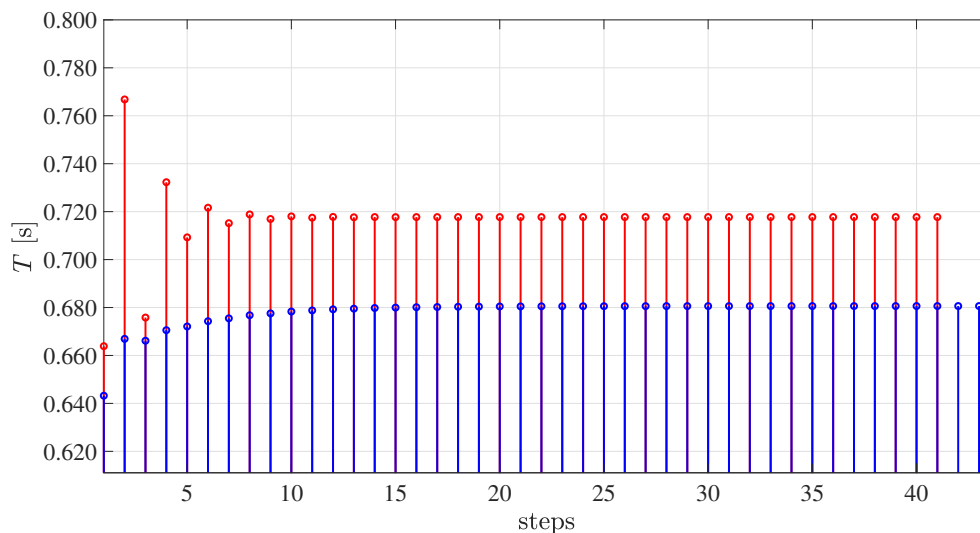
(a) Event history of S .(b) Event history of T .

Figure 6.6: Event histories of step length and step period during Case Study II with a 10% uncertainty on both masses and lengths. In blue, the gait without any parametric uncertainty with the proposed IDA-PBC. In red, the same gait with uncertainty. The CBR with parametric uncertainty results to be slower since it performs 41 steps versus the 43 steps of the CBR without parametric uncertainty within the same simulation time.

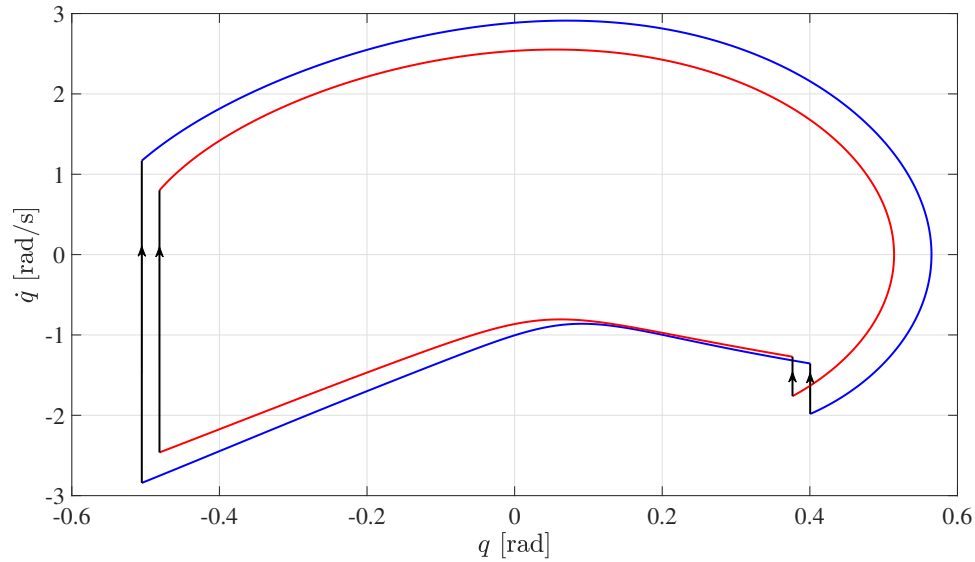


Figure 6.7: Limit cycles comparison during Case Study II. In blue, the gait generated with the proposed IDA-PBC, without any parametric uncertainty. In red, the gait generated with the same controller, in presence of parametric uncertainties.

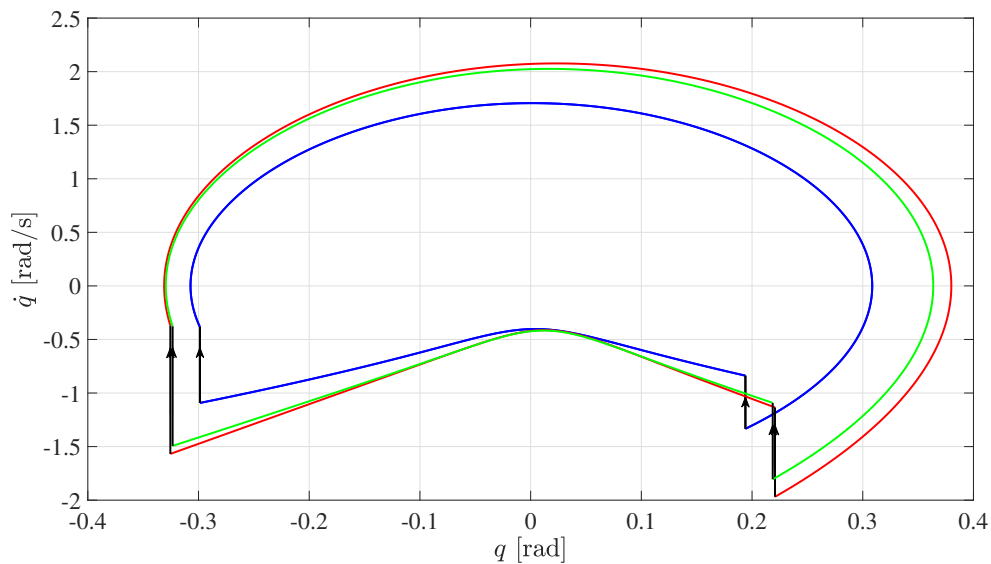


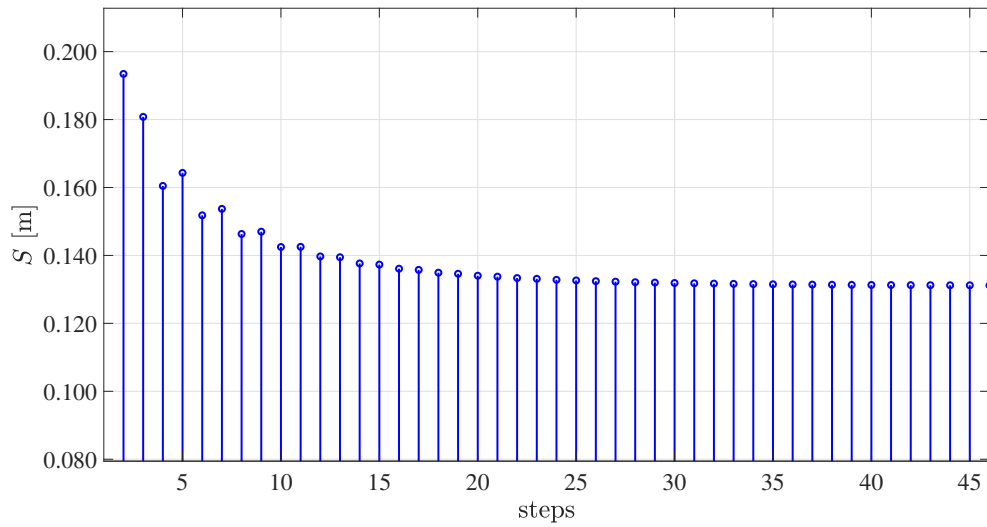
Figure 6.8: Limit cycles comparison. In green, the passive gait. In blue, the Case Study I. In red, the Case Study II.

6.6.3 Case Study III: Small Gait Generation via SIDA-PBC with Dissipative Forces

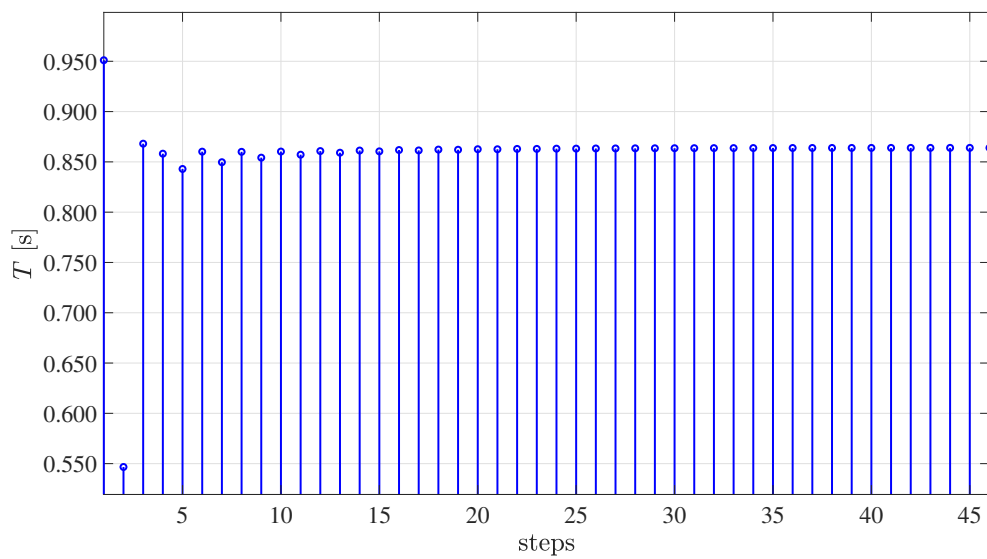
In order to generate the small gait, the controller (A.21) is designed as shown in Section 6.3 through the following set of gains $k_1 = -0.01$, $k_2 = -15$, $k_3 = 0.92$ experimentally tuned complying with **C.1**. The simulation is carried out for 40 s. The obtained gait has a very small step length $S = 0.1312$ m and a big step period $T = 0.8639$ s. The event histories of S and T are depicted in Figure 6.9.

6.6.4 Case Study IV: Large Gait Generation via SIDA-PBC with Dissipative Forces

In order to generate the large gait, the controller (A.21) is designed as shown in Section 6.3 through the following set of gains $k_1 = -0.15$, $k_2 = 0$, $k_3 = 0$, experimentally tuned complying with **C.1**. The simulation, as for Case Study III, lasts for 40 s. The obtained gait has a bigger step length, $S = 0.6084$ m, and a smaller step period, $T = 0.7144$ s, than the passive gait. The event histories of S and T are depicted in Figure 6.10. The comparison of the obtained limit cycles in the third and the fourth case studies with the passive gait is depicted in Figure 6.11.

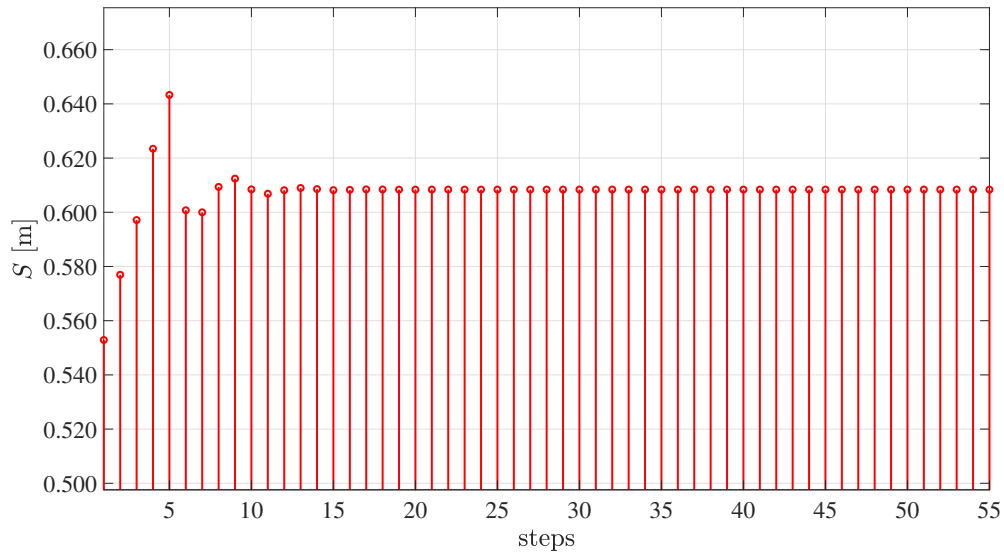


(a) Event history of S .

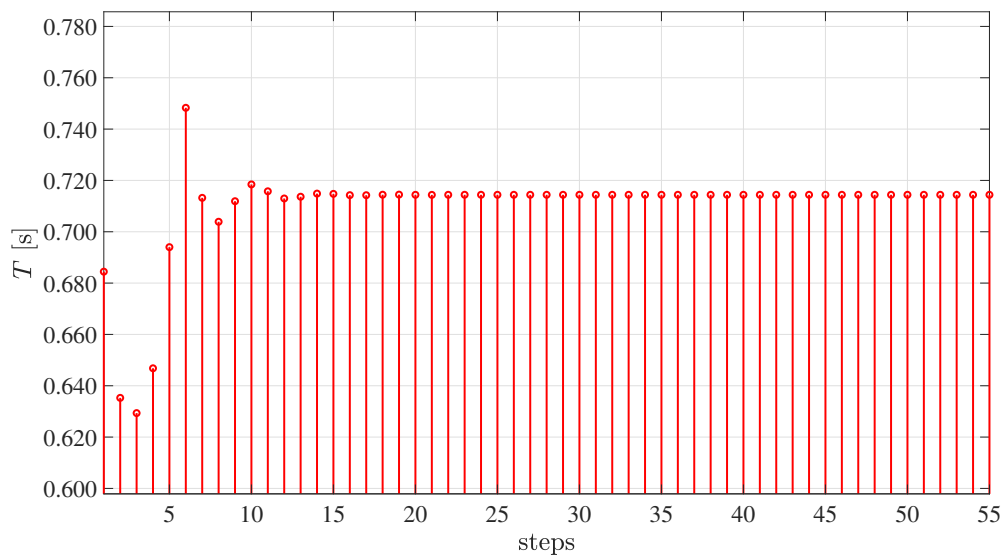


(b) Event history of T .

Figure 6.9: Event histories of the step length and the step period during Case Study III.



(a) Event history of S .



(b) Event history of T .

Figure 6.10: Event histories of the step length and the step period during a Case Study IV.

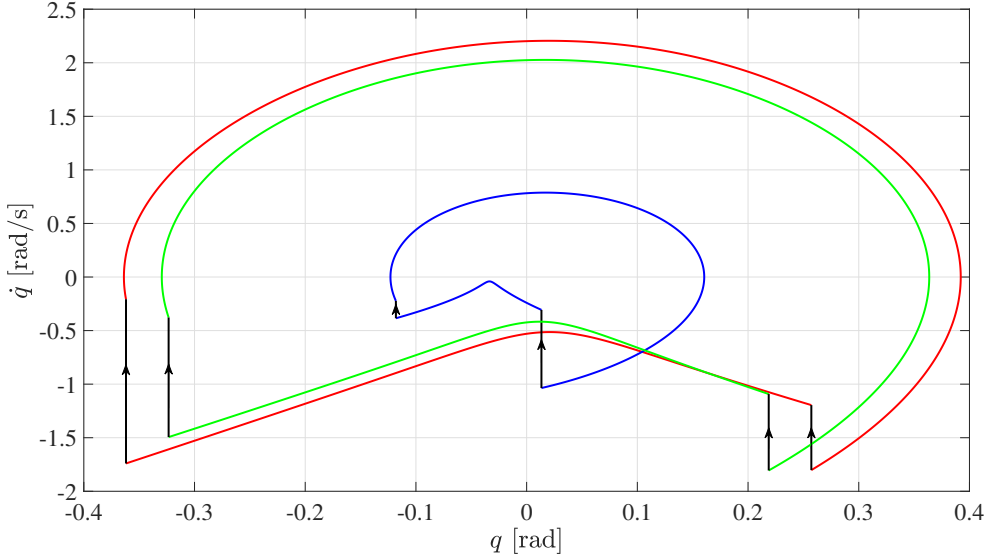


Figure 6.11: Limit cycles comparison. In green, the passive gait. In blue, the Case Study III. In red, the Case Study IV.

6.6.5 Case Study V: Small Gait Generation via EPD-PBC

In order to generate the small gait, the controller (6.29) is designed as shown in Section 6.4 with $k_{pd} = -30$. The simulation is carried out for 40 s. The offset ζ has been experimentally tuned to $\frac{\pi}{24}$ rad, leading to a controller which exhibits gaits that are comparable with the others presented in this thesis. The obtained gait has a smaller step length, $S = 0.4899$ m, and a bigger period, $T = 0.7418$ s, than the passive one. The event histories of S and T are depicted in Figure 6.12.

6.6.6 Case Study VI: Large Gait Generation via EPD-PBC

In order to generate the large gait, the controller (6.29) is designed as shown in Section 6.4 with $k_{pd} = 30$. The simulation, as for Case Study V, lasts for 40 s. The offset ζ , as for Case Study V, has been experimentally tuned to $\frac{\pi}{24}$ rad. The obtained gait has a bigger step

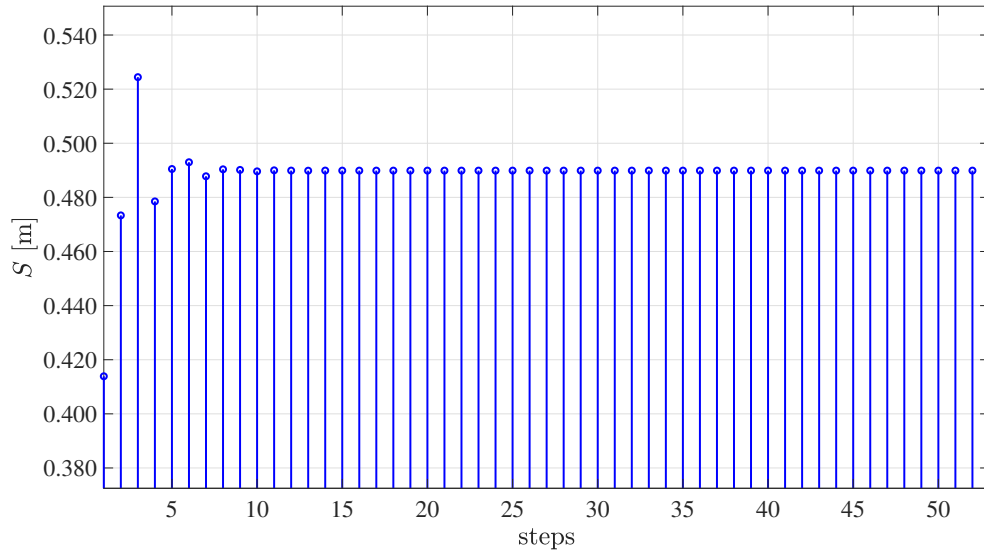
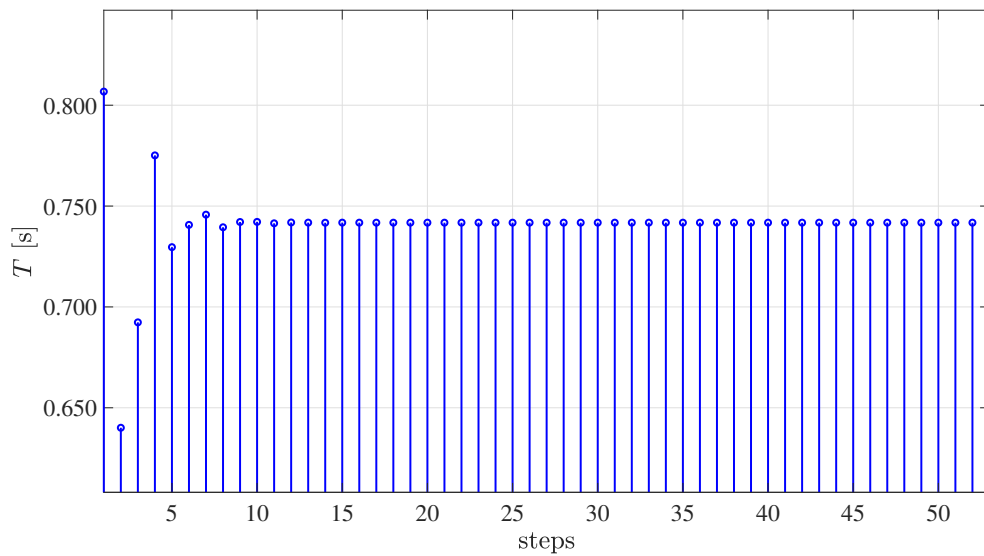
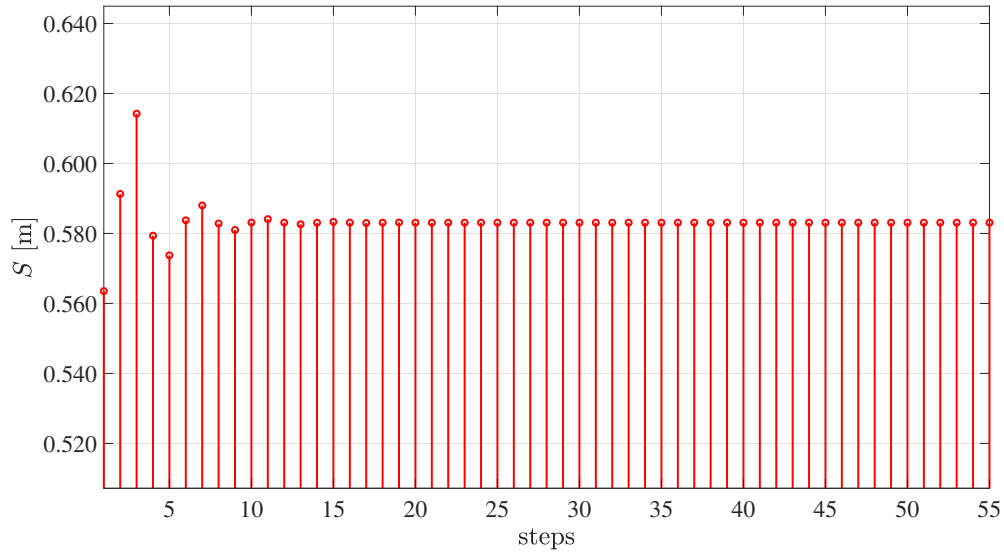
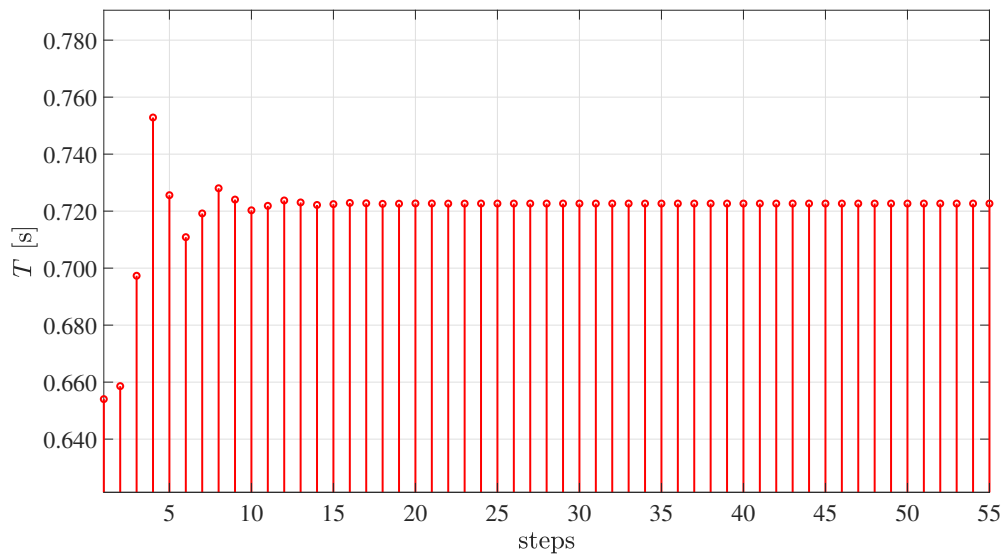
(a) Event history of S .(b) Event history of T .

Figure 6.12: Event histories of the step length and the step period during Case Study V.

length, $S = 0.5831$ m, and a smaller step period, $T = 0.7227$ s, than the passive one. The event histories of S and T are depicted in Figure 6.13.



(a) Event history of S .



(b) Event history of T .

Figure 6.13: Event histories of the step length and the step period during Case Study VI.

The comparison of the limit cycles obtained in the fifth and sixth case studies with the passive gait is depicted in Figure 6.14.

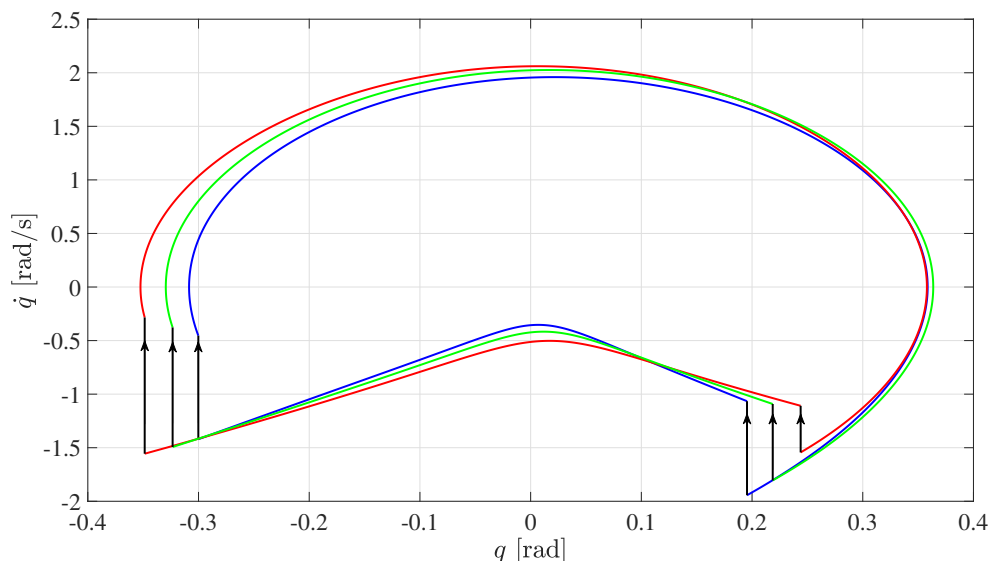


Figure 6.14: Limit cycles comparison. In green, the passive gait. In blue, the Case Study V. In red, the Case Study VI.

6.6.7 Case Study VII: Small Gait Generation via EPOD-PBC

In order to generate the small gait, the controller (6.30) is designed as shown in Section 6.5 through the gain $k_{pd} = -280$. The simulation is carried out for 40 s. The obtained gait has a small step length $S = 0.4399$ m and a large step period $T = 0.7457$ s. The event histories of the step length S and the period T are depicted in Figure 6.15.

6.6.8 Case Study VIII: Large Gait Generation via EPOD-PBC

In order to generate the large gait, the controller (6.30) is designed as shown in Section 6.5 through the gain $k_{pd} = 160$. The simulation, as for Case Study VII, lasts for 40 s. The obtained gait has a bigger step length, $S = 0.6394$ m, and a smaller step period, $T = 0.7286$ s, than the passive gait. The event histories of the step length S and the step period T are depicted in Figure 6.16. The limit cycles obtained in

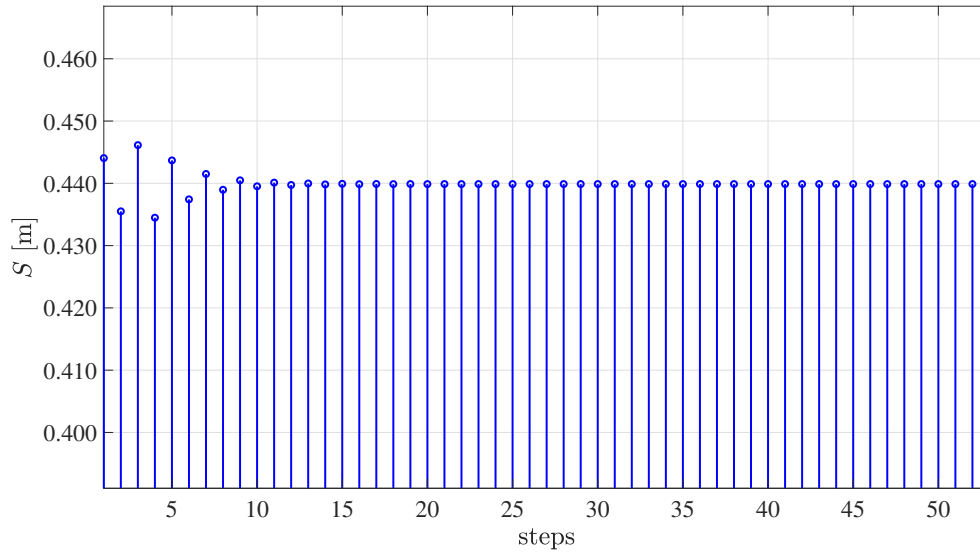
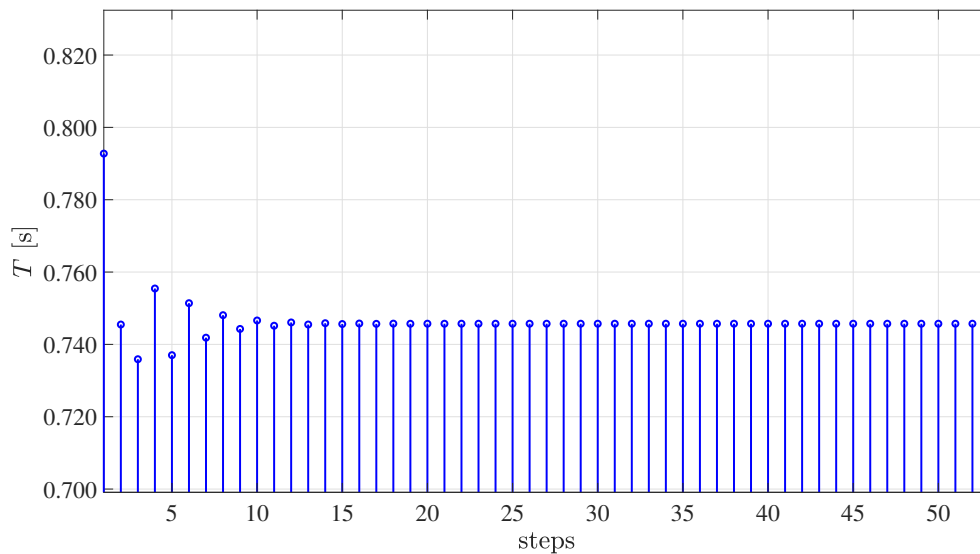
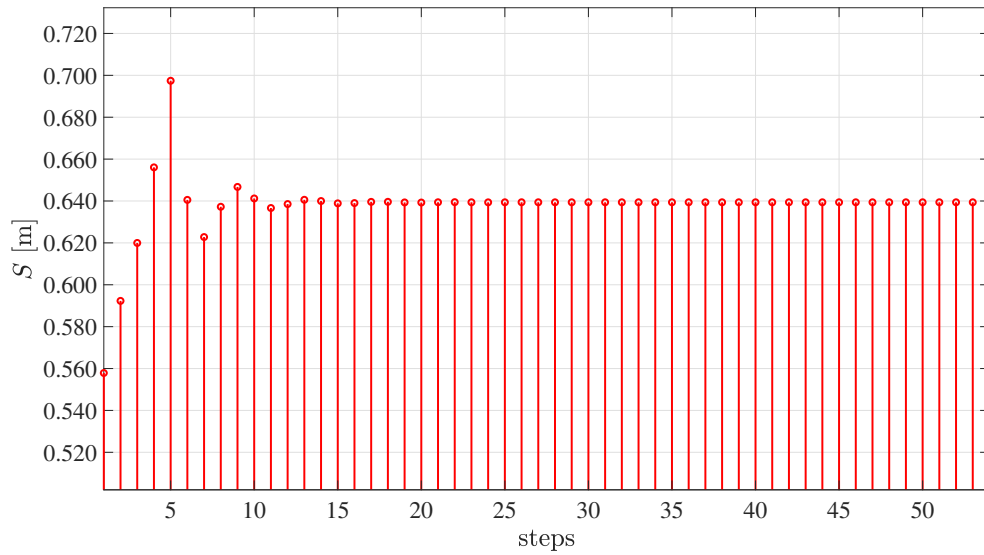
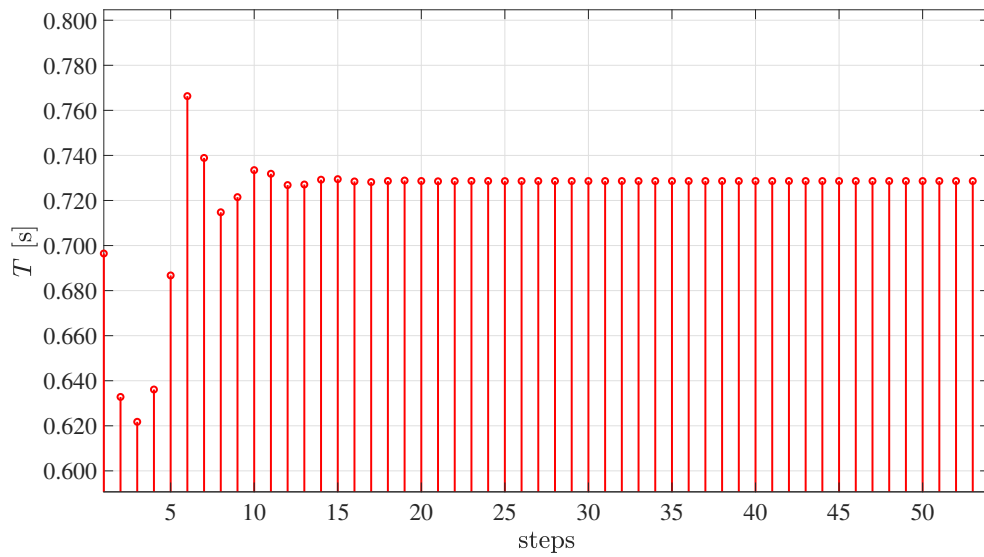
(a) Event history of S .(b) Event history of T .

Figure 6.15: Event histories of the step length and the step period during Case Study VII.

these two last examined case studies are compared with the passive gait within Figure 6.17.



(a) Event history of S .



(b) Event history of T .

Figure 6.16: Event histories of the step length and the step period during Case Study VIII.

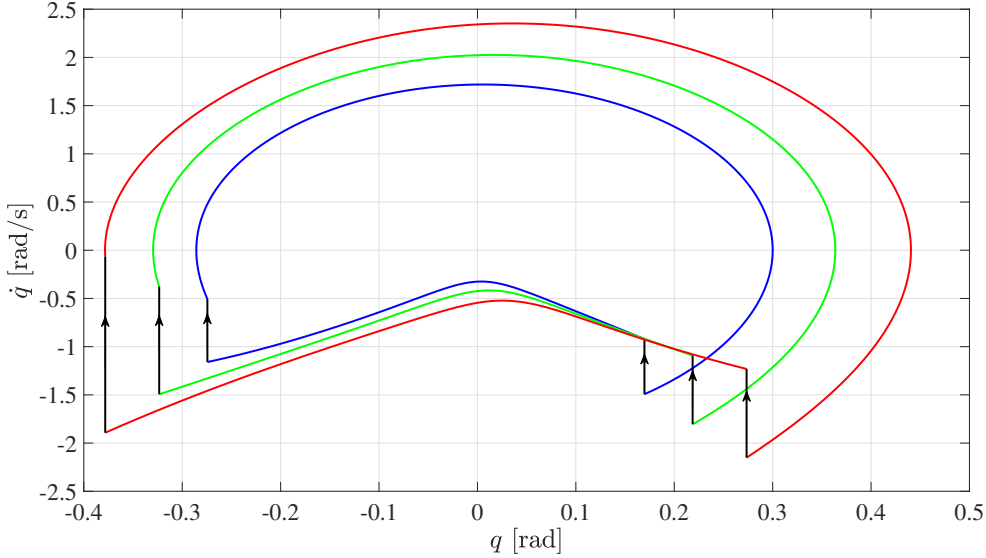


Figure 6.17: Limit cycles comparison. In green, the passive gait. In blue, the Case Study VII. In red, the Case Study VIII.

6.7 Performance Comparison

The comparisons depicted in Figure 6.8, Figure 6.11, Figure 6.14, and Figure 6.17 between the limit cycles relative to all the case studies and the passive gait, as well as the event histories of the parameters S and T depicted in Figure 6.3, Figure 6.10, Figure 6.13, and Figure 6.16, show that all the controllers are comparable with respect to the generation of gaits larger than the passive one. For what concerns those methods based on dissipative forces in particular, the EPOD can increase the step length of the passive gait of ≈ 0.1 m ($\approx +20\%$), versus the ≈ 0.07 m ($\approx +15\%$) of the SIDA-PBC, and the ≈ 0.05 m ($\approx +10\%$) of the EPD. The maximum period decrease among methodologies based on dissipative forces is of ≈ 0.02 s ($\approx -3\%$), obtained by employing the SIDA-PBC. Performance of IDA-PBC are strongly influenced by the choice of $\gamma(q_1)$ and $a_{11}(q)$, *i.e.*, by the desired inertia matrix. IDA-PBC increases the step length of the passive gait of ≈ 0.004 m ($\approx +0.75\%$) of with $\gamma(q_1)$ as in (6.2) and $a_{11}(q)$ as in (6.8) whereas designing $\gamma(q_1)$ as in (6.13) and $a_{11}(q)$ as in (6.14) leads to an increase of ≈ 0.34 m

($\approx +65\%$) which represents the biggest step increment achieved in the numerical simulation carried out in the thesis. In the same time, IDA-PBC with such a choice of $\gamma(q_1)$ and $a_{11}(q)$ leads to the maximum period decrease experienced during simulations, which is of ≈ 0.05 s ($\approx -7\%$).

On the other hand, the blue limit cycles in Figure 6.8, Figure 6.11, Fig. 6.14, and Fig. 6.17 show that IDA-PBC is more effective in creating narrow limit cycles compared to the SIDA-PBC, EPOD-PBC, and the EPD-PBC. This is certified by the event histories in Figure 6.2 which shows that the IDA-PBC can produce stable gaits with the smallest step length, $S = 0.0417$ m ($\approx -92\%$ compared to the passive step length), and the biggest time period, $T = 1.149$ s ($\approx +100\%$ compared to the passive step period), than the others. Comparable results are achievable using SIDA-PBC, which leads to a small limit cycle with $S = 0.1312$ m ($\approx -75\%$ compared to the passive step length) and $T = 0.8639$ s ($\approx +20\%$ compared to the passive step period).

Summarizing, all the methodologies proposed in this work can produce new gaits characterized by a simultaneous increment of S and reduction of T or vice-versa, in the same biomimetic fashion as the approaches proposed in [16] and [49]. Total energy shaping has proved to be worth being exploited to generate both large and small gaits, compared to kinetic-energy shaping only methods. In particular, IDA-PBC can go beyond CL in generating large gaits, as manifest in Figure 6.5. Besides, comparing the results of this work with those achieved in [49], where a partial IDA-PBC approach without potential energy shaping is employed, emerges that adding the potential energy shaping stage has beneficial effects in the generation of small gaits. The smallest gait generated in [49], using IDA-PBC reduced to kinetic energy shaping only, has $S = 0.2012$ m and $T = 0.9996$ s as parameters, while the values exhibited by the total energy shaping, achieved using the proposed version of IDA-PBC, are $S = 0.0417$ m and, $T = 1.149$ s. Therefore, differently from the approaches presented in [16] and [49], the former being more suitable to generate large gaits whereas the latter being more appropriate to create small ones, the IDA-PBC proposed in this thesis can be exploited indifferently to face both large

and small gait generation, showing performance that surpasses past methodologies. Furthermore, the stumbling block which usually prevents standard IDA-PBC to be widely applied, that is, the solution of PDEs, has been partially removed, thus extending the range of applicability of the proposed method. Moreover, if the sought goal is to generate gaits spreading from very small to large ones, SIDA-PBC with dissipative forces seems to represent a good alternative to IDA-PBC, especially if compared to other control strategies based on the exploitation of dissipative forces, such as EPD-PBC and EPOD-PBC.

The gait parameters arising from the application of the different control policies deployed in this chapter have been collected in Table 6.2 to help compare the performance of the total energy shaping methodologies and the kinetic energy shaping ones available in the literature.

Table 6.2: Comparison between step length values (S) and step period values (T) obtained carrying out simulations of the CBR model. In green, no control action (passive gait). In blue, the total energy shaping approaches proposed in this thesis (both small and large gait). In red, the kinetic energy shaping methodologies referenced in this chapter [16] (large gait), [49] (small gait).

controller	passive gait	small gait	large gait
no	$S = 0.5347 \text{ m}, T = 0.7347 \text{ s}$	-	-
IDA-PBC	-	$S = 0.4871 \text{ m}, T = 0.7854 \text{ s}$	$S = 0.5387 \text{ m}, T = 0.7322 \text{ s}$
IDA-PBC	-	$S = 0.0417 \text{ m}, T = 1.1490 \text{ s}$	$S = 0.8738 \text{ m}, T = 0.6806 \text{ s}$
SIDA-PBC	-	$S = 0.1312 \text{ m}, T = 0.8639 \text{ s}$	$S = 0.6084 \text{ m}, T = 0.7144 \text{ s}$
EPD-PBC	-	$S = 0.4899 \text{ m}, T = 0.7418 \text{ s}$	$S = 0.5831 \text{ m}, T = 0.7227 \text{ s}$
EPOD-PBC	-	$S = 0.4399 \text{ m}, T = 0.7457 \text{ s}$	$S = 0.6394 \text{ m}, T = 0.7286 \text{ s}$
CL [16]	-	-	$S = 0.7784 \text{ m}, T = 0.7118 \text{ s}$
IDA-PBC [49]	-	$S = 0.2012 \text{ m}, T = 0.9996 \text{ s}$	-

Chapter 7

Energy Shaping for Gait Robustification

Conservation of energy is the physical principle that motivates passive dynamic walking [17, 53]. Consequently, a limit cycle can be regarded as an energy-conserving orbit corresponding to a specific mechanical energy value $E^* \in \mathbb{R}$ [17, 22, 23, 47, 53]. One of the main drawbacks of limit cycle walking is that finding the correct set of initial conditions such that the system converges to the limit cycle is hard. From an alternative point of view, initial conditions related to a limit cycle are extremely sensitive to perturbations. The objective of this chapter is to provide a methodology to extend the range of possible initial conditions leading to periodic walking, *i.e.*, to enlarge the basin of attraction of a given limit cycle. As shown in [22], one possible approach is to build an output variable, namely

$$e = E(x) - E^*, \quad (7.1)$$

with $E(x) \in \mathbb{R}$ the energy of the system. Suppose that the system has been written in the hybrid zero dynamics form, as in [22]. If the output dynamics \dot{e} converge exponentially fast to zero, then, based on results about HZD for planar bipeds [66, 67], the set of states such that $e = 0$ and $\dot{e} = 0$ constitute an hybrid invariant zero dynamics manifold. Such states are those for which $E(x) = E^*$, hence the system has been exponentially stabilized at the energy level E^* with the beneficial effects

that its basin of attraction has been enlarged, as illustrated in [22]. To prove stability for the overall system, Poincaré maps are proposed in [22]. One drawback of employing such a method is that it recasts stability analysis as a standard equilibrium stabilization problem, leading to very conservative results, as explained in [24]. Conversely, it is more useful to exploit the notion of stability of an invariant set, which is the closed orbit associated with the periodic solution [24, 87]. Poincaré maps require linearizing the system at the fixed point. Hence, they only hold locally in a neighborhood of the point, in contrast with the target of the paper that is the enlargement of the basin of attraction of the periodic solution. In contrast, invariant-set theorems led to global or almost-global stability results [88]. In the previous chapter, EPD-PBC has been exploited to accomplish a gait generation task. In the current chapter, EPD-PBC is designed to enlarge the basin of attraction of the gait exhibited by the CBR, going beyond the approach presented in [22], in the sense that it yields less conservative stability results based on invariant-set theory.

Remark. *In order to ensure consistency with the other chapters of this thesis, results in this chapter have been particularized for 2-DoF mechanical systems. However, it should be noted that they can be easily extended to systems with a number of DoFs greater than two.*

7.1 EPD-PBC Design within HZD Formulation

As shown in [4], EPD-PBC can be adequately expressed to take into account HZD formulation. To achieve gait robustification, differently from Section 6.3, where the scalar $e(x)$ is defined in order to comply with (6.28), in this context $e(x)$ is designed such that

$$e(x) = \begin{cases} e_1(x) = 0 & \text{if } x \in Z, \\ e_2(x) \neq 0 & \text{if } x \in \mathbb{R}^4 - Z. \end{cases} \quad (7.2)$$

Besides, $e(x)$ is selected as the output variable of the hybrid mechanical system (3.18). From now on, the dependency on x in e is omitted to shorten the notation. To enlarge the basin of attraction of the limit cycle related to a certain gait, exponential stabilization to an invariant level set of the total mechanical energy of the system has to be achieved. Such a Hamiltonian value, namely $H^* \in \mathbb{R}$, is the one corresponding to the limit cycle, constant due to the principle of conservation of energy. Suppose that (3.18) already exhibits a stable periodic gait. The choice

$$e = H(x) - H^*, \quad (7.3)$$

which is similar to (7.1), meets (7.2) and realizes the sought goal, that is, e exponentially converge to zero implying that the system (3.18) is stabilized at H^* despite impacts, as it will be demonstrated in the next sections.

The hybrid system (3.18) with control input given by (A.27) and output variable (7.3) becomes

$$\Sigma_{zd} = \begin{cases} \dot{x} = f(x) + g(x)u_{pd}(x, e) & (x, e) \in X \setminus S, \\ \dot{e} = r(x) + w(x)u_{pd}(x, e) & (x, e) \in X \setminus S, \\ x^+ = \Delta(x^-) & (x^-, e^-) \in S, \\ e^+ = \Delta(e^-) & (x^-, e^-) \in S. \end{cases} \quad (7.4)$$

with $f(x) = J(x)\nabla H(x)$, $r(x) = \nabla_x H(x)^T J(x)\nabla_x H(x)$, $g(x) = G(x)$, and $w(x) = \nabla_x H(x)^T G(x)$ which are assumed to be locally continuous Lipschitz functions. Moreover, as consequence of (7.3), the sign of the pumping-and-damping matrix $R_{pd}(x)$ (A.26) changes accordingly to the actual value of the Hamiltonian $H(x)$ respect to the target value H^* . Conversely, if $k_{pd} < 0$, then the following condition

$$R_{pd}(x)e = G_p(q)k_{pd}G_p^T(q)e^2 \leq 0, \quad (7.5)$$

always holds true.

7.2 Zero Dynamics Stability Analysis

The goal of this section is to show that, through (A.27), the zero dynamics submanifold is both forward invariant and attractive, and that the closed-loop system (7.4) is exponentially stable to it.

Firstly, assume that Z is the largest invariant set in the set

$$\{x \in X \mid \nabla_x^T H(x) R_{pd}(x) \nabla_x H(x) e = 0\}. \quad (7.6)$$

To prove exponential stability of the closed-loop system respect to Z , the storage function

$$V(e) = \frac{1}{2} e^2 \geq 0, \quad (7.7)$$

positive everywhere except for $e = 0$, is selected. The output variable e constitutes an isolated minimum for the storage function $V(e)$ in the zero dynamics submanifold Z , that is

$$\begin{aligned} \nabla_e V(e)|_{x \in Z} &= e|_{x \in Z} = 0, \\ \nabla_e^2 V(e)|_{x \in Z} &= 1 > 0. \end{aligned} \quad (7.8)$$

Then, the time derivative of $V(e)$ is

$$\dot{V}(e) = \frac{\partial V(e)}{\partial e} \dot{e} = e \dot{e}, \quad (7.9)$$

while the time derivative of the output dynamics is

$$\begin{aligned} \dot{e} &= \dot{H}(x) - \dot{H}^* = \nabla_x H(x)^T \dot{x} = \\ &= \nabla_x H(x)^T (J(x) + R_{pd}(x)) \nabla_x H(x) = \\ &= \nabla_x H(x)^T R_{pd}(x) \nabla_x H(x) = \\ &= \nabla_p H(x)^T G_p(q) k_{pd} e G_p^T(q) \nabla_p H(x) \\ &= l(x) e, \end{aligned} \quad (7.10)$$

where $l(x) = \nabla_p H(x)^T G_p(q) k_{pd} G_p^T(q) \nabla_p H(x) \leq 0$ with $k_{pd} < 0$. Notice that $J(x)$ has been exploited to cancel out the related quadratic

term. Substituting (7.10) into (7.9) yields

$$\begin{aligned}\dot{V}(e) &= \nabla_p H(x)^T G_p(q) k_{pd} e^2 G_p^T(q) \nabla_p H(x) = \\ &= 2l(x) \frac{1}{2} e^2 = 2l(x) V(e) \leq 0.\end{aligned}\quad (7.11)$$

Relation (7.11) with (7.8) proves the exponential stability of (7.4) with respect to Z . Given (7.8), the following holds

$$\nabla^T H_x(x) R_{pd}(x) \nabla H_x(x) e|_{x \in Z} = 0. \quad (7.12)$$

Attractivity of Z is proved applying LaSalle's invariance principle, taking into account (7.11) and assumption (7.6).

To prove the forward invariance of Z , the restriction of the transverse dynamics to the zero dynamics submanifold must be considered

$$\dot{e}|_{x \in Z} = r(x)|_{x \in Z} + w(x) u_{pd}(x, e)|_{x \in Z}. \quad (7.13)$$

Since $e = 0$ in Z , then $u_{pd}(x, 0)|_{x \in Z} = 0$. Besides, since $\dot{e} = \dot{H}(x)$, equation (7.13) can be rewritten as $\dot{H}(x)|_{x \in Z} = r(x)|_{x \in Z}$. Since the mechanical energy is constant during swing dynamics due to the absence of dissipation, then $\dot{e}|_Z = \dot{H}(x)|_Z = 0$ holds, proving the forward invariance of Z which, now, can be profitably defined as

$$Z = \{x \in X | e = 0, \dot{e} = 0\}. \quad (7.14)$$

Finally, hybrid invariance is automatically achieved in (7.10), where output dynamics convergence exponentially fast to Z , under the control law (A.27). Moreover, the exponential rate of convergence can be adjusted by profitably tuning the gain k_{pd} in $l(x)$.

The benefits of such results are twofold.

1. Suppose that a limit cycle exists and it is a periodic solution of the zero dynamics. In that case, if the related mechanical energy belongs to the zero dynamics submanifold, its stability is automatically guaranteed by using the stability theory of invariant sets, rather than Poincaré map analysis [87].

2. The stability of the closed-loop system restricted to the zero dynamics is the prerequisite to guarantee the stability of the closed-loop system's full-order dynamics.

7.3 Full Dynamics Stability Analysis

The results of the previous section hold only for the hybrid zero dynamics and the associated submanifold. Once that exponential stability of a periodic solution is guaranteed, and that such property is valid under continuous and discrete dynamics, such a result must be transferred to the full order system, *i.e.*, system (7.4) not restricted to Z . Since (7.4) meets the hypotheses outlined in [69], it is possible to conclude that the exponential stability of a periodic orbit belonging to the hybrid restriction dynamics implies the exponential stability of the same periodic orbit for the full-order system (for the detailed demonstration, see [69]). In particular, the following conditions must be verified:

- FS.1** for Z in (7.14), $S \cap Z$ is a $(2n - 1)$ dimensional hybrid invariant submanifold of Z ;
- FS.2** system (7.4) has a exponentially stable periodic orbit O contained in Z , which is transverse to the reset map S ;
- FS.3** the storage function $V(e)$ is positive definite locally around the orbit O , it decreases during swing dynamics as showed in (7.11), and its value is zero on the orbit;
- FS.4** if the scalar e is measured right after any impact and it is defined as e_i , where i stands for the $i - th$ impact event, then the sequence of the storage functions $V(e_i)$, evaluated at every impact, is decreasing.

The first condition is true because Z is a hybrid invariant submanifold. **FS.2** and **FS.3** above are satisfied if the energy value of a given periodic orbit O , transverse to S by hypothesis, belongs to Z , as demonstrated in (7.11). Finally, since an uncontrolled passive walker

dissipates kinetic energy at every impact (supposed perfectly inelastic), while mechanical energy is constant during swing dynamics, $H(x)$ decreases to the passive value at every foot strike. When the biped is controlled using $u_{pd}(x)$ in (A.27) with e in (7.3), the only effect is in the swing phase, where $V(e)$ exponentially decreases to zero as pointed out in (7.11). Hence, summing the dissipation during the continuous dynamics, achieved via control, and the dissipation naturally taking place at discrete events, the consequence is that $V(e_i)$ constitutes a decreasing sequence of values.

7.4 Numerical Evaluation

The current section aims to demonstrate the effectiveness of the designed controller for the CBR in enlarging the basin of attraction of existing gaits. The nominal dynamic parameters chosen for the CBR are $m_H = 10$ kg, $m = 5$ kg, $a = 0.5$ m, $b = 0.5$ m, $g = 9.8$ m/s², and $\varphi = 3$ deg. The robot is underactuated with the control torque applied only at the hip joint.

Two case studies will be analyzed in the following. The objective is the robustification, with respect to perturbations on initial conditions, of the limit cycle, related to an already exhibited gait, whether it is the passive one or it has been generated via a preliminary energy-shaping approach, like those presented in Sections 6.2, 6.3, 6.4, and 6.5, for instances.

Tests are performed on a standard personal computer, using the Matlab *ODE45* routine together with the event detection option active, to evaluate the hits between the swing foot and the ground. The controller is implemented at a discrete-time step of 0.01 s. The simulations last 20 s. The average computation time of the controller is ≈ 0.12 ms with a standard deviation of ≈ 0.41 ms.

7.4.1 Case Study I: Passive Gait Robustification

In the first case study, only the EPD-PBC is applied, without any energy shaping, to test the performance in terms of robustification of the passive gait to perturbed initial conditions. Passive gait is exhibited by the CBR without control, starting by the initial conditions

$$x_P(0) = [0.2187, -0.3234, -1.0918, -0.3772]^T,$$

where the first two are generalized coordinates whereas the last two are generalized velocities, for the same reasons already explained in Section 6.6 for gait generation. Passive gait parameters are known to be $S_P = 0.5347$ m, $T_P = 0.7347$ s, $H_P = 153.0787$ J for the chosen CBR [23], where the last parameter is the constant value of the Hamiltonian associated with the passive limit cycle.

EPD-PBC enlarges the basin of attraction of the passive gait. Firstly, uniform perturbations on initial conditions have been considered. Three distinct sets of perturbed initial conditions were obtained multiplying x_{0P} by 0.8 (small perturbation), 0.7 (medium perturbation), and 0.6 (large perturbation), respectively [22]. The control gain for each initial condition has been experimentally tuned as $k_{pd} = -1$, $k_{pd} = -10.2$, and $k_{pd} = -8.4$, respectively.

Figure 7.1 shows the limit cycle in the phase plane of the controlled CBR starting from $0.6x_P(0) = [0.1312, -0.1940, -0.6551, -0.2263]^T$ with $k_{pd} = -8.4$. Both the part of the cycle related to the swing angle (blue line) and the one associated with the stance angle (green line) converge to the passive limit cycle (red line). The CBR recovers the passive gait after a large perturbation on the initial state thanks to EPD-PBC, which thus enlarges the basin of attraction of the passive limit cycle. The periodic motion associated with the first leg, which is the swing one at the beginning of the simulation, is depicted in Figure 7.2 (since the gait is symmetric, this figure holds for the other leg also, though with a different initial condition).

Figure 7.3 shows the convergence of the storage function $V(e)$ to zero. At every impact, the value of $V(e)$ is smaller than (or equal to) the value of the same function at the previous foot strike. This gives an

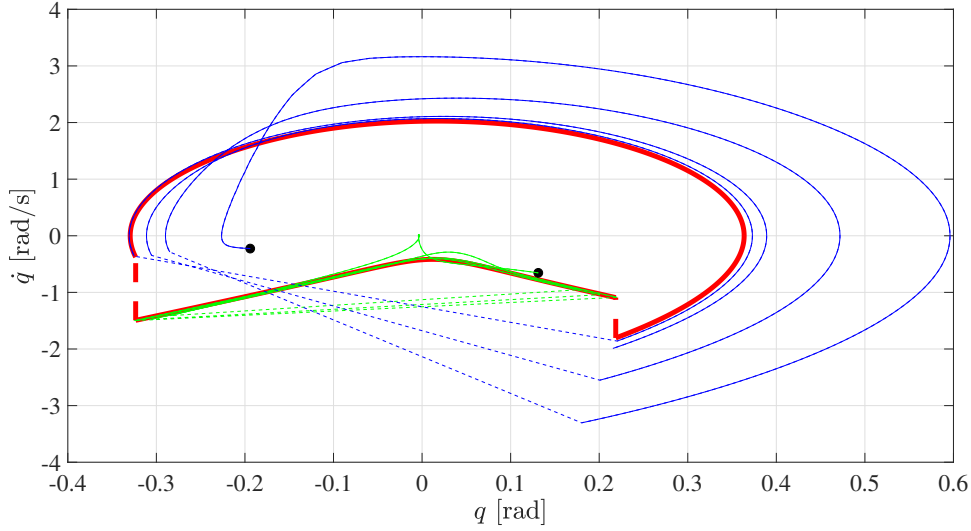


Figure 7.1: Limit cycle comparison during Case Study I. Red arcs represent the passive limit cycle. Green arc represents the component of the limit cycles relative to q_1 , while blue arc represents the component of the limit cycles relative to q_2 during a test carried out starting by perturbed initial conditions. Black dots represent initial conditions. Both green and blue arcs converge to red ones using EPD-PBC with $k_{pd} = -8.4$.

experimental confirmation that the passivity of the switched systems is the right hypothesis.

To further enlighten increment of robustness to initial conditions, nonuniform perturbations have been taken into account (*i.e.*, distinct perturbations on every component of $x_P(0)$ were considered). Ten further simulations have been carried out, each one starting from a different initial condition $x_{P_i}(0)$ with $i = 1, \dots, 10$ obtained multiplying $x_P(0)$ by as many diagonal matrices whose elements have been randomly computed to lie in the set $\{0.8, 0.7, 0.6\}$.

For the sake of comparison, the same initial conditions have been used to test performances of the min-norm control (MNC) employed in [22]. Results of simulations with EPD-PBC and MNC have been collected in TABLE 7.1, where *PG* indicates the passive gait while

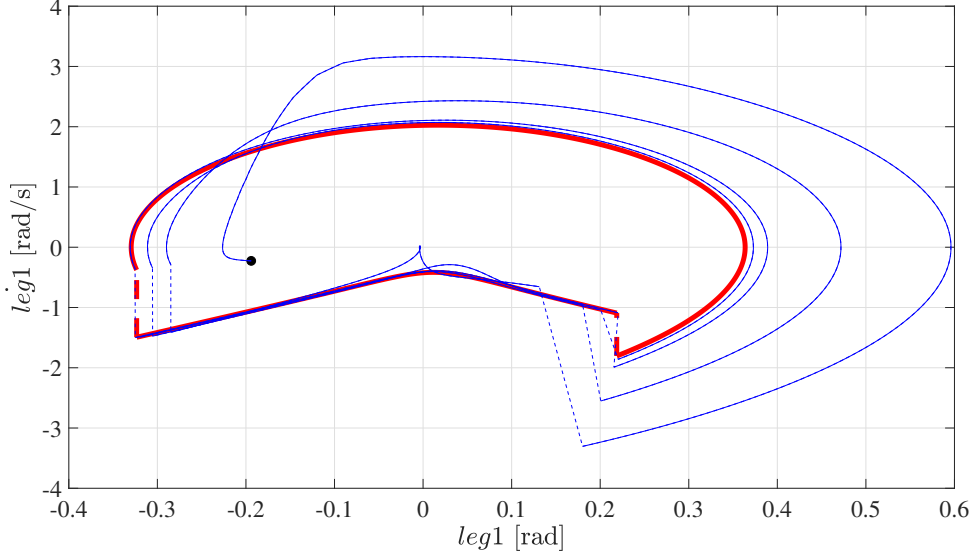


Figure 7.2: Limit cycles comparison for the first leg during Case Study I. Red arcs represent the passive limit cycle. Same legend and condition of Fig. 7.1 hold.

NG indicates a new gait characterized by $S_N = 0.5351 m$, $T_N = 0.7282 s$, and $H_N = 153.12 J$. Control gains have been firstly tuned to face uniform disturbances. Then, they have been tested in all ten simulations. Those reported in the table are the best ones for each methodology ($k_{mn} = c/\epsilon$ with $c = 1$ and $\epsilon = 0.5$, see [22] for further details).

By inspecting TABLE 7.1, it is clear that both methodologies increase CBR robustness to initial conditions. EPD-PBC is more suitable to increase the basin of attraction of the passive limit cycle, compared to MNC. The passive gait has been recovered in 4 out of 10 total trials, with $k_{pd} = -1$. On the other hand, MNC never succeeds to recover the passive limit cycle, as evident by the new gait created. MNC cannot enlarge the basin of attraction of the passive limit cycle for perturbations equal or greater than those considered in this paper. Another crucial aspect is that EPD-PBC avoids robot falling as many times as done by MNC. In conclusion, EPD-PBC exhibits the same performances of MNC in increasing the overall robustness, but it is

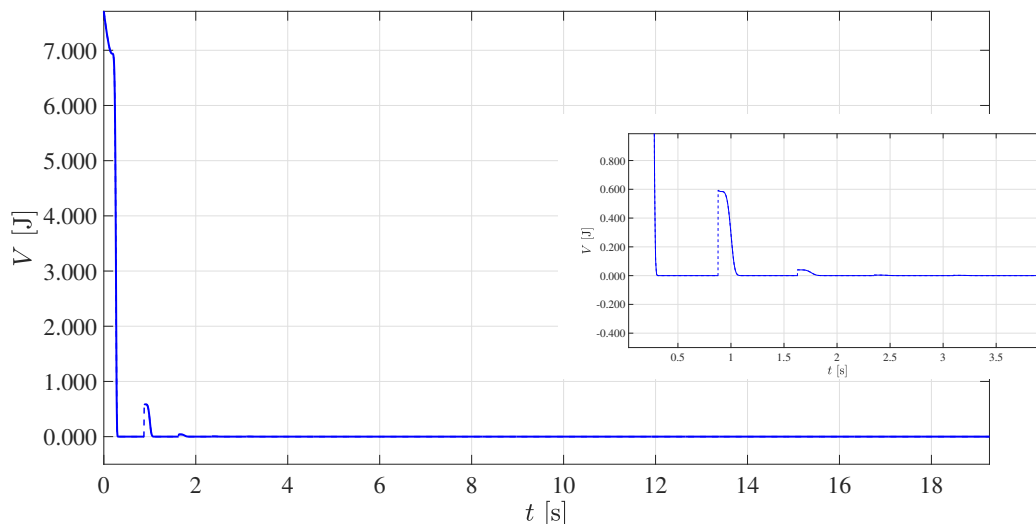


Figure 7.3: Storage function convergence during Case Study I. Storage function converges to zero in a simulation carried out starting from perturbed initial conditions using EPD-PBC with $k_{pd} = -8.4$. As highlighted by the box on the right, the value of the storage function at every impact is less than (or equal to) the value at the previous impact.

more effective in recovering the passive gait, as a possible consequence of the almost global stability results obtained via invariant sets theory.

7.4.2 Case Study II: Generated Gait Robustification

In this section, EPD-PBC has been applied after energy shaping. The energy of the system has been shaped through the IDA-PBC procedure proposed in [1] and presented, in this thesis, in Sections 4.2.1 and 6.2, for what concerns the methodological procedure and the application to the CBR, respectively. Energy-shaping is motivated by the possibility to generate new gaits. As remarked in [53], the gait exhibited by a CBR emerges from its particular inertial and geometrical properties. If both inertia and geometry are fixed, as well as the slope of the incline,

Table 7.1: Comparison between EPD-PBC and MNC during Case Study I

$x_P(0)$	EPD-PBC	MNC
	$k_{pd} = -1$	$k_{mn} = 2$
1	-	-
2	PG	NG
3	PG	-
4	-	-
5	-	-
6	PG	-
7	-	NG
8	-	NG
9	-	-
10	PG	NG

the energy flow between the walking surface and the robot is fixed too, driving biped dynamics towards its passive limit cycle with energy H_P . As shown in [23], control approaches similar to EPD-PBC and MNC fail in stabilizing target energies values which significantly differs from H_P (i.e., $H^* \gg H_P$ or $H^* \ll H_P$). In some cases, the resulting gait is exactly the passive one while, in others, new gaits arise, whose energies are different. Then, to stabilize a desired H^* , it is necessary to change how the robot and the ground interact, modifying both the inertial and the geometrical properties of the biped. Therefore, its kinetic and potential energies must be shaped.

A novel gait has been generated via an inner IDA-PBC control loop. Since it is not required to add dissipation in this task, the damping-injection step has been skipped. Hence, IDA-PBC has been reduced to the energy shaping phase only. The obtained gait has $S_{ida} = 0.5329 \text{ m}$ and $T_{ida} = 0.7717 \text{ s}$ as parameters, while its energy is $H_{ida} = 227.8194 \text{ J}$. Notice how this gait is significantly slower than the passive one. Simulation has been performed starting from

$[0.1959, -0.2902, -0.9576, -0.2700]^T$, which corresponds to a uniform 10% perturbation on the passive initial conditions

$$x_{ida}(0) = [0.2177, -0.3224, -1.0640, -0.3000]^T,$$

without introducing the proposed EPD-PBC. The same procedure adopted in Section 6.2 has been followed, appropriately adapted to take into account the actuation at the hip instead of the ankle. The CBR falls after few simulation seconds, showing that this novel limit cycle has a very narrow basin of attraction.

Then, an outer EPD-PBC loop, with $k_{pd} = -0.7$ and $H^* = 227.8194 J$ has been implemented. As shown in Fig. 7.4, the limit cycle (blue line) converges to the target one (green line) which partially surrounds the passive one (red line) placed here as a reference. Thanks to the EPD-PBC, the CBR keeps walking, demonstrating its usefulness to increase the robustness of newly generated gaits.

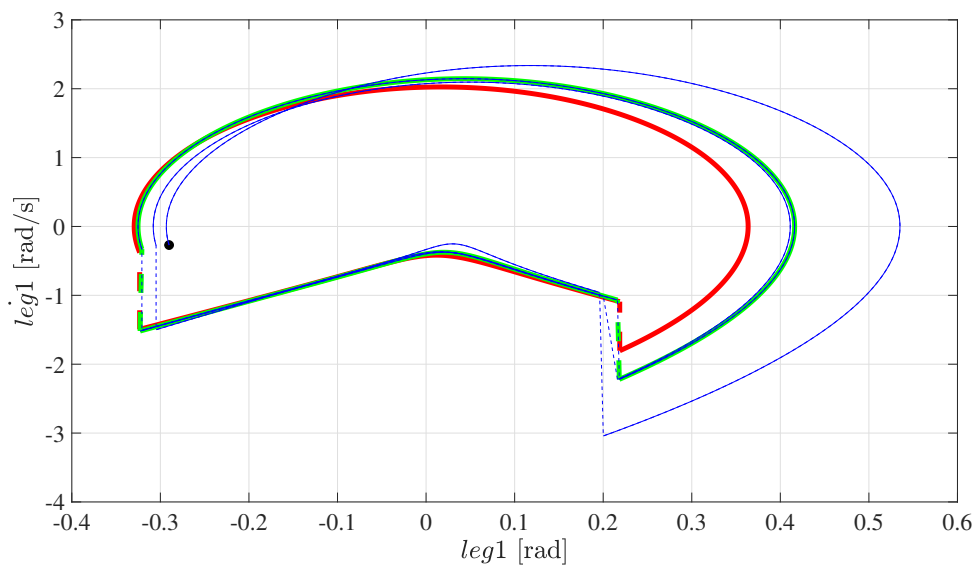


Figure 7.4: Limit cycles comparison for the first leg during Case Study II. Red arcs represent the passive limit cycle without energy shaping. Green arcs represent the gait generated through IDA-PBC starting from nominal initial conditions. Blue arcs represent the same gait starting from perturbed initial conditions. Black dot represents perturbed initial conditions. Blue arcs converge to green ones using EPD-PBC with $k_{pd} = -1$.

Chapter 8

Conclusion and Future Research

In this thesis, the versatility of energy shaping to tackle different control problems concerning underactuated mechanical systems has been highlighted. In particular, approaches belonging to the realm of IDA methodologies, namely IDA-PBC, SIDA-PBC, EPD-PBC, and EPOD-PBC have been deployed to achieve several control objectives: *i)* equilibrium stabilization; *ii)* gait generation; *iii)* gait robustification.

Firstly, a constructive solution to deal with IDA-PBC for underactuated two-degree-of-freedom mechanical systems has been presented. The proposed strategy combines the attributes of the parameterized IDA-PBC with those of the algebraic IDA-PBC: *i)* it provides explicit solutions of the PDEs arising from the matching process without requiring the a priori knowledge of the desired total energy; *ii)* the singularity in the generalized momenta, usually appearing in the desired interconnection matrix within state-of-the-art methodologies is avoided; *iii)* it does not put any constraint on the structure of the original system's inertia matrix. For these reasons, the proposed methodology overcomes the limitations inherent to both parameterized IDA-PBC and algebraic IDA-PBC. It is indeed a useful tool in the control of two-degree-of-freedom mechanical systems with underactuation degree one. Such a methodology has been exploited to face both the equilib-

rium stabilization of the TORA system and the gait generation of the CBR, exhibiting performances that are comparable to or better than other state-of-the-art approaches, as confirmed by numerical simulations which have been carried out. Then, several control methodologies using dissipative forces, as the SIDA-PBC, the EPD-PBC control, and the EPOD-PBC, have been used to generate stable gaits for the CBR. Due to the switching conditions produced by the impact of the swing leg with the ground, it has been possible to generate a stable gait in a CBR by relaxing the stability condition of the controllers mentioned in Appendix A. In particular, it has shown that the SIDA-PBC, with the inclusion of dissipative forces, is efficient in the generation of gaits not exhibited by the uncontrolled system, especially compared to EPD-PBC and EPOD-PBC controllers. Both IDA-PBC and the approaches based on dissipative forces can generate both small and large gaits, showing performance that justifies shaping the total energy of the biped rather than the kinetic energy only, as done in [16] and [49], instead. To tackle the gait robustification problem, a control design using EPD-PBC with HZD has been exploited to enlarge the basin of attraction of the passive limit cycle of the CBR, as well as, to enlarge the basin of attraction of the gaits generated through energy shaping, the latter created through IDA-PBC, further proving the flexibility of IDA methodologies to tackle different control problems. Numerical simulations and comparisons with other techniques validated the approach. Future work will focus on: *i*) generalizing the presented approaches to systems with higher degrees of freedom than two and higher underactuation degree than one; *ii*) extending the results and the ideas concerning gait generation to more complex biped models, from planar biped robots to 3D bipeds, *i.e.*, systems not constrained to move in the sagittal plane only; *iii*) investigating methods to guide the parameter selection for gait generation in terms of step length and step period specifications; *iv*) formalizing the presented results based on IDA methodologies to stabilize the gaits (*i.e.*, the orbital stabilization problem), and not only to generate them; *v*) implementing such methods on real hardware, with the proper adaptations to avoid foot scuffing, as mentioned at the end of Section 3.2.4.

Appendix A

IDA Methodologies

In this Appendix, the basic concepts about IDA-PBC, SIDA-PBC, EPD-PBC, and EPOD-PBC, are given. Such methodologies are repeatedly referred to as *IDA methodologies*, throughout the thesis. Such a choice has been made to stress out that SIDA-PBC, EPD-PBC, and EPOD-PBC, can be seen as a modification of IDA-PBC, which is the progenitor of the methodologies based on interconnection and damping assignment, having been the first to be proposed, in [9]. So, grouping together such different approaches paves the way to remark their common origin, as well as, to enlighten their differences. In particular, SIDA-PBC with dissipative forces represents a generalization of IDA-PBC, because gyroscopic forces have been substituted by more general dissipative ones [89] while the energy shaping and damping injection are carried out simultaneously, rather than in separate steps [21]. Besides, SIDA-PBC, EPD-PBC, and EPOD-PBC can be grouped in a further subgroup, namely the group of methodologies based on dissipative forces, since the control action is carried out only using such kind of forces. All the approaches proposed in this work have been exploited to control 2-DoFs mechanical systems, hence, the brief description outlined in this Appendix has been particularized for 2-DoFs mechanical systems too, for the sake of consistency with the rest of the thesis.

A.1 IDA-PBC for Applications to 2-DoF Mechanical Systems

This section is intended to give the preliminary concepts about the IDA-PBC. The systems addressed in this thesis can be described using (3.1), particularized for 2-DoF mechanical systems as

$$\begin{bmatrix} \dot{q} \\ \dot{p} \end{bmatrix} = \begin{bmatrix} O_2 & I_2 \\ -I_2 & O_2 \end{bmatrix} \begin{bmatrix} \nabla_q H(q, p) \\ \nabla_p H(q, p) \end{bmatrix} + \begin{bmatrix} 0_2 \\ G_p \end{bmatrix} u(q, p), \quad (\text{A.1})$$

with $q = [q_1 \ q_2]^T \in \mathbb{R}^2$ the generalised coordinates vector, $p = [p_1 \ p_2]^T \in \mathbb{R}^2$ the generalised momenta vector, $G_p \in \mathbb{R}^2$ the constant input mapping port, and $u(q, p) \in \mathbb{R}$ the scalar control input.

The Hamiltonian $H(q, p)$ is expressed as in (3.2), with $M(q) \in \mathbb{R}^{2 \times 2}$ defined as

$$M(q) = \begin{bmatrix} b_{11}(q) & b_{12}(q) \\ b_{12}(q) & b_{22}(q) \end{bmatrix} \quad (\text{A.2})$$

The IDA-PBC wants to bring the system (A.1) into the desired closed-loop expression

$$\begin{bmatrix} \dot{q} \\ \dot{p} \end{bmatrix} = \begin{bmatrix} O_2 & M^{-1}(q)M_d(q) \\ -M_d(q)M^{-1}(q) & J_2(q, p) - G_p k_d G_p^T \end{bmatrix} \begin{bmatrix} \nabla_q H_d(q, p) \\ \nabla_p H_d(q, p) \end{bmatrix} \quad (\text{A.3})$$

with

$$J_d(q, p) = \begin{bmatrix} O_2 & M^{-1}(q)M_d(q) \\ -M_d(q)M^{-1}(q) & J_2(q, p) \end{bmatrix} \quad (\text{A.4})$$

the desired, skew-symmetric interconnection matrix such that $J_d(q, p) = -J_d(q, p)^T \in \mathbb{R}^{4 \times 4}$,

$$R_d = \begin{bmatrix} O_2 & O_2 \\ O_2 & -G_p k_d G_p^T \end{bmatrix} \quad (\text{A.5})$$

the desired, positive semidefinite dissipation matrix such that $R_d(q, p) \geq 0 \in \mathbb{R}^{4 \times 4}$, where $k_d > 0 \in \mathbb{R}$ is a positive damping gain, and $H_d(q, p) \in \mathbb{R}$ is the desired Hamiltonian scalar function, *i.e.*

$$H_d(q, p) = \frac{1}{2} p^T M_d^{-1}(q) p + V_d(q). \quad (\text{A.6})$$

The following crucial conditions must be satisfied:

- C.1** $M_d(q) \in \mathbb{R}^{2 \times 2}$ is the desired mass matrix which must be positive definite ($M_d(q) > 0$) and symmetric ($M_d(q) = M_d(q)^T$);
- C.2** $V_d(q) \in \mathbb{R}$ is the desired potential energy scalar function which must admit a minimum in the desired equilibrium $q^* = \operatorname{argmin} V_d(q)$;
- C.3** $J_2(q, p) \in \mathbb{R}^{2 \times 2}$ is the assigned interconnection matrix which must be skew-symmetric ($J_2(q, p) = -J_2(q, p)^T$).

Notice that, for mechanical systems, because of **C.2**, the desired equilibrium point $(q, p) = (q^*, 0_2)$ corresponds to the minimum of the total energy $(q^*, 0_2) = \operatorname{argmin} H_d(q, p)$.

Problem Statement: Find a control-law matching the pH system (A.1) with the desired closed-loop pH system (A.3), satisfying **C.1**, **C.2**, and **C.3**.

Matching (A.1) with the target closed-loop (A.3) yields the following set of PDEs (*i.e.*, the matching equations)

$$G_p^\perp (\nabla_q H(q, p) - M_d(q) M^{-1}(q) \nabla_q H_d(q, p) + J_2(q, p) M_d^{-1}(q) p) = 0. \quad (\text{A.7})$$

Defined $G_p^\perp \in \mathbb{R}^{1 \times 2}$ as the left annihilator of G_p , the matching process, as explained in Section 2.3, changes accordingly to the methodology adopted. Notice that, in case of fully actuated systems, the PDEs (A.7) are trivially satisfied since G_p^\perp is a null matrix. Therefore, the potential and kinetic energies can be shaped as desired. In general, for fully actuated system, only the potential energy is shaped to avoid nonlinear cancellations, reducing the robustness of the closed loop.

The non-parameterized IDA-PBC fixes the structure of $J_2(q, p)$ in (A.7), defining the family of admissible $H_d(q, p)$ satisfying the matching equations.

The algebraic IDA-PBC fixes the desired total energy $H_d(q, p)$ exactly. For mechanical systems, this means that $M_d(q)$ and $V_d(q)$ are previously defined. In this way, the matching equations (A.7) become algebraic with $J_2(q, p)$ as unknown.

The parameterized IDA-PBC fixes the structure of $H_d(q, p)$. For mechanical systems, this means that a parameterization of $M_d(q)$ and $V_d(q)$ is defined. This splits the matching equations (A.7) into two subsets of PDEs, namely the KE-ME

$$\begin{aligned} G_p^\perp (\nabla_q (p^T M^{-1}(q)p) - M_d(q)M^{-1}(q)\nabla_q (p^T M_d^{-1}(q)p) \\ + 2J_2(q, p)M_d^{-1}(q)p) = 0, \end{aligned} \quad (\text{A.8})$$

and the PE-ME

$$G_p^\perp (\nabla_q V(q) - M_d(q)M^{-1}(q)\nabla_q V_d(q)) = 0. \quad (\text{A.9})$$

Both the KE-ME and the PE-ME are solved with respect to the chosen parameterization for $M_d(q)$ and $V_d(q)$, which in turn gives some constraints on $J_2(q, p)$ as clear from (A.8).

Regardless of the chosen approach, at the end of the matching process, the terms $V_d(q)$, $M_d(q)$, and $J_2(q, p)$ are known. Hence, the energy-shaping control law can be computed as

$$\begin{aligned} u_{es}(q, p) = (G_p^T G_p)^{-1} G_p^T (\nabla_q H(q, p) - M_d(q)M^{-1}(q)\nabla_q H_d(q, p) \\ + J_2(q, p)M_d^{-1}(q)p), \end{aligned} \quad (\text{A.10})$$

which defines a strict minimizer of the potential energy in the desired equilibrium $(q, p) = (q^*, 0_2)$. Moreover, a damping injection term

$$u_{di}(q, p) = -k_d G_p^T \nabla_p H_d(q, p) \quad (\text{A.11})$$

guarantees the asymptotic stability of the desired equilibrium if the passive output

$$y_d(q, p) = G_p^T \nabla_p H_d(q, p) = G_p^T M_d^{-1}(q)p \quad (\text{A.12})$$

is detectable (see Remark 3.2.21 in [83]). The final control law is thus

$$u(q, p) = u_{es}(q, p) + u_{di}(q, p). \quad (\text{A.13})$$

For more details see [63].

A.2 SIDA-PBC with Dissipative Forces for Applications to 2-DoF Mechanical Systems

In IDA-PBC, gyroscopic forces included in the desired dynamics simplify the solution of the KE-ME. Such kind of forces translates into the presence of the free skew-symmetric matrix $J_2(q, p)$ in the matching equations. As a consequence, the number of PDEs to be solved is reduced. Such free skew-symmetric term is intrinsic in IDA-PBC, due to its pH formulation, while it was added to the CL method for the first time in [90], where it is shown that the PDEs of the CL method extended with gyroscopic forces and those of IDA-PBC are the same, and later exploited in [91].

As shown in [21], SIDA-PBC with Dissipative Forces assigns a target pH system with a more general structure than the one considered in IDA-PBC, *i.e.*

$$\begin{bmatrix} \dot{q} \\ \dot{p} \end{bmatrix} = \begin{bmatrix} 0_2 & M^{-1}(q)M_d(q) \\ -M_d(q)M^{-1}(q) & 0_2 \end{bmatrix} \begin{bmatrix} \nabla_q H_d(q, p) \\ \nabla_p H_d(q, p) \end{bmatrix} + \begin{bmatrix} 0 \\ C(q, p) \end{bmatrix}, \quad (\text{A.14})$$

where the function $C(q, p) \in \mathbb{R}^2$ represents a mapping to be defined which is referred to as dissipative forces in [21]. Such kind of forces, whose adoption was originally proposed in [89], are more general than the usual gyroscopic ones represented, in standard IDA-PBC, by the skew-symmetric matrix $J_2(q, p)$. Hence, dissipative forces, though they do not reduce the complexity of the PDEs [10], extend the realm of application of IDA-PBC to a wider class of systems [21].

Substituting gyroscopic forces with dissipative ones, the KE-ME (A.8) becomes

$$G_p^\perp (\nabla_q (p^T M^{-1}(q)p) - M_d(q)M^{-1}(q)\nabla_q (p^T M_d^{-1}(q)p) + 2C(q, p)) = 0, \quad (\text{A.15})$$

while the PE-ME (A.9) remains unchanged.

Since $C(q, 0) = 0_n$, the related mapping can be expressed as

$$C(q, p) = \Lambda(q, p)M_d^{-1}(q)p \quad (\text{A.16})$$

for a matrix $\Lambda(q, p) \in \mathbb{R}^{2 \times 2}$ defined as

$$\Lambda(q, p) := \begin{bmatrix} \Lambda_{11}(q, p) & \Lambda_{12}(q, p) \\ \Lambda_{21}(q, p) & \Lambda_{22}(q, p) \end{bmatrix}, \quad (\text{A.17})$$

with $\Lambda_{ij}(q, p) \in \mathbb{R}$. The mapping $C(q, p)$ must be quadratic in p and thus, without loss of generality, it can be written as

$$2C(q, p) = \sum_{i=1}^2 (p^T M_d^{-1}(q) Q_i M_d^{-1}(q) p) e_i, \quad (\text{A.18})$$

with $Q_i \in \mathbb{R}^{2 \times 2}$ free matrices to be chosen and $e_i \in \mathbb{R}^2$ the Euclidean basis vector.

Therefore, the desired closed-loop dynamics can be written as

$$\begin{bmatrix} \dot{q} \\ \dot{p} \end{bmatrix} = \begin{bmatrix} 0_2 & M^{-1}(q)M_d(q) \\ -M_d(q)M^{-1}(q) & \Lambda(q, p) \end{bmatrix} \begin{bmatrix} \nabla_q H_d(q, p) \\ \nabla_p H_d(q, p) \end{bmatrix}. \quad (\text{A.19})$$

A necessary condition for stability of the equilibrium point of the closed-loop system is

$$p^T M_d^{-1}(q) \Lambda(q, p) M_d^{-1}(q) p \leq 0. \quad (\text{A.20})$$

Once the matching equations (A.15) and (A.9) are solved, then the control input can be algebraically computed as

$$u(q, p) = (G_p^T G_p)^{-1} G_p^T \left[\nabla_q H(q, p) - M_d(q) M^{-1}(q) \nabla_q H_d(q, p) + \Lambda(q, p) M_d^{-1}(q) p \right]. \quad (\text{A.21})$$

which replaces the standard IDA-PBC controller (A.13) and carries out energy shaping and damping injection simultaneously.

A.3 EPD-PBC for Applications to 2-DoF Mechanical Systems

As shown in Appendix A.1, within the IDA-PBC methodology, there exist two distinctive control actions which are, contrarily to the SIDA-PBC, carried out in two consecutive steps, namely, the energy shaping $u_{es}(q, p)$ and the damping injection $u_{di}(q, p)$.

If the energy shaping stage is ignored, *i.e.* $H_d(q, p) = H(q, p)$ and $J_2(q, p) = 0$, the IDA-PBC reduces to a controller which only dissipates the initial energy of the system. Then, the resulting control law comes out to be

$$u(q, p) = u_{di}(q, p) = -k_d G_p^T \nabla_p H(q, p), \quad (\text{A.22})$$

while the closed-loop system (A.3) becomes

$$\begin{bmatrix} \dot{q} \\ \dot{p} \end{bmatrix} = \begin{bmatrix} 0_2 & I_2 \\ -I_2 & R_d(q) \end{bmatrix} \begin{bmatrix} \nabla_q H(q, p) \\ \nabla_p H(q, p) \end{bmatrix}, \quad (\text{A.23})$$

which asymptotically converges to its natural equilibrium, given that the passive output is detectable, due to the dissipation condition

$$R_d \leq 0, \quad (\text{A.24})$$

where

$$R_d = -G_p k_d G_p^T. \quad (\text{A.25})$$

with $k_d \geq 0$. An alternative to (A.25) is

$$R_{pd} = G_p k_{pd} e(q, p) G_p^T. \quad (\text{A.26})$$

which relaxes the classical dissipation condition (A.24). R_{pd} is positive definite in some regions of the state space while, in other regions, it is negative semidefinite, leading to a control action which pumps energy into the system and damps energy from the system accordingly to the sign of R_{pd} . The pumping-and-damping matrix (A.26) yields to an EPD-PBC with the following structure

$$\begin{aligned} u_{pd}(q, p) &= k_{pd} e(q, p) G_p^T \nabla_p H(q, p) \\ &= k_{pd} e(q, p) G_p^T M^{-1}(q) p, \end{aligned} \quad (\text{A.27})$$

with $k_{pd} \in \mathbb{R}$ a given control gain and $e(q, p)$ a suitable scalar function which will be chosen accordingly to the selected control objective (*e.g.*, gait generation or gait robustification). Through such a control law, the time derivative of the total energy $H(q, p)$ becomes

$$\dot{H}(q, p) = p^T M^{-1}(q) G_p k_{pd} e(q, p) G_p^T M^{-1}(q) p, \quad (\text{A.28})$$

whose sign changes accordingly with the sign of the function $e(q, p)$.

The same methodology was proposed by [92] to stabilize a pendulum in its upright position.

A.4 EPOD-PBC

The control methodology presented in the previous section can be slightly modified by designing a function $e(q, p)$ such to be always positive. Albeit such a choice does not lead to an EPD-PBC controller, it brings to a control law that is different from the standard damping injection term of the IDA-PBC because of the dependency on the generalized coordinate vector introduced by $e(q, p)$. It is indeed equivalent to an energy damping controller, dissipating energy for $k_{pd} < 0$. On the other hand, it reduces to an energy pumping controller for $k_{pd} > 0$. The $u_{pod}(q, p)$ term assumes the role of a dissipative force for $k_{pd} < 0$.

Appendix B

Existence of the Integrals

B.1 Existence of the integral within equation (4.11)

To guarantee a closed-form solution for the integral in (4.11), from the fundamental theorem of calculus, it is necessary to show that the integrand is an integrable function. Since the continuity implies the integrability, in the Riemann sense, to accomplish the task, it is sufficient to show that the argument of the integral is a continuous function over the set $[1, q_1]$. The integrand of (4.11) is a fractional function. Notice that the quotient of two continuous functions is continuous if the denominator is not equal to zero. The numerator is the gradient of the plant's potential energy. Therefore, it is a conservative force that is continuous everywhere by definition ($V(q)$ is a class \mathcal{C}_2 function due to its relationship with the Hamiltonian). Regarding the continuity of the denominator, specific conditions will be expressed in the next subsection. As a matter of fact, the integrand's continuity in (4.11) is strongly related to the integrand's continuity in (4.17).

B.2 Existence of the integral within equation (4.17)

Starting from the considerations provided in the previous subsection, the integrand of (4.17) is a fractional function too. The numerator and the denominator are continuous because they are a linear combination of the plant's inertia matrix terms and their gradients. Hence, the continuity of the integrand reduces to avoid that the denominator becomes zero, as given by the following condition

$$k_1 b_{12}([\sigma \ f_4(q, \sigma)]) + k_2 b_{22}([\sigma \ f_4(q, \sigma)]) \neq 0,$$

which yields to

$$k_2 \neq -\frac{k_1 b_{12}([\sigma \ f_4(q, \sigma)])}{b_{22}([\sigma \ f_4(q, \sigma)])}. \quad (\text{B.1})$$

It is thus necessary to find upper and lower bounds for k_2 to satisfy (B.1). This is equivalent to compute the bounds for $b_{12}(q_1, q_2)$ and $b_{22}(q_1, q_2)$. Such bounds exist if and only if $M(q)$ is bounded too. A study about the boundedness of the inertia matrix of serial robot manipulators was carried out in [93]. At the same time, several examples are provided for many underactuated 2-DoF mechanical systems (the Acrobot, the Pendubot, the cart-pole, the crane, the rotating pendulum, the inertia-wheel pendulum, the magnetic suspension, the ball-and-beam, and the TORA) [70], that are precisely the target of this thesis (where the CBR is added to the list, and others can be found in the literature). Moving from this assumption, it is possible to always satisfy (B.1) through the following (very) conservative condition

$$k_2 > \left| \frac{k_1 \max(b_{12}([\sigma \ f_4(q, \sigma)]))}{\min(b_{22}([\sigma \ f_4(q, \sigma)])} \right|, \quad (\text{B.2})$$

where the given bounds exist due to the boundedness of $M(q)$. Hence, the integral in (4.17) exists and it is well-defined. In turn, this yields to the existence of the integral in (4.11). As a matter of fact, $f_2(q, c_1)$

in (4.17) cannot be zero since it is an exponential continuous function. Therefore, the function $\gamma(q, c_1)$ in (4.16) cannot be zero since $f_3(\cdot, \cdot)$ is a nonzero continuous function. Since the product of a finite number of continuous functions is still a continuous function, and since $\gamma(q, c_1)$ cannot be zero, the denominator in (4.11) is a nonzero continuous function. This yields to the existence of the integral in (4.11).

Bibliography

- [1] P. Arpentì, F. Ruggiero, and V. Lippiello, “A Constructive Methodology for the IDA-PBC of Underactuated 2-DoF Mechanical Systems with Explicit Solution of PDEs,” *International Journal of Control, Automation, and Systems (IJCAS)*, 2022 (in press).
- [2] P. Arpentì, F. Ruggiero, and V. Lippiello, “Interconnection and damping assignment passivity-based control for gait generation in underactuated compass-like robots,” in *2020 IEEE International Conference on Robotics and Automation*, (Paris, France), 2020.
- [3] M. Nacusse, P. Arpentì, F. Ruggiero, and V. Lippiello, “Gait Generation for Underactuated Compass-Like Robots Using Dissipative Forces in the Controller,” *IFAC-PapersOnLine*, vol. 53, no. 2, pp. 9023–9030, 2020. 21th IFAC World Congress.
- [4] P. Arpentì, A. Donaire, F. Ruggiero, and V. Lippiello, “Energy pumping-and-damping for gait robustification in underactuated planar biped robots within the hybrid zero dynamics framework,” in *2020 IEEE-RAS International Conference on Humanoid Robots, Humanoids 2020*, 2021 (in press).
- [5] R. Tedrake, “Underactuated robotics: Algorithms for walking, running, swimming, flying, and manipulation (course notes for mit 6.832),” May 2021.
- [6] M.-W. Spong, “Partial feedback linearization of underactuated mechanical systems,” in *Proceedings of IEEE/RSJ International*

- Conference on Intelligent Robots and Systems (IROS'94)*, vol. 1, (Munich, Germany), pp. 314–321, 1994.
- [7] R. Ortega, A. Loria, P. J. Nicklasson, and H. Sira-Ramirez, *Passivity-based control of Euler–Lagrange systems*. Communications and Control Engineering, Berlin: Springer, September 1998.
- [8] R. Ortega, A. Donaire, and J.-G. Romero, *Passivity-Based Control of Mechanical Systems*, pp. 167–199. Feedback Stabilization of Controlled Dynamical Systems—In Honor of Laurent Praly, Lecture Notes in Control and Information Sciences, Berlin/Heidelberg: Springer, 2017.
- [9] R. Ortega, A. Van Der Schaft, B. Maschke, and G. Escobar, “Interconnection and damping assignment passivity-based control of port-controlled Hamiltonian systems,” *Automatica*, vol. 38, no. 4, pp. 585–596, 2002.
- [10] N. Crasta, R. Ortega, H. K. Pillai, and J. G. R. Velazquez, “The Matching Equations of Energy Shaping Controllers for Mechanical Systems are not Simplified with Generalized Forces,” *IFAC Proceedings Volumes*, vol. 45, no. 19, pp. 48–53, 2012. 4th IFAC Workshop on Lagrangian and Hamiltonian Methods for Non Linear Control.
- [11] A. Donaire, R. Mehra, R. Ortega, S. Sumeet, J. Romero, K. Faruk, and N.-M. Singh, “Shaping the energy of mechanical systems without solving partial differential equations,” *IEEE Transactions on Automatic Control*, vol. 61, no. 4, pp. 1051–1056, 2016.
- [12] J.-W. Grizzle, C. Chevallereau, R.-W. Sinnet, and A.-D. Ames, “Models, feedback control, and open problems of 3d bipedal robot walking,” *Automatica*, vol. 50, no. 8, pp. 1955–1988, 2014.
- [13] C. Chevallereau, D. Djoudi, and J. W. Grizzle, “Stable Bipedal Walking With Foot Rotation Through Direct Regulation of the

- Zero Moment Point,” *IEEE Transactions on Robotics*, vol. 24, no. 2, pp. 390–401, 2008.
- [14] J. Gottschall and R. Kram, “Energy cost and muscular activity required for propulsion during walking,” *Journal of applied physiology (Bethesda, Md. : 1985)*, vol. 94, pp. 1766–72, 06 2003.
- [15] D.-A. Winter, “Energy generation and absorption at the ankle and knee during fast, natural, and slow cadences,” *Clinical orthopaedics and related research*, p. 147—154, May 1983.
- [16] J. Holm and M.-W. Spong, “Kinetic energy shaping for gait regulation of underactuated bipeds,” in *IEEE International conference on control applications*, (San Antonio, Texas, USA), pp. 1232–1238, 2008.
- [17] T. McGeer, “Passive dynamic walking,” *The International Journal of Robotics Research*, vol. 9, no. 2, pp. 62–82, 1990.
- [18] M.-W. Spong and F. Bullo, “Controlled symmetries and passive walking,” *Proceeding IFAC Triennial World Congress*, (Barcelona, Spain), 2002.
- [19] M.-W. Spong and G. Bhatia, “Further results on control of the compass gait biped,” in *Proceedings 2003 IEEE/RSJ International Conference on Intelligent Robots and Systems (IROS 2003)*, (Las Vegas, NV, USA), pp. 1933–1938, 2003.
- [20] M.-W. Spong, J. Holm, and D. Lee, “Passivity-based control of bipedal locomotion,” *IEEE Robotics & Automation Magazine*, vol. 12, no. 2, pp. 30–40, 2007.
- [21] A. Donaire, R. Ortega, and J. Romero, “Simultaneous interconnection and damping assignment passivity-based control of mechanical systems using dissipative forces,” *Systems & Control Letters*, vol. 94, pp. 118 – 126, 2016.

- [22] R.-W. Sinnet and A.-D. Ames, “Energy shaping of hybrid systems via control lyapunov functions,” in *2015 American Control Conference (ACC)*, (Chicago, IL), pp. 5992–5997, 2015.
- [23] A. Goswami, B. Espiau, and A. Keramane, “Limit Cycles in a Passive Compass Gait Biped and Passivity-Mimicking Control Laws.,” *Autonomous Robots*, no. 4, pp. 273–286, 1997.
- [24] H. K. Khalil, *Nonlinear systems; 3rd ed.* Upper Saddle River, NJ: Prentice-Hall, 2002.
- [25] J. Yamaguchi, E. Soga, S. Inoue, and A. Takanishi, “Development of a bipedal humanoid robot-control method of whole body cooperative dynamic biped walking,” in *Proceedings 1999 IEEE International Conference on Robotics and Automation (Cat. No.99CH36288C)*, vol. 1, pp. 368–374 vol.1, 1999.
- [26] S. Kajita and K. Tani, “Study of dynamic biped locomotion on rugged terrain-theory and basic experiment,” in *Fifth International Conference on Advanced Robotics 'Robots in Unstructured Environments*, vol. 1, pp. 741–746, 1991.
- [27] J. Geursen, D. Altena, C. Massen, and M. Verduin, “A model of the standing man for the description of his dynamic behaviour,” *Agressologie*, vol. 17B, pp. 63–69, 1976.
- [28] S. Kajita, F. Kanehiro, K. Kaneko, K. Yokoi, and H. Hirukawa, “The 3d linear inverted pendulum mode: a simple modeling for a biped walking pattern generation,” in *Proceedings 2001 IEEE/RSJ International Conference on Intelligent Robots and Systems. Expanding the Societal Role of Robotics in the the Next Millennium*, vol. 1, pp. 239–246, 2001.
- [29] S. Kajita, M. Morisawa, K. Miura, S. Nakaoka, K. Harada, K. Kaneko, F. Kanehiro, and K. Yokoi, “Biped walking stabilization based on linear inverted pendulum tracking,” in *2010*

IEEE/RSJ International Conference on Intelligent Robots and Systems, pp. 4489–4496, 2010.

- [30] S. Kajita, T. Yamaura, and A. Kobayashi, “Dynamic walking control of a biped robot along a potential energy conserving orbit,” *IEEE Transactions on Robotics and Automation*, vol. 8, no. 4, pp. 431–438, 1992.
- [31] A. Goswami, “Postural stability of biped robots and the foot-rotation indicator (fri) point,” *The International Journal of Robotics Research*, vol. 18, no. 6, pp. 523–533, 1999.
- [32] M. Vukobratovic and B. Borovac, “Zero-moment point - thirty five years of its life.,” *I. J. Humanoid Robotics*, vol. 1, pp. 157–173, 03 2004.
- [33] A. Takanishi, M. Ishida, Y. Yamazaki, and I. Kato, “Realization of dynamic walking by the biped walking robot wl-10rd.,” pp. 459–466, Dec. 1985.
- [34] Jun Ho Choi and J. W. Grizzle, “Planar bipedal walking with foot rotation,” in *Proceedings of the 2005, American Control Conference, 2005.*, vol. 7, pp. 4909–4916, 2005.
- [35] J. H. Park and K. D. Kim, “Biped robot walking using gravity-compensated inverted pendulum mode and computed torque control,” in *Proceedings. 1998 IEEE International Conference on Robotics and Automation (Cat. No.98CH36146)*, vol. 4, pp. 3528–3533, 1998.
- [36] B. J. Stephens and C. G. Atkeson, “Push recovery by stepping for humanoid robots with force controlled joints,” in *2010 10th IEEE-RAS International Conference on Humanoid Robots*, pp. 52–59, 2010.
- [37] T. Takenaka, T. Matsumoto, and T. Yoshiike, “Real time motion generation and control for biped robot -3rd report: Dynamics er-

- ror compensation-,” in *2009 IEEE/RSJ International Conference on Intelligent Robots and Systems*, pp. 1594–1600, 2009.
- [38] J. Pratt, J. Carff, S. Drakunov, and A. Goswami, “Capture point: A step toward humanoid push recovery,” in *2006 6th IEEE-RAS International Conference on Humanoid Robots*, pp. 200–207, 2006.
- [39] J. Pratt and R. Tedrake, *Velocity-Based Stability Margins for Fast Bipedal Walking*, pp. 299–324. 01 1970.
- [40] J. Rebula, F. Canas, J. Pratt, and A. Goswami, “Learning capture points for humanoid push recovery,” in *2007 7th IEEE-RAS International Conference on Humanoid Robots*, pp. 65–72, 2007.
- [41] M. H. Raibert, “Hopping in legged systems — modeling and simulation for the two-dimensional one-legged case,” *IEEE Transactions on Systems, Man, and Cybernetics*, vol. SMC-14, no. 3, pp. 451–463, 1984.
- [42] R. Blickhan, “The spring-mass model for running and hopping,” *Journal of Biomechanics*, vol. 22, no. 11, pp. 1217–1227, 1989.
- [43] M. Ahmadi and M. Buehler, “Controlled passive dynamic running experiments with the arl-monopod ii,” *IEEE Transactions on Robotics*, vol. 22, no. 5, pp. 974–986, 2006.
- [44] M. H. Raibert, *Legged Robots That Balance*. USA: Massachusetts Institute of Technology, 1986.
- [45] G. Zeglin and B. Brown, “Control of a bow leg hopping robot,” in *Proceedings. 1998 IEEE International Conference on Robotics and Automation (Cat. No.98CH36146)*, vol. 1, pp. 793–798 vol.1, 1998.
- [46] S. Mochon and T.-A. McMahon, “Ballistic walking,” *Journal of Biomechanics*, vol. 13, no. 1, pp. 49–57, 1980.

- [47] T. McGeer, “Passive walking with knees,” in *Proceedings., IEEE International Conference on Robotics and Automation*, vol. 3, pp. 1640–1645, 1990.
- [48] A.-D. Kuo, “The six determinants of gait and the inverted pendulum analogy: A dynamic walking perspective,” *Human Movement Science*, vol. 26, no. 4, pp. 617–656, 2007.
- [49] V. De-León-Gómez, V. Santibañez, and J. Sandoval, “Interconnection and damping assignment passivity-based control for a compass-like biped robot,” *International Journal of Advanced Robotic Systems*, vol. 14, no. 4, 2017.
- [50] S. Collins, A. Ruina, R. Tedrake, and M. Wisse, “Efficient bipedal robots based on passive-dynamic walkers,” *Science*, vol. 307, no. 5712, pp. 1082–1085, 2005.
- [51] M. Yeatman, G. Lv, and R. Gregg, “Passivity-based control with a generalized energy storage function for robust walking of biped robots,” Annual American Control Conference, (Milwaukee, USA), 2018.
- [52] P. B. Wieber, R. Tedrake, and S. Kuindersma, “Modeling and control of legged robots,” in *Springer Handbook of Robotics* (B. Siciliano and O. Khatib, eds.), pp. 1203–1234, Springer International Publishing, 2016.
- [53] A. Goswami, B. Thuilot, and B. Espiau, “Compass-like biped robot Part I: Stability and bifurcations of passive gaits,” *Institut National de Recherche en Informatique et en Automatique (INRIA), Technical Report 2996*, 1996.
- [54] K. Fujimoto and S. Toshiharu, “Canonical transformations and stabilization of generalized Hamiltonian systems,” *System & Control Letters*, vol. 42, pp. 217–227, 2001.

- [55] A. Bloch, N. Leonard, and J. Marsden, “Controlled lagrangians and the stabilization of mechanical systems. I. The first matching theorem,” *IEEE Transactions on Automatic Control*, vol. 45, no. 12, pp. 2253–2270, 2000.
- [56] A. Bloch, D. Chang, N. Leonard, and J. Marsden, “Controlled lagrangians and the stabilization of mechanical systems. II. Potential shaping,” *IEEE Transactions on Automatic Control*, vol. 46, no. 10, pp. 1556–1571, 2000.
- [57] R. Ortega, A. Van Der Schaft, I. Mareels, and B. Maschke, “Putting energy back into control,” *IEEE Control Systems Magazine*, pp. 18–33, 2001.
- [58] J.-A. Acosta, R. Ortega, and A. Astolfi, “Interconnection and damping assignment passivity-based control of mechanical systems with underactuation degree one,” *IEEE Transactions on Automatic Control*, vol. 50, pp. 1936–1955, 2005.
- [59] V. Duindam, *Port-Based Modelling and Control for Efficient Bipedal Walking Robots*. PhD thesis, Ph.D. Dissertation, University of Twente, 2006.
- [60] R. Ortega and E. Garcia-Canseco, “Interconnection and damping assignment passivity-based control: A survey,” *European Journal of Control*, vol. 10, pp. 432–450, 2004.
- [61] M. Zhang, R. Ortega, Z. Liu, and H. Su, “A new family of interconnection and damping assignment passivity-based controllers,” *International Journal of Robust and Nonlinear Control*, vol. 27, no. 1, pp. 50–65, 2017.
- [62] K. Nunna, M. Sassano, and A. Astolfi, “Constructive interconnection and damping assignment for port-controlled hamiltonian systems,” *IEEE Transactions on Automatic Control*, vol. 60, no. 9, pp. 2350–2361, 2015.

- [63] R. Ortega, M. Spong, F. Gómez-Estern, and G. Blankenstein, “Stabilization of a class of underactuated mechanical systems via interconnection and damping assignment,” *IEEE Transactions on Automatic Control*, vol. 47, no. 8, pp. 1218–1233, 2002.
- [64] D. Serra, F. Ruggiero, A. Donaire, L.-R. Buonocore, V. Lippiello, and B. Siciliano, “Control of nonprehensile planar rolling manipulation: A passivity-based approach,” *IEEE Transactions on Robotics*, vol. 35, no. 2, pp. 317–329, 2019.
- [65] A.-D. Ames, K. Galloway, K. Sreenath, and J.-W. Grizzle, “Rapidly Exponentially Stabilizing Control Lyapunov Functions and Hybrid Zero Dynamics,” *IEEE Transactions on Automatic Control*, vol. 59, no. 4, pp. 876–891, 2014.
- [66] E.-R. Westervelt, J.-W. Grizzle, and D.-E. Koditschek, “Hybrid zero dynamics of planar biped walkers,” *IEEE Transactions on Automatic Control*, vol. 48, no. 1, pp. 42–56, 2003.
- [67] E.-R. Westervelt, J.-W. Grizzle, C. Chevallereau, J.-H. Choi, and B. Morris, *Feedback Control of Dynamic Bipedal Robot Locomotion*. London, UK: Taylor & Francis/CRC Press, 2007.
- [68] B. Morris and J.-W. Grizzle, “Hybrid Invariant Manifolds in Systems With Impulse Effects With Application to Periodic Locomotion in Bipedal Robots,” *IEEE Transactions on Automatic Control*, vol. 54, no. 8, pp. 1751–1764, 2009.
- [69] H. Sadeghian, C. Ott, G. Garofalo, and G. Cheng, “Passivity-based control of underactuated biped robots within hybrid zero dynamics approach,” in *2017 IEEE International Conference on Robotics and Automation (ICRA)*, (Singapore), pp. 4096–4101, 2017.
- [70] Y. Liu and H. Yu, “A survey of underactuated mechanical systems,” *IET Control Theory Applications*, vol. 7, no. 7, pp. 921–935, 2013.

- [71] C.-J. Wan, D.-S. Bernstein, and V.-T. Coppola, “Global stabilization of the oscillating eccentric rotor,” *Nonlinear Dynamics*, vol. 10, pp. 49–62, 1996.
- [72] A. Morillo, M.-R. Bolivar, and V. Acosta, “feedback stabilization of the TORA system via interconnection and damping assignment control,” 17th IFAC World Congress, (Seoul, KR), pp. 3781–3786, 2008.
- [73] D.-A. Dirksz, J.-M.-A. Scherpen, and R. Ortega, “Interconnection and damping assignment passivity-based control for port-Hamiltonian mechanical systems with only position measurements,” 47th IEEE Conference on Decision and Control, (Cancun, MX), pp. 4957–4962, 2008.
- [74] M. Jankovic, D. Fontaine, and P.-V. Kokotovic, “TORA example: Cascade and passivity-based control designs,” *IEEE Transactions on Control Systems Technology*, vol. 4, no. 3, pp. 292–297, 1996.
- [75] R. Olfati-Saber, “Nonlinear control and reduction of underactuated systems with symmetry I: Actuated shape variables case,” 40th IEEE Conference on Decision and Control, (Orlando, FL, US), pp. 4158–4163, 2001.
- [76] A. Pavlov, B. Jansen, N. van der Wouw, and H. Nijmeijer, “Experimental output regulation for the TORA system,” 44th IEEE Conference on Decision and Control, (Sevilla, ES), pp. 1108–1113, 2005.
- [77] T. Tanighuchi and M. Sugeno, “Piecewise multi-linear model based control for TORA system via feedback linearization,” International MultiConference of Engineers and Computer Scientist, (Honk Kong, CN), 2018.
- [78] K. Tanaka, T. Tanighuchi, and H.-O.-M. Wang, “Model-based fuzzy control of the TORA: Fuzzy regulator and fuzzy observer design via LMIs that rapresent decay rate, disturbance rejection,

- robustness, optimality,” 1998 IEEE International Conference on Fuzzy Systems Proceedings., (Anchorage, AK, US), 1998.
- [79] L.-C. Hung, H.-P. Lin, and H.-Y. Chung, “Design of self-tuning fuzzy sliding mode control for TORA system,” *Expert Systems with Applications*, vol. 32, no. 1, pp. 201–212, 2007.
- [80] A. Isidori, *Nonlinear Control Systems (3rd ed.)*. Berlin: Springer-Verlag, 1995.
- [81] P.-A. Bhounsule, J. Cortell, and A. Ruina, “Design and control of Ranger: An energy-efficient, dynamic walking robot,” *Adaptive Mobile Robotics*, pp. 441–448, 2012.
- [82] M. Ryalat and D. Laila, “A simplified IDA—PBC design for underactuated mechanical systems with applications,” *European Journal of Control*, vol. 27, pp. 1–16, 2016.
- [83] A. Van Der Schaft, “ L_2 -gain and passivity techniques in nonlinear control,” Communications and Control Engineering, Berlin: Springer, 2017. ISBN 978-3-319-49991-8.
- [84] A.-D. Kuo, “Energetics of Actively Powered Locomotion Using the Simplest Walking Model ,” *Journal of Biomechanical Engineering*, vol. 124, pp. 113–120, 09 2001.
- [85] M. Alexander.-R., “Mechanics of fossil vertebrates,” *Journal of the Geological Society*, vol. 146, no. 1, pp. 41–52, 1989.
- [86] D. Grieve and R.-J. Gear, “The relationships between length of stride, step frequency, time of swing and speed of walking for children and adults,” *Ergonomics*, vol. 9, no. 5, pp. 379–399, 1966.
- [87] B. Yi, R. Ortega, D. Wu, and W. Zhang, “Orbital stabilization of nonlinear systems via Mexican sombrero energy shaping and pumping-and-damping injection,” *Automatica*, vol. 112, 2020.

- [88] Ö. Karabacak, R. Wisniewski, and J. Leth, “On the almost global stability of invariant sets,” in *2018 European Control Conference (ECC)*, pp. 1648–1653, 2018.
- [89] D. E. Chang, “Generalization of the IDA-PBC method for stabilization of mechanical systems,” in *18th Mediterranean Conference on Control and Automation, MED’10*, pp. 226–230, 2010.
- [90] G. Blankenstein, R. Ortega, and A. J. V. D. Schaft, “The matching conditions of controlled Lagrangians and IDA-passivity based control,” *International Journal of Control*, vol. 75, no. 9, pp. 645–665, 2002.
- [91] D. E. Chang, A. M. Bloch, N. E. Leonard, J. E. Marsden, and C. A. Woolsey, “The equivalence of controlled lagrangian and controlled hamiltonian systems,” *ESAIM: Control, Optimisation and Calculus of Variations*, vol. 8, pp. 393–422, 2002.
- [92] K. J. Astrom, J. Aracil, and F. Gordillo, “A family of smooth controllers for swinging up a pendulum,” *Automatica*, vol. 44, pp. 1841–1848, July 2008.
- [93] F. Ghorbel, B. Srinivasan, and M.-W. Spong, “On the uniform boundedness of the inertia matrix of serial robot manipulators,” *Journal of Robotic Systems*, vol. 15, pp. 17–28, 1998.